01 Sep 1991

Design of automotive structural components using high strength sheet steels structural strength of cold-formed steel beams under dynamic loads

Chi-Ling Pan

Wei-Wen Yu
Missouri University of Science and Technology, wwy4@mst.edu

Civil Engineering Study 91-4
Cold-Formed Steel Series

Sixteenth Progress Report

DESIGN OF AUTOMOTIVE STRUCTURAL COMPONENTS USING HIGH STRENGTH SHEET STEELS

STRUCTURAL STRENGTH OF COLD-FORMED STEEL BEAMS UNDER DYNAMIC LOADS

by

Chi-Ling Pan
Research Assistant

Wei-Wen Yu
Project Director

A Research Project Sponsored by the American Iron and Steel Institute

September 1991

Department of Civil Engineering
University of Missouri-Rolla
Rolla, Missouri

TABLE OF CONTENTS

TABLE OF CONTENTS (Cont.)

LIST OF TABLES

LIST OF TABLES (cont.)

LIST OF TABLES (cont.)

LIST OF TABLES (cont.)

LIST OF TABLES (cont.)

LIST OF FIGURES

LIST OF FIGURES (Cont.)

LIST OF FIGURES (Cont.)

LIST OF FIGURES (Cont.)

LIST OF FIGURES (Cont.)

I. INTRODUCTION

It has long been recognized that material properties and stress-strain relationships of sheet steels can be influenced by the strain rate. A considerable amount of theoretical and experimental research have been undertaken in the past to study material properties and the behavior of structures under dynamic loads and impact loads. In view of the fact that in the current AISI Automotive Steel Design Manual[1], the design criteria for effective design width are based on the test results under static loading condition, the objective of this investigation was to study the validity of these effective design width formulas for the design of cold-formed steel structural members subjected to dynamic loads.

In order to investigate the structural behavior and strength of cold-formed steel members under dynamic loads, the material properties of three selected sheet steels (35XF, 50XF, and 100XF) have been studied at the University of Missouri-Rolla. The test results of the static and dynamic mechanical properties in tension and compression under different strain rates were established in the first phase of the project. The nominal yield strengths of these three types of sheet steels ranged from 35 to 100 ksi and the range of strain rates varied from 10^{-4} to 1.0 in./in./sec.. Details of the tension and compression coupon tests were presented in the Eleventh and Twelfth Propress Reports[2,3].

In Phase II of the project, the structural behavior and strength of cold-formed steel members having both unstiffened and stiffened elements were studied experimentally and analytically for stub columns and beams subjected to dynamic loads. Two materials (35XF and 50XF) were used in this phase of study. The test results of 97 stub columns with evaluation were summarized in the Fifteenth Progress Report[6].

During the period from August 1989 through April 1990, fifteen (15) beam specimens using channel sections and fifteen (15) beam specimens using hat sections were tested to study the strength of structural members having unstiffened and stiffened compression elements, respectively. These test specimens were fabricated from 35XF sheet steel. The strain rates ranged from 10^{-5} to 10^{-2} in./in./sec.. The test results were presented in the Thirteenth and Fourteenth Propress Reports[4,5],

The study of beam specimens fabricated from 50XF sheet steel subjected to dynamic loads was initiated in March 1991. Fifteen (15) beam specimens using channel sections and fifteen (15) beam specimens using hat sections were tested for the purpose of studying the behavior of unstiffened and stiffened compression elements, respectively. The strain rates for these beam tests varied from 10^{-5} to 10^{-2} in./in./sec..

In Chapter II, the experimental investigation of beam specimens is discussed in detail. The test data of beam specimens fabricated from two types of sheet steels (35XF and 50XF) are evaluated in Chapter III. Finally, the results of beam tests are summrized in Chaper IV.

II. EXPERIMENTAL INVESTIGATION OF BEAM SPECIMENS

A. GENERAL

The research project sponsored by the American Iron and Steel Institute (AISI) at University of Missouri-Rolla has been concentrated on a study of the effect of strain rate on mechanical properties of sheet steels and the structural behavior and strength of cold-formed steel members subjected to dynamic loads. The objective of this experimental investigation was to study whether the available effective design formulas using dynamic material properties can be adequately used for the design of structural members subjected to dynamic loads.

The materials used in this phase of the study were 35XF and 50XF sheet steels with nominal yield strengths equal to approximately 35 ksi to 50 ksi, respectively. A total of 15 hat-shaped beams were fabricated from 35XF sheet steel and 15 hat-shaped beams were fabricated from 50XF sheet steel. These specimens were tested to study the strength of stiffened elements. For the strength of unstiffened elements, 15 beam specimens using channel sections were fabricated from 35XF sheet steel and 15 beam specimens using channel sections were fabricated from 50XF sheet steel. These specimens were cold-formed to shape by Holloway Machine Company in Springfield, Missouri.

The configurations of beam specimens having stiffened and unstiffened elements are shown in Figures 2.1 and 2.2, respectively. The

designation of test specimens is presented in Table 2.1. Tables 2.2 to 2.5 show the specimen number, test speed, strain rate, w/t ratio, and full length of each individual test specimen. The strain rates used in the tests varied from 10^{-5} to 10^{-2} in./in./sec.. A total of 60 beam specimens were tested and are discussed in this study.

B. MATERIAL PROPERTIES

The sheet steels used to fabricate beam specimens are 35XF and 50XF. The mechanical properties of these two types of sheet steels were presented in the Eleventh and Twelfth Progress Reports. Tables 2.6 and 2.7 present the average values of mechanical properties including yield strength (F_y) in tension and compression, proportional limit (F_{pr}), tensile strength (F_u), and elongation in 2-inch gage length for 35XF and 50XF sheet steels tested under different strain rates. The nominal thicknesses of 35XF and 50XF sheet steels are 0.085 inch and 0.077 inch, respectively.

Figures 2.3 and 2.4 show comparisons of typical stress-strain relationships for the 35XF sheet steel subjected to longitudinal tension and compression under different strain rates of 10^{-4}, 10^{-2}, and 1.0 in./in./sec.. The typical stress-strain relationships for 50XF sheet steel under tension and compression are shown in Figures 2.5 and 2.6. Based on the material test results, empirical equations were derived and presented in the Twelfth Progress Report. The yield strength, tensile strength, and proportional limit were used to evaluate the strength of structural members.

C. BEAM TESTS FOR STIFFENED ELEMENTS

1. Specimens. Beam tests were used to study the local buckling and postbuckling strengths of compression elements. In order to investigate the behavior and strength of stiffened compression elements, the webs of hat-shaped beam specimens were designed to be fully effective without web crippling according to the AISI Specification[7]. The lengths of beam specimens were designed to be long enough to prevent shear lag effects.

Prior to April 1990, a total of 15 hat-shaped beam specimens fabricated from 35XF sheet steel have been tested and reported in the Thirteenth Progress Report[4]. These specimens have stiffened elements with w/t ratios ranging from 29.05 to 76.64. Since March 1991, a total of 15 hat-shaped beam specimens were fabricated from 50XF sheet steel and tested to study the local buckling and postbuckling strengths of stiffened elements with w/t ratios ranging from 26.28 to 66.08. Tables 2.8 and 2.9 give the span lengths and dimensions of beam test specimens fabricated from 35XF and 50XF sheet steels, respectively. Figure 2.7 shows the hat-shaped beam specimens used for beam tests.

As shown in Figure 2.8, T-sections were used in the tests at loading points (one-eighth of span length) to prevent web crippling failure. Six 1/4-in. dia., high strength bolts were used to connected each T-section to each web of beam specimens. Three aluminum bars were connected to the tension flanges at midspan and quarter points to prevent hat section from

opening. Additional aluminum bars were placed close to the bearing plates at both ends of beam specimens.

2. Strain Measurements. Twelve (12) foil strain gages were mounted on each individual hat-shaped beam specimen. The arrangements of strain gages are shown in Figure 2.9. Three paired strain gages (No. 1-2, 3-4, and 9-10) were mounted along the longitudinal centerline of compression flange. The paired strain gages (No. 3-4) were placed at midspan of beam specimens. The other two paired strain gages (No. 1-2 and 9-10) were placed at a distance equal to the overall width of the stiffened compression flange on each side of the midspan of specimens. The load-strain diagrams obtained from these three paired strain gages were used to determine the local buckling load by means of the modified strain reversal method, which is discussed in Reference 8.

Strain gages (No. 5 and 6) placed along both edges of stiffened compression flange were used to measure edge strains for determining the strain rate used in the test. Strain gages (No. 7 and 8) placed on the top of webs were used to study the distribution of compressive stress in the web. Strain gages (No. 11 and 12) placed along the edges of tension flanges were used to determine the yield moment of specimen and to study the shift of the neutral axis during the test.

3. Instrumentation and Test Procedure. All beam tests were performed by using the 880 Material Test System with a capacity of 110 kips located in the Engineering Reasearch Laboratory at University of

Missouri-Rolla. As shown in Figure 2.10, the MTS 880 automated test system consists of three components : the load frame, the control console, and the CAMAC (Computer Automated Measurement and Control) data acquisition. The main data acquisition module used in this system is a Kinetic Systems Model 4022 Transient Recorder. The unit has 64 simultaneously sampling input channels. The maximum rate to acquire test data for this unit is 25,000 sets of reading per second. For all tests, the maximum load range of 20 kips and the maximum stroke ranges of 2.5 or 1.0 inches were selected for the function generator of the test machine. The ramp time was programmed to have a constant speed in accordance with the calculated strain rate for each beam specimen.

Figure 2.11 shows the test setup for beam specimens. The beam was simply supported and the load was applied from the lower compression platen to the specimen. The tension flanges at both ends of the beam specimens are clamped to 4-inch wide bearing plates. Two wooden blocks were placed between beam webs at both ends of beam specimens. Two LVDT (Linear Variable Differential Transformer) were used at the midspan to measure the beam deflections and to check any rotation of beam specimens during the test. The applied load, actuator displacement, strains from 12 strain gage outputs, and the deflections from two LVDT outputs were recorded and stored in the CAMAC memory. After the data have been acquired, it was downloaded to the Data General MV-10000 Computer for analysis purpose.

4. Test Results. The failure mode of the beam specimens varies with the width-to-thickness ratio of the stiffened compression flange. The local buckling load can be detected based on the load-strain diagram obtained from the paired strain gages attached back to back along the longitudinal centerline of the stiffened flange. As shown in Figure 2.12, no local buckling occured in specimens with small w/t ratios. The local buckling occured in the elastic range for the specimens having large w/t ratios. After local buckling occurred in the test specimen, the stresses in the compression flange redistributed across the flange until edge stresses reached to the maximum. A typical local buckling pattern of the stiffened compression flange during the test is shown in Figure 2.13. For the specimen with a large w/t ratio, the typical load-strain relationship is shown in Figure 2.14.

Two typical load-displacement relationships are shown in Figures 2.15 to 2.16 for beam specimens fabricated from 35XF sheet steel and tested under different strain rates. The average w/t ratios of compression flanges and the strain rates used in the tests are indicated in each figure. Similarly, Figures 2.17 to 2.19 show typical load-displacement diagrams for hat-shaped beam specimens fabricated from 50XF sheet steel. Figure 2.20 shows the positions of the neutral axis determined from strain gage readings of a compact section (Specimen 3A0A). It can be seen that the neutral axis remained the same position as long as the stress in the cross section was in the elastic range. The neutral axis shifted away from the bottom flange when the tensile strain in the bottom flange of the hat-shaped beam exceeded its yield strain. The

load-deflection diagram can be obtained from the LVDT readouts. As expected, beam deflection increased linearly corresponding to the applied load in the early stage of tests. The nonlinear load-defection relationship was noted when (1) local buckling occured in the compression flange (specimens with medium or large w/t ratios) or (2) yield point reached in the tension flange (specimens with small w/t ratios). A constant speed was applied to the test specimen during the test. Similar to load-deflection relationship, the strain rate could not be retained constant when the specimen attained the aforementioned conditions. Therefore, the value of strain rate was defined by a linear protion of the slope of the strain-time curve. A typical strain-time diagram is shown in Figure 2.21. The tested critical load , yield load, and ultimate load for each beam specimen are presented in Chapter III.

D. BEAM TESTS FOR UNSTIFFENED ELEMENTS

1. Specimens. In this phase of experimental investigation, Beam specimens using channel sections made of 35XF and 50XF sheet steels were tested to study the local buckling and postbuckling strengths of unstiffened elements affected by strain rate. The webs of channel sections were designed to be fully effective without web crippling in accordance with the AISI Specification[7]. Figure 2.22 shows the cross section of beam test specimen. To prevent each channel specimen from lateral buckling, aluminum bars were used to connect two channel sections together to form the beam specimen. In order to reduce the influence of hole on the area of cross section, small-size, high strength bolts were used in the fabrication of beam specimens.

A total of 15 beam test specimens fabricated from 35XF sheet steel have been tested and reported in the Thirteenth Progress Report[4]. These specimens had unstiffened compression flanges with w/t ratios from 9.03 to 20.99. In addition, 15 beam specimens were fabricated from 50XF sheet steel and tested to study the local buckling and postbuckling strengths of unstiffened elements with w/t ratios ranging from 8.78 to 20.57 since March 1991. Tables 2.10 and 2.11 give the span lengths and dimensions of all beam specimens fabricated from 35XF and 50XF sheet steels, respectively.

2. Strain Measurements. Eight (8) foil strain gages were placed at midspan of each specimen. Two paired strain gages (No. 1-2 and 5-6) were mounted along the tips of unstiffened compression flanges for the purpose of determining the local buckling load. By using the modified strain reversal method[8], the critical local buckling load was obtained from load-strain relationships of these paired strain gages. Two strain gages (No. 3 and 4) were mounted on the supported edges of unstiffened compression flanges to measure the edge strains for determining the strain rate used for the test. The edge stresses of unstiffened compression flanges can be determined from these strain readings using the stress-strain diagram. Strain gages (No. 7 and 8) mounted along the edges of tension flanges were used to determine the yield load of the specimen and to study the shift of the neutral axis during the test. The locations of strain gages placed on beam specimens are shown in Figure 2.23.

3. Instrumentation and Test Procedure. The test setup for the beam specimens using channel sections is illustrated in Figure 2.24. The instrumentation and the test procedure used for this phase of study are the same as that used for the hat-shaped beam tests described in Section C, except that two 4-in. wide bearing plates were placed on the top of compression flanges at the location of one-eighth span length (loading points) from end supports. The tension flanges at both ends of the beam specimens are clamped to 4-in. wide bearing plates, and two wooden blocks were placed between the webs of two channel sections at each end of beam specimens. Same as hat-shaped beam specimens, two LVDT were used to measure the beam deflections and to monitor any rotation of beam specimens during the test.

Load range 3 with a maximum load equal to 20 kips and stroke range 3 with a maximum displacement equal to 1.0 in. were selected for the function generator of the 880 MTS test machine. To achieve a constant-speed test, the ramp time was programmed in accordance with the calculated strain rate for each beam specimen. The strain rates for all tests ranged from 10^{-5} to 10^{-2} in./in./sec..

4. Test Results. Similar to the beam tests for the study of stiffened compression elements, no local buckling occured in the unstiffened compression flanges of the specimens with small w/t ratios. For specimens fabricated from 35XF sheet steel with medium w/t ratios, the unstiffened flanges buckled locally in the inelastic range. The local buckling occured in the elastic range for specimens fabricated from 35XF

sheet steel with large w/t ratios and specimens fabricated from 50XF sheet steel with medium and large w/t ratios. Typical load-strain relationships for the specimens with large w/t ratios is shown in Figure 2.25.

The failure mode of the beam specimens varies with the w/t ratio of unstiffened compression flanges. For most of the specimens with small w/t ratios and some of the specimens with medium w/t ratios, the top compression flanges near loading plates buckled as specimens reached the maximum loads. For the specimens with large w/t ratios, local buckling occured at the location between two loading points as expected. Figure 2.26 shows the typical failure for the channel beam with a large w/t ratio. Three typical load-displacement relationships are shown in Figures 2.27 to 2.29 for beam specimens fabricated from 35XF sheet steel and tested under different strain rates. The average w/t ratio of unstiffened compression elements and strain rates used in the tests are indicated in each figure. Similarly, Figures 2.30 to 2.32 show three typical load-displacement curves for beam specimens fabricated from 50XF sheet steel. A typical strain-time curve for the medium strain rate is shown in Figure 2.33. The tested critical load and yield load for each beam specimen are presented and evaluated in Chapter III.

III. EVALUATION OF EXPERIMENTAL DATA

A. GENERAL

Two types of beam specimens were tested to study the stiffened and unstiffened compression elements subjected to dynamic loads. The width-to-thickness ratio of stiffened and unstiffened elements controls the failure mode of the beam. Since the material properties and stress-strain relationships can be influenced by strain rate, comparisons between the experimental results and the failure loads predicted by the current AISI Automotive Steel Design Manual[1] using static and dynamic material properties are presented in this chapter. In order to consider the effect of cold-work on the strength of beams, comparisions are also made between the test results and the predicted loads for compact sections.

B. BEAM TESTS FOR THE STUDY OF STIFFENED ELEMENTS

Hat-shaped beam specimens fabricated from 35XF and 50XF sheet steels were tested for studying the postbuckling strength of stiffened compression elements. All beam specimens were subjected to pure moments between two loading points located at one-eighth of span length from end supports. The weight of test beam specimen and the cross beam placed on the top of the specimen are light enough (approximate 70 lbs.) to be neglected in the evaluation of test results. The compressive yield stress obtained from material tests was used for calculating the critical local buckling moment (M_{cr}) and the tested tensile stress was used to evaluate

the yield moment (M_y) and the the ultimate moment (M_u) for all beam specimens.

1. Critical Local Buckling Strength. The compression element of beam specimens may buckle locally in the elastic or inelastic range, depending on the w/t ratio of the compression element. The elastic critical local buckling stress, $(f_{cr})_E$, of stiffened compression elements subjected to a uniform compression can be calculated by using Equation 3.1 which is derived from Bryan's differential equation based on small deflection.

$$(f_{cr})_E = \frac{k\pi^2 E}{12(1-\mu^2)(w/t)^2} . \qquad (3.1)$$

where E = modulus of elasticity

μ = Poisson's ratio = 0.3 for steel

k = buckling coefficient

t = thickness of element

w = width of element

If the critical buckling stress exceeds the proportional limit, the compression element buckles in the inelastic range. Therefore, the concept of tangent modulus[9] can be applied to calculate the inelastic buckling stress, $(f_{cr})_I$, by using Equation 3.2.

$$(f_{cr})_I = F_y - \frac{F_{pr}(F_y - F_{pr})}{(f_{cr})_E} \qquad (3.2)$$

where F_y = compressive yield stress of steel

F_{pr} = proportional limit of steel

$(f_{cr})_E$ = elastic critical local buckling stress

The critical local buckling moment ($(M_{cr})_{comp}$) of a beam can be predicted by using Equation 3.3. The buckling cofficient used to compute the critical buckling stress, f_{cr}, ($(f_{cr})_E$ or $(f_{cr})_I$) in Equation 3.3 is equal to 4.0 for stiffened compression elements supported along both longitudinal edges. Consequently, the computed critical buckling moment can be calculated as follows :

$$(M_{cr})_{comp} = S_{xc} f_{cr} \qquad (3.3)$$

where f_{cr} = critical buckling stress

S_{xc} = elastic section modulus of the full cross section relative to the compression flange

The tested critical buckling moments of beam specimens were determined from the product of the bending arm (L/8) and one half of the tested critical buckling load ($P_{cr}/2$) as follows :

$$(M_{cr})_{test} = \frac{P_{cr} L}{16} \qquad (3.4)$$

where P_{cr} = tested critical buckling load

L = span length of beam specimen

The computed critical moments determined from Equation 3.3 and the tested critical moments obtained from Equation 3.4 are presented in Tables 3.1 and 3.2 for 35XF and 50XF sheet steels, respectively. The tested critical local buckling loads ($(P_{cr})_{test}$) listed in column (3) of Tables 3.1 and 3.2 were determined from load-strain relationships by using the modified strain reversal method. The computed local buckling moments listed in column (4) of Tables 3.1 and 3.2 were calculated on the basis of dynamic material properties.

From load-strain relationships of beam specimens, it can be observed that no local buckling occured in the specimens with small w/t ratios for both sheet steels. The comparisons of computed and tested local critical moments are listed in column (6) of Tables 3.1 and 3.2. The mean values of $(M_{cr})_{test}/(M_{cr})_{comp}$ ratios for specimens fabricated from 35XF and 50XF sheet steels are 1.076 and 0.977 with standard deviations of 0.066 and 0.109, respectively. Similar to the results of stub-column tests presented in the Fifteenth Progress Report[6], it seems that the computed buckling moments for hat-shaped beams fabricated from 50XF sheet steel are slightly less conservative than the beams fabricated from 35XF sheet steel. It was noted that the number of half sine waves developed in the stiffened compression flanges of the specimens having large w/t ratios is the same for all tests regardless of the strain rate used for the test.

2. Ultimate Flexural Strength. According to the AISI Specification[7], two methods can be used to calculate the ultimate strength of beams. One is based on the initiation of yielding using the effective

section and the other is based on the inelastic reserve capacity. The concept of the effective width design can be used to calculate the effective section properties.

(a) Effective Width Formulas. According to the AISI Automotive Steel Design Manual[1], the effective design width of compression elements can be used for determining the load-carrying capacity of the member when the slenderness factor λ exceeds a value of 0.673.

$$\lambda = 1.052\left[\frac{w}{t}\right]\frac{\sqrt{\frac{f}{E}}}{\sqrt{k}} \qquad (3.5)$$

where f = stress in the element

E = modulus of elasticity of the steel, 29500 ksi

k = buckling coefficient for the flat plate

w = flat width of the element

t = thickness of the element

Equation 3.5 with $f = F_y$ is valid for materials with yield strengths up to F_y = 80 ksi. For stiffened compression elements with a higher yield strength, a recent research[10] suggests that a reduced yield strength be substituted for the limiting value of f in Equation 3.5 and in all subsequent calculations to determine the bending capacity of the member. The reduced yield strength for a stiffened compression element, F_{yrs}, is obtained as follows :

$$F_{yrs} = \left[1.0 - 0.2\sqrt{\frac{w}{t}}\sqrt{\frac{F_y}{E}}\right]F_y \qquad (3.6)$$

The above expression was obtained from tests with w/t ratios ranging from 18 to 137, F_y values ranging from 84 to 153 ksi, and $\sqrt{w/t}\sqrt{F_y/E}$ values from 0.27 to 0.84.

At $\lambda \leq 0.673$, the limit width-thickness ratio (at which full capacity is achievable) can be evaluated as

$$\left[\frac{w}{t}\right]_{lim} = 0.64\sqrt{\frac{kE}{f}} \qquad (3.7)$$

For fully stiffened compression elements under uniform stress, k = 4, which gives a limiting w/t value as follows[1] :

$$\left[\frac{w}{t}\right]_{lim} = S = 1.28\sqrt{\frac{E}{f}} \qquad (3.8)$$

For w/t exceeding the value S, the effective width, b, is less than the actual width w. For the purpose of calculating of sectional properties, the effective width is divided into two parts and each half is positioned adjacent to each stiffening element. Thus the width (w-b) is considered to be removed at the center of the flat width when evaluating the section properties. The value of b is calculated from the 1986 AISI Automotive Steel Design Manual[1] given in Equation 3.9 as follows :

$$b = w\left[\frac{1 - \frac{0.22}{\lambda}}{\lambda}\right] \qquad (3.9)$$

The current effective width formulas for the stiffened and unstiffened compression elements used in the AISI Cold-Formed Steel Design Manual[7] are listed in Appendix A.

(b) Yield Flexural Strength. Based on the initiation of yield in the effective section, the computed yield moment ($(M_y)_{comp}$) of a beam can be calculated by using the following equation :

$$(M_y)_{comp} = F_y S_e \qquad (3.10)$$

where F_y = static or dynamic yield stress of steel

S_e = elastic section modulus of effective section

The computed yield moment was determined on the basis of the effective design width formulas (Equations 3.9) with the extreme compression or tension stress at yield point (F_y). The tested yield moments of beam specimens were determined from the product of bending arm (L/8) and one half of the yield load ($P_y/2$) as follows :

$$(M_y)_{test} = \frac{P_y L}{16} \qquad (3.11)$$

The tested yield load (F_y) shown above was determined from the load-strain relationship for each individual specimen. Tables 3.3(a) and 3.3(b) compare the computed and tested yield moments for 35XF sheet steel. Similarly, Tables 3.4(a) and 3.5(b) present the values for 50XF sheet steel. The computed yield moments listed in column (4) of Tables 3.3(a) and 3.4(a) are based on the static tensile yield stresses, while the values listed in column (4) of Tables 3.3(b) and 3.4(b) are based on the dynamic tensile stresses corresponding to the strain rate used in the

test. The tested yield moments are listed in Column (5) of Tables 3.3 and 3.4.

Comparisons of the computed yield moments based on the static yield stresses and the tested yield moments are listed in column (6) of Tables 3.3(a) and 3.4(a). The mean values of $(M_y)_{test}/(M_y)_{comp}$ ratios for the hat-spaped sections made of 35XF and 50XF sheet steels are 1.321 and 1.057 with standard deviations of 0.148 and 0.126, respectively. Comparsions of computed yield moments based on the dynamic yield stresses and the tested yield moments are listed in column (6) of Tables 3.3(b) and 3.4(b). The mean values and standard deviations of $(M_y)_{test}/(M_y)_{comp}$ ratios are (1.237 and 0.102) for 35XF sheet steel and (1.028 and 0.117) for 50XF sheet steel.

As expected, the ratios of tested to computed yield moments listed in Tables 3.3(a) and 3.4(a) are larger than those listed in Tables 3.3(b) and 3.4(b), because the latter table takes into account the effect of strain rate on yield stress. It is noted that all computed yield moments are lower than the tested yield moments for using 35XF sheet steel. However for using 50XF sheet steel, some computed yield moments are higher than the tested yield moments. It is also noted from those tables that the tested yield moment increases with strain rate for specimens having the same w/t ratios.

It has been recognized that cold-forming operation increases the yield stress and tensile strength of the steel particularly in the corners

of cross sections. In order to consider the effect of cold-work on the bending strength of the beam, comparisons are made between the tested and computed yield moments for beam specimens with small w/t ratios (compact section). According to the AISI Cold-Formed Steel Design Manual[7], the strength of a compact section (i.e. $\rho = 1$) including the cold work of forming may be determined by substituting F_{ya} for F_y as follows when $F_{uv}/F_{yv}>1.2$, $R/t<7$, and minimum included angle$< 120°$:

$$F_{ya} = CF_{yc} + (1-C)F_{yf} \tag{3.12}$$

where

F_{ya} = Average tensile yield stress of the beam flange.

C = Ratio of the total corner cross-sectional area of the controlling flange to the full cross-sectional area of the controlling flange.

F_{yf} = Weighted average tensile yield stress of flat portions.

$F_{yc} = B_c F_{yv}/(R/t)^m$, tensile yield stress of corners. (3.13)

$B_c = 3.69(F_{uv}/F_{yv})-0.819(F_{uv}/F_{yv})^2 -1.79$ (3.14)

$m = 0.192(F_{uv}/F_{yv})-0.068$ (3.15)

R = Inside bend radius.

F_{yv} = Tensile yield stress of virgin steel.

F_{uv} = Ultimate tensile strength of virgin steel.

The computed yield moments for Specimen series 3A considering cold-work of forming and tested yield moments are presented in the lower portions of Tables 3.3(a) and 3.3(b) for hat-shaped beam specimens

fabricated from 35XF sheet steel. The mean values and standard deviations are based on 5 beam specimens. These two tables indicate the improvements of computed yield moments when cold-work of forming was considered. However, in Tables 3.4(a) and 3.4(b), the effect of cold-work of forming was not considered for the computed yield moments for the beam specimens fabricated from 50XF sheet steel, because the average tensile yield stress of the beam flange computed from Equation 3.12 was found to be unusually large as a result of large ratios C and F_{uv}/F_{yv}.

(c) Inelastic Reserve Capacity. The inelastic reserve capacity of flexural members, which allows partial yielding of a cross section, is recognized in the current AISI Automotive Steel Design Manual[1]. It can be used to predict the ultimate moments of flexural members provided that such members satisfy the specific requirements. The ultimate strengths of hat sections or track sections with yielded tension flanges may be calculated on the basis of inelastic reserve capacity. According to AISI Specification[7], the inelastic flexural reserve capacity may be used when the following conditions are met :

(1) The member is not subject to twisting or to lateral, torsional, or torsional-flexural buckling.

(2) The effect of cold forming is not included in determining the yield point F_y.

(3) The ratio of the depth of the compressed potion of the web to its thickness does not exceed λ_1(Equation 3.19).

(4) The shear force does not exceed $0.35F_y$ times the web area (hxt).

(5) The angle between any web and the vertical does not exceed 30 degrees.

Figure 3.1 shows the stress distribution in sections with yielded tension flanges at ultimate moment. The inelastic stress distribution in the cross section depends on the maximum strain in the compression flange. The following equations can be used to compute the values of y_c, y_t, y_p, and y_{tp} shown in Figure 3.1 and the ultimate moment, M_u. For the purpose of simplicity, midline dimensions were used in the calculations[12].

$$y_c = \frac{b_t - b_c + 2d}{4} \tag{3.16a}$$

$$y_t = d - y_c \tag{3.16b}$$

$$y_p = \frac{y_c}{C_y} \tag{3.16c}$$

$$y_{cp} = y_c - y_p \tag{3.16d}$$

$$y_{tp} = y_t - y_p \tag{3.16e}$$

$$M_u = F_y t\left[b_c y_c + 2y_{cp}(y_p + \frac{y_{cp}}{2}) + \frac{4}{3}(y_p)^2 + 2y_{tp}(y_p + \frac{y_{tp}}{2}) + b_t y_t\right] \tag{3.17}$$

where b_c = effective width of the compression flange

b_t = total width of the tension flange

d = depth of the section

t = thickness of the section

C_y = compression strain factor for stiffened compression elements without intermediate stiffeners, which can be determined as follows :

$$C_y = 3 \qquad \text{for} \quad w/t \leq \lambda_1 \qquad (3.18a)$$

$$C_y = 3 - 2\left(\frac{w/t - \lambda_1}{\lambda_2 - \lambda_1}\right) \qquad \text{for} \quad \lambda_1 < w/t < \lambda_2 \qquad (3.18b)$$

$$C_y = 1 \qquad \text{for} \quad w/t \geq \lambda_2 \qquad (3.18c)$$

where $$\lambda_1 = \frac{1.11}{\sqrt{F_y/E}} \qquad (3.19)$$

$$\lambda_2 = \frac{1.28}{\sqrt{F_y/E}} \qquad (3.20)$$

According to the AISI Automotive Steel Design Manual[1], The computed ultimate moments obtained from Equation 3.17 should not exceed the limit of 1.25 $S_e F_y$. The tested ultimate moments of beam specimens were determined from the product of bending arm (L/8) and one half of the ultimate load ($P_u/2$) as follows :

$$(M_u)_{test} = \frac{P_u L}{16} \qquad (3.21)$$

Tables 3.5(a) and 3.5(b) present the computed ultimate moments computed from Equation 3.17 and the tested umtimate moments obtained from the tests for 35XF sheet steel. Tables 3.6(a) and 3.6(b) present the similar values for 50XF sheet steel. Similar to Tables 3.3 and 3.4, Tables 3.5(a) and 3.6(a) use static tensile stresses while Tables 3.5(b)

and 3.6(b) use dynamic yield stresses corresponding to the strain rate used in the test. The tested ultimate loads are listed in column (3) of Tables of 3.5 and 3.6. Comparsions of the computed ultimate moments based on the static yield stresses and the tested ultimate moments are listed in Column (6) of Tables 3.5(a) and 3.6(a). The mean value of $(M_u)_{test}/(M_u)_{comp}$ ratios for hat-shaped sections made of 35XF and 50XF sheet steels are 1.270 and 1.063 with standard deviations of 0.198 and 0.075, respectively. Comparisons between the computed ultimate moments based on the dynamic yield stresses and the tested ultimate moments are listed in column (6) of Tables of 3.5(b) and 3.6(b). The mean values and standard deviations of $(M_u)_{test}/(M_u)_{comp}$ ratios are (1.191 and 0.169) for using 35XF sheet steel and (1.036 and 0.063) for using 50XF sheet steel.

It is noted from column (6) of these tables that the ratio of the tested ultimate moment to the computed ultimate moment decreases with increasing w/t ratio. Figure 3.2 shows graphically a typical moment-displacement diagram for the beam specimen. The computed critical moment($(M_{cr})_{comp}$), yield moment($(M_y)_{comp}$), and ultimate moment($(M_u)_{comp}$) are marked in this figure for the purpose of comparison. It can be seen from Figure 3.2 that for Specimen 3B1A the critical buckling moment is greater than the yield moment. This is because the stress in the compression flange at the initiation of yielding is less than the critical local buckling stress as shown in Figure 3.3(b). The critical local buckling moment was calculated according to the stress distribution shown in Figure 3.3(c) and assuming that the strain diagram is linear.

Figure 3.4 shows the load-strain diagrams of a hat-shaped beam specimen 3A1AX using 50XF sheet steel. The curves shown in Figure 3.4(a) are drawn from the readings of paired strain gages (5 and 6) mounted on the compression flange of the beam. The readings of the paired strain gages (11 and 12) mounted on the tension flanges of the beam are shown in Figure 3.4(b). It can be seen that the bottom flanges of the hat-shaped beam reached the yield point first, because the neutral axis is close to the top flange. By comparing Figure 3.4 with the results obtained from the material tests as shown in Figures 2.5 and 2.6, It is noted that the strains of the beam specimen remained in the plastic range as the beam specimen reached its maximum capacity. Figure 3.5 shows the similar plots for the specimen 3C1B using 35XF sheet steel.

Figures 3.6 and 3.7 show graphically the effect of strain rate on the ratios of the tested ultimate moment to the computed ultimate moment obtained from Tables 3.5(a) and 3.5(b), respectively. Similarly, Figures 3.8 and 3.9 show the strain rates vs. the ratios of the tested ultimate moment to the computed ultimate moment obtained from Tables 3.6(a) and 3.6(b). Tables 3.7 and 3.8 list the average tested ultimate moments for beam specimens with stiffened flanges using 35XF and 50XF sheet steels, respectively. Each value given in Tables 3.7 and 3.8 and each point shown in Figures 3.6 through 3.9 is the average of two values obtained from two similar tests.

By comparing the mean values and standard deviations of $(M_u)_{test}/(M_u)_{comp}$ ratios listed in Tables 3.5(a) and 3.6(a) with those

listed in Tables 3.5(b) and 3.6(b), it can be seen that the computed ultimate moments using dynamic yield stresses are better than the computed ultimate moments using static stresses. Similar to the results of stub-column specimens for studying stiffened elements reported in the Fifteenth Propress Report[6], all computed ultimate moments are lower than the tested ultimate moments for using 35XF sheet steel. However for using 50XF sheet steel, some computed ultimate moments are higher than the tested ultimate moments. Therefore, the prediction of ultimate moments for hat-shaped beams fabricated from 50XF sheet steel were found to be less conservative than the beams fabricated from 35XF sheet steel. It is also noted from Tables 3.7 and 3.8 that the tested ultimate moment increases with strain rate for specimens having the same w/t ratios.

C. BEAM TESTS FOR THE STUDY OF UNSTIFFENED ELEMENTS

Beam specimens using channel sections fabricated from 35XF and 50XF sheet steels were tested for studying the postbuckling strength of unstiffened elements. All beam specimens were subjected to pure moments between two loading points located at one-eighth span length from end supports. As mention in Chapter III, the webs of specimens were designed to be fully effective. Lateral-torsional buckling of channel beams was prevented by using lateral supports provided by aluminum angles connected to the top and bottom flanges. The weights of test beam and the cross beam placed on the top of the specimen (approximate 70 lbs.) are small as compared to the ultimate loads and were neglected in the evaluation of test results. The compressive yield stress obtained from material tests was used for calculating the critical local buckling load (P_{cr}) and

the tensile stress was used to evaluate the yield moment (M_y) for all specimens.

1. Critical Local Buckling Strength. Like stiffened elements, unstiffened elements of beams may buckle locally in the elastic or inelastic range, depending on the w/t ratio of the compression element. The critical local buckling stress (f_{cr}) can be computed by using Equation 3.1 or Equation 3.2 for the unstiffened element subjected to a uniform compressive stress. The value of buckling coefficient (k) used to calculate the critical buckling stress is 0.43 in this phase of study. The critical local buckling moment ($(M_{cr})_{comp}$) can be predicted by using Equation 3.3.

The computed and tested critical local buckling moments of beam specimens are given in Tables 3.9 and 3.10 for 35XF and 50XF sheet steels, respectively. The tested critical local buckling loads listed in column (3) of Tables 3.9 and 3.10 were determined from load-strain diagrams by using the modified strain reversal method. The computed critical local buckling moments listed in those Tables were calculated on the basis of the dynamic material properties. The values given in column (2) of Tables 3.9 and 3.10 are the average values of two critical local buckling stresses of unstiffened compression flanges of beams.

It was noted that no local buckling occured in the specimens with small and medium w/t ratios for 35XF sheet steel, and the specimens with small w/t ratios for 50XF sheet steel. All tested critical buckling

moments are greater than the computed critical local buckling moments. This is because that a value of 0.43 was used as the buckling coefficient for unstiffened compression flanges ignoring any effect of rotational edge restraint provided by the adjoining webs.

Column (6) of Tables 3.9 and 3.10 show the comparisons between the computed and tested critical local buckling moments. The mean values of $(M_{cr})_{test}/(M_{cr})_{comp}$ ratios for using 35XF and 50XF sheet steels are 1.405 and 1.211 with standard deviations of 0.060 and 0.147, respectively. Similar to the results of hat-shaped beam tests, it seems that the computed buckling moments for specimens fabricated from 50XF sheet steel are less conservative than specimens fabricated from 35XF sheet steel.

2. Ulatimate Flexural Strength. It is assumed that a channel beam reaches its ultimate section strength when the maximum edge stress in the compression flanges reaches the yield stress of steel. The ultimate section strengths of all channel beams can be calculated by using Equation 3.10. The effective width formulas (Equations 3.9) can be applied for the calculation of the elastic section modulus of the effective section to be used in Equation 3.10. A buckling coefficient of 0.43 was used to calculate the effective width of an unstiffened compression element. Therefore, the limit of w/t ratio $((w/t)_{lim})$ for the unstiffened compression elements will be expressed as follows :

$$\left[\frac{w}{t}\right]_{lim} = 0.42\sqrt{\frac{E}{f}} \qquad (3.22)$$

Similar to the stiffened compression elements, the AISI Automotive Steel Design Manual[1] suggests that a reduced yield strength should be substituted for the limiting value of f in all calculations to determine the ultimate moment of the beam having unstiffened compression elements with a yield strength greater than 80 ksi. The reduced yield strength for an unstiffened compression element, F_{yru}, is obtained as follows :

$$F_{yru} = \left[1.079 - 0.6\sqrt{\frac{w}{t}}\sqrt{\frac{F_y}{E}} \right] F_y \leq F_y \qquad (3.23)$$

This expression was obtained from the tests with w/t ratios from 5.6 to 53, F_y values ranging from 84 to 153 ksi, and $\sqrt{w/t}\sqrt{F_y/E}$ values from 0.13 to 0.53.

The computed and tested ultimate moments of channel beams fabricated from 35XF sheet steel are given in Tables 3.11(a) and 3.11(b). Tables 3.12(a) and 3.12(b) present the similar values for using 50XF sheet steel. The computed ultimate moments based on the static tensile yield stresses are given in column (4) of Tables 3.11(a) and 3.12(a), while the computed ultimate moments based on dynamic tensile yield stresses are given in Tables 3.11(b) and 3.12(b). The computed ultimate moments ($(M_y)_{comp}$) listed in those tables were calculated by using Equation 3.10. The tested ultimate moments listed in those tables were determined from the product of bending arm (L/8) and one half of the tested failure load as given in Equation 3.11. Comparisons of computed ultimate moments based on the static yield stresses and the tested ultimate moments are listed in column (6) of Tables 3.11(a) and 3.12(a) for 35XF and 50XF sheet steels, respectively. The mean values of $(M_u)_{test}/(M_y)_{comp}$ ratios listed in

Tables 3.11(a) and 4.12(a) are 1.299 and 1.121 with standard deviations of 0.096 and 0.040, respectively. The values listed in column (6) of Tables 3.11(b) and 3.12(b) are comparisons between the computed ultimate moments based on the dynamic yield stresses and the tested ultimate moments. The mean values and standard deviations of $(M_u)_{test}/(M_y)_{comp}$ ratios are (1.228, 0.052) for using 35XF sheet steel and (1.094, 0.026) for using 50XF sheet steel.

For the purpose of comparison, Figures 3.10 and 3.11 show graphically the effect of strain rate on the ratios of the tested ultimate moment to the computed ultimate moment obtained from Tables 3.11(a) and 4.11(b). Similarly, Figures 3.12 and 3.13 show the strain rates vs. the ratios of the tested ultimate moment to the computed ultimate moment obtained from Tables 3.12(a) and 3.12(b). The horizontal axis represents logarithmic strain rate while the vertical axis represents the ratio of the tested ultimate moment to the computed ultimate moment. The tests performed at strain rate of 10^{-4} in./in./sec. are considered to be the static loading conditions. Tables 3.13 and 3.14 list average failure moments for beam specimens using 35XF and 50XF sheet steels, respectively. Each value listed in Tables 3.13 and 3.14 and each point shown in Figures 3.10 through 3.13 is the average of two values obtained from similar tests.

For Specimen series 4A (specimens with small w/t ratios), the computed ultimate moments considered cold-work of forming and tested ultimate moments are presented in the lower portions of Tables 3.11(a) and 3.11(b) for channel beams fabricated from 35XF sheet steel. The lower

portions of Tables 3.12(a) and 3.12(b) present the similar data for beam specimens fabricated from 50XF sheet steel. The mean values and standard deviations listed in the lower portions of Tables 3.11 and 3.12 are based on 5 beam specimens. It can seen that the computed yield moments can be improved by considering cold-work of forming.

From Tables 3.11 and 3.12, it can be seen that the computed ultimate moments using the dynamic yield stresses are better than the computed ultimate moments using the static yield stresses. A better prediction of ultimate moments can be obtained by considering the cold work effect for specimens with small w/t ratios. Similar to the results for studying hat-shaped beams, the computed ultimate moments for channel beams fabricated from 50XF sheet steel are less conservative than the beams fabricated from 35XF sheet steel. It is observed from Tables 3.13 and 3.14 that the tested ultimate moment increases with strain rate for specimens having the same w/t ratios.

D. DEFLECTION OF BEAM SPECIMENS

As shown in Figure 3.14, the deflection (d) of beam specimen was measured by placing two LVDTs (Linear Variable Differential Transformer) at midspan. The measured deflection under service moment which was considered to be 60% of the computed yield moment was obtained from the moment-deflection relationship. The computed deflection ($(d)_{comp}$) was calculated by using the following theoretical deflection equation :

$$(d)_{comp} = \frac{9M_s L^2}{128EI_e} \qquad (3.24)$$

where E = modulus of elasticity

I_e = effective moment of inertia under service moment

L = span length of beam

M_s = service moment

For studying the hat-shaped beam specimens, Equations A-5 and A-6 (Procedure II) listed in Appendix A were used to calculate the effective moment of inertia, while Procedure I was used to calculate the effective moment of inertia for channel beam specimens.

Tables 3.15 and 3.16 compare the deflections calculated from Equation 3.24 and the tested deflections measured from the LVDT reading under service moment for hat-shaped beam specimens fabricated from 35XF and 50XF sheet steels, respectively. Similarly, Tables 3.17 and 3.18 show the comparison of computed and tested deflections for the channel beam specimens fabricate from 35XF and 50XF sheet steels. The mean values and standard deviations are given in each table. It is noted that the values of the measured deflection are less than the values of computed deflection for most cases.

IV. CONCLUSIONS

To study the postbuckling strength of stiffened and unstiffened compression elements, two types of beam specimens fabricated from two sheet steels (35XF and 50XF sheet steels) were tested under different strain rates. Prior to April 1990, 15 hat-shaped beam specimens and 15 channel beam specimens fabricated from 35XF sheet steel were tested to study the strength of stiffened and unstiffened compression elements. The test results were presented in the Thirteenth Propress Report[4]. During the period from February through May 1991, 15 additional hat-shaped beams and 15 channel beams fabricated from 50XF sheet steel were also tested. The test results obtained from all beam tests are presented and evaluated in this report.

Based on the available test results, the following tentative conclusions may be drawn for the effect of strain rate on the strength of cold-formed steel beams fabricated from 35XF and 50XF sheet steels :

1. For most cases, the yield moment and ultimate moment of beam specimens fabricated from 35XF and 50XF sheet steels increase with increasing strain rate.
2. Better prediction can be obtained for the computed yield and ultimate moments using the dynamic yield stresses as compared with the computed yield and ultimate moments using the static yield stresses.

3. For beam specimens using hat sections and channels with small w/t ratios, a better prediction of yield moments can be achieved by considering the cold-work of forming except for the hat-shaped beam specimens fabricated from 50XF sheet steel.
4. The computed yield and ultimate moments based on the AISI Automotive Steel Design Manual[1] were found to be conservative for most beam tests.
5. From the beam tests using hat sections and channels, the computed moments for the beams fabricated from 50XF sheet steel were found to be less conservative than the beams fabricated from 35XF sheet steel.
6. It was found that the computed ultimate moments of beam specimens having stiffened flanges are less conservative than the beam specimens with unstiffened flanges by using the current design criteria.
7. The computed midspan deflections under service moments are larger than the deflections measured from tests for most cases.

ACKNOWLEDGMENTS

The research work reported herein was conducted in the Department of Civil Engineering at the University of Missouri-Rolla under the sponsorship of the American Iron and Steel Institute.

The financial assistance granted by the Institute and the technical guidance provided by members of the Task Force on Automotive Structural Design and the AISI Automotive Applications Committee and the AISI staff are gratefully acknowledged. These members are: Messrs. S. J. Errera (Chairman), J. Borchelt, R. Cary, J. D. Harrington, F. L. Cheng, A. M. Davies, J. D. Grozier, C. Haddad, C. S. Jayanth, A. L. Johnson, C. M. Kim, R. W. Lautensleger, J. P. Leach, K. H. Lin, J. N. Macadam, H. Mahmood, D. Malen, J. McDermott, J. G. Schroth, P. G. Schurter, T. N. Seel, M. F. Shi, M. Sheh, and M. T. Vecchio. An expression of thanks is also due to Mr. D. L. Douty for his help.

All materials used in the experimental study were donated by Inland Steel Company and LTV Steel Company.

Appreciation is expressed to Messrs. K. Haas, J. Bradshaw, F. Senter, and S. Gabel, staff of the Department of Civil Engineering, for their technical support and to Mr. M. Y. Shan for his valuable assistance in the preparation and performance of the tests. The advice provided by Dr. J. E. Minor, Chairman of the UMR Department of Civil Engineering, is greatly appreciated.

REFERENCES

1. American Iron and Steel Institute, Automotive Steel Design Manual , 1986 Edition, Revision 3 - February 1991.

2. Kassar, M. and Yu, W.W., "Design of Automotive Structural Components Using High Strength Sheet Steels: The Effect of Strain Rate on Mechanical Proporties of Sheet Steels", Eleventh Progress Report, Civil Engineering Study 89-2, University of Missouri-Rolla, January 1989.

3. Kassar, M. and Yu, W.W., "Design of Automotive Structural Components Using High Strength Sheet Steels: The Effect of Strain Rate on Compressive Mechanical Proporties of Sheet Steels", Twelfth Progress Report, Civil Engineering Study 89-3, University of Missouri-Rolla, August 1989.

4. Kassar, M. and Yu, W.W., "Design of Automotive Structural Components Using High Strength Sheet Steels: Structural Strengths of Cold-Formed Steel Members Under Dynamic Loads of Sheet Steels", Thirteenth Progress Report, Civil Engineering Study 90-1, University of Missouri-Rolla, May 1990.

5. Kassar, M. and Yu, W.W., "Design of Automotive Structural Components Using High Strength Sheet Steels: Effect of Strain Rate on Material Properties of Sheet Steels and Structural Strengths of Cold-Formed Steel Members", Fourteenth Progress Report, Civil Engineering Study 90-2, University of Missouri-Rolla, May 1990.

6. Pan, C.L. and Yu, W.W., "Design of Automotive Structural Components Using High Strength Sheet Steels: Structural Strength of Cold-Formed Steel Members Under Dynamic Loads", Fifteenth Progress Report, Civil Engineering Study 90-3, University of Missouri-Rolla, Nov. 1990.

7. American Iron & Steel Institute, Specification for the Design of Cold-Formed Steel Structural Members, 1986 Edition with the 1989 Addendum.

8. Johnson, A. L. and Winter, G., "The Structural Performance of Austenitic Stainless Steel Members," Report No. 327, Cornell University, Nov. 1966.

9. Bleich, F., Buckling Strength of Metal Structures, New York: McGraw-Hill Book Company, 1952.

10. Pan, L.C., "Effective Widths of High Strength Cold-Formed Steel Members", PhD Thesis, University of Missouri-Rolla, 1987.

11. American Iron & Steel Institute, Specification for the Design of Cold-Formed Steel Structural Members, September, 1980.

12. Yu, W. W., Cold-Formed Steel Design, New York: John Wiley & Sons Inc., 1991.

Table 2.1

Designation of Test Specimens Used in This Study

1st Digit	1st Letter	2nd Digit	2nd Letter
Section Type (Group)	w/t Ratio (Case)	Strain-Rate (in./in./sec.)	Test No.
3- Hat-Shaped Section for Beam Test	A- Small Ratio	0- 0.00001	A- 1st Test
	B- Medium Ratio	1- 0.0001	B- 2nd Test
4- Channel Section for Beam Test	C- Large Ratio	2- 0.01	

Note: The fifth character (X) in the designation of test specimens represents the specimen fabricated from 50XF sheet steel.

Table 2.2

Number of Performed Beam Tests
Hat Sections Having Stiffened Compression Flanges
(35XF Sheet Steel)

Spec.	Test Speed (in./min.)	Strain Rate (in./in./sec.)	w/t	Full Length (in.)	No. of Tests Performed
3A0A	0.023	0.00001	29.15	47.0	1
3A1A	0.23	0.0001	30.00	47.0	1
3A1B	0.23	0.0001	29.85	47.0	1
3A2A	23.0	0.01	29.05	47.0	1
3A2B	23.0	0.01	30.17	47.0	1
3B0A	0.038	0.00001	55.91	77.0	1
3B1A	0.38	0.0001	55.11	77.0	1
3B1B	0.38	0.0001	55.91	77.0	1
3B2A	38.0	0.01	55.82	77.0	1
3B2B	38.0	0.01	55.97	77.0	1
3C0A	0.15	0.00001	76.17	95.0	1
3C1A	1.50	0.0001	76.64	95.0	1
3C1B	1.50	0.0001	76.57	95.0	1
3C2A	150.0	0.01	76.62	95.0	1
3C2B	150.0	0.01	76.03	95.0	1

Table 2.3

Number of Performed Beam Tests
Hat Sections Having Stiffened Compression Flanges
(50XF Sheet Steel)

Spec.	Test Speed (in./min.)	Strain Rate (in./in./sec.)	w/t	Full Length (in.)	No. of Tests Performed
3A0AX	0.12	0.00001	26.28	41.0	1
3A1AX	1.20	0.0001	26.82	41.0	1
3A1BX	1.20	0.0001	26.79	41.0	1
3A2AX	120.0	0.01	26.82	41.0	1
3A2BX	120.0	0.01	26.71	41.0	1
3B0AX	0.20	0.00001	46.07	61.0	1
3B1AX	2.00	0.0001	46.10	61.0	1
3B1BX	2.00	0.0001	46.11	61.0	1
3B2AX	200.0	0.01	46.16	61.0	1
3B2BX	200.0	0.01	45.99	61.0	1
3C0AX	0.24	0.00001	66.08	71.0	1
3C1AX	2.40	0.0001	65.31	71.0	1
3C1BX	2.40	0.0001	66.07	71.0	1
3C2AX	240.0	0.01	66.08	71.0	1
3C2BX	240.0	0.01	65.31	71.0	1

Table 2.4

Number of Performed Beam Tests
Channel Sections Having Unstiffened Compression Flanges
(35XF Sheet Steel)

Spec.	Test Speed (in./min.)	Strain Rate (in./in./sec.)	w/t	Full Length (in.)	No. of Tests Performed
4A0A	0.043	0.00001	9.28	41.0	1
4A1A	0.43	0.0001	9.16	41.0	1
4A1B	0.43	0.0001	9.16	41.0	1
4A2A	43.0	0.01	9.22	41.0	1
4A2B	43.0	0.01	9.03	41.0	1
4B0A	0.045	0.00001	15.13	47.0	1
4B1A	0.45	0.0001	15.16	47.0	1
4B1B	0.45	0.0001	14.93	47.0	1
4B2A	45.0	0.01	15.04	47.0	1
4B2B	45.0	0.01	15.16	47.0	1
4C0A	0.082	0.00001	20.93	69.0	1
4C1A	0.82	0.0001	20.99	69.0	1
4C1B	0.82	0.0001	20.93	69.0	1
4C2A	82.0	0.01	20.99	69.0	1
4C2B	82.0	0.01	20.93	69.0	1

Table 2.5

Number of Performed Beam Tests
Channel Sections Having Unstiffened Compression Flanges
(50XF Sheet Steel)

Spec.	Test Speed (in./min.)	Strain Rate (in./in./sec.)	w/t	Full Length (in.)	No. of Tests Performed
4A0AX	0.075	0.00001	8.83	35.0	1
4A1AX	0.75	0.0001	8.78	35.0	1
4A1BX	0.75	0.0001	8.84	35.0	1
4A2AX	75.0	0.01	8.83	35.0	1
4A2BX	75.0	0.01	8.85	35.0	1
4B0AX	0.12	0.00001	15.28	45.0	1
4B1AX	1.20	0.0001	15.31	45.0	1
4B1BX	1.20	0.0001	15.31	45.0	1
4B2AX	120.0	0.01	15.39	45.0	1
4B2BX	120.0	0.01	15.35	45.0	1
4C0AX	0.17	0.00001	20.48	63.0	1
4C1AX	1.70	0.0001	20.48	63.0	1
4C1BX	1.70	0.0001	20.50	63.0	1
4C2AX	170.0	0.01	20.57	63.0	1
4C2BX	170.0	0.01	20.54	63.0	1

Table 2.6

Average Mechanical Properties of 35XF Sheet Steel Used in the Experimental Study Under Different Strain Rates

Strain Rate in./in./sec.	$(F_y)_c$ (ksi)	$(F_{pr})_c$ (ksi)	$(F_y)_t$ (ksi)	$(F_u)_t$ (ksi)	Elongation (%)
0.0001	29.83	17.79	32.87	49.35	38.90
0.01	31.92	20.03	36.40	51.76	36.80
1.0	36.91	*****	42.37	56.63	40.90

Table 2.7

Average Mechanical Properties of 50XF Sheet Steel Used in the Experimental Study Under Different Strain Rates

Strain Rate in./in./sec.	$(F_y)_c$ (ksi)	$(F_{pr})_c$ (ksi)	$(F_y)_t$ (ksi)	$(F_u)_t$ (ksi)	Elongation (%)
0.0001	49.68	38.64	49.50	72.97	31.00
0.01	52.51	40.05	51.60	74.87	27.00
1.0	54.79	*****	54.66	78.73	25.80

Notes:

1) $(F_y)_c$ and $(F_{pr})_c$ are based on longitudinal compression coupon tests.
2) $(F_y)_t$ and $(F_u)_t$ and Elongation are determined from longitudinal tension coupon tests.
3) Elongation was measured by using a 2-in. gage length.

Table 2.8

Dimensions of Beam Specimens with Stiffened Flanges
(35XF Sheet Steel)

Spec.	BC (in.)	D (in.)	BT (in.)	t (in.)	w/t	Span Length (in.)
3A0A	2.960	1.510	1.010	0.085	29.15	43.00
3A1A	3.033	1.462	1.012	0.085	30.00	43.00
3A1B	3.020	1.477	1.017	0.085	29.85	43.00
3A2A	2.952	1.515	1.020	0.085	29.05	43.00
3A2B	3.047	1.470	1.012	0.085	30.17	43.00
3B0A	5.235	2.445	1.235	0.085	55.91	73.00
3B1A	5.167	2.460	1.255	0.085	55.11	73.00
3B1B	5.235	2.435	1.230	0.085	55.91	73.00
3B2A	5.227	2.435	1.220	0.085	55.82	73.00
3B2B	5.240	2.440	1.232	0.085	55.97	73.00
3C0A	6.957	2.926	1.490	0.085	76.17	91.00
3C1A	6.997	2.947	1.483	0.085	76.64	91.00
3C1B	6.991	2.954	1.481	0.085	76.57	91.00
3C2A	6.995	2.934	1.483	0.085	76.62	91.00
3C2B	6.945	2.945	1.485	0.085	76.03	91.00

Note : * For symbols of dimensions, see Figure 2.7.
* The inside bend radius (R) is 0.15625 (5/32) in. for all specimens.

Table 2.9

Dimensions of Beam Specimens with Stiffened Flanges
(50XF Sheet Steel)

Spec.	BC (in.)	D (in.)	BT (in.)	t (in.)	w/t	Span Length (in.)
3A0AX	2.490	1.250	0.769	0.077	26.28	37.0
3A1AX	2.532	1.256	0.757	0.077	26.82	37.0
3A1BX	2.529	1.263	0.757	0.077	26.79	37.0
3A2AX	2.532	1.258	0.757	0.077	26.82	37.0
3A2BX	2.523	1.242	0.767	0.077	26.71	37.0
3B0AX	4.014	1.999	1.006	0.077	46.07	57.0
3B1AX	4.016	1.989	1.028	0.077	46.10	57.0
3B1BX	4.017	1.994	1.028	0.077	46.11	57.0
3B2AX	4.021	1.990	1.036	0.077	46.16	57.0
3B2BX	4.008	1.996	1.029	0.077	45.99	57.0
3C0AX	5.555	2.505	1.260	0.077	66.08	67.0
3C1AX	5.495	2.508	1.275	0.077	65.31	67.0
3C1BX	5.554	2.498	1.258	0.077	66.07	67.0
3C2AX	5.555	2.465	1.295	0.077	66.08	67.0
3C2BX	5.495	2.503	1.258	0.077	65.31	67.0

Note : * For symbols of dimensions, see Figure 2.7.
* The inside bend radius (R) is 0.15625 (5/32) in. for all specimens.

Table 2.10

Dimensions of Beam Specimens with Unstiffened Flanges
(35XF Sheet Steel)

Spec.	BC (in.)	D (in.)	t (in.)	w/t	Span Length (in.)
4A0A	1.030	2.020	0.085	9.28	37.00
4A1A	1.020	2.007	0.085	9.16	37.00
4A1B	1.020	2.025	0.085	9.16	37.00
4A2A	1.025	2.012	0.085	9.22	37.00
4A2B	1.009	2.020	0.085	9.03	37.00
4B0A	1.527	2.517	0.085	15.13	43.00
4B1A	1.530	2.510	0.085	15.16	43.00
4B1B	1.510	2.530	0.085	14.93	43.00
4B2A	1.520	2.520	0.085	15.04	43.00
4B2B	1.530	2.510	0.085	15.16	43.00
4C0A	2.020	3.020	0.085	20.93	65.00
4C1B	2.025	3.010	0.085	20.99	65.00
4C1C	2.020	3.010	0.085	20.93	65.00
4C2A	2.025	3.030	0.085	20.99	65.00
4C2B	2.020	3.020	0.085	20.93	65.00

Note : * For symbols of dimensions, see Figure 2.20.
* The inside bend radius (R) is 0.15625 (5/32) in. for all specimens.

Table 2.11

Dimensions of Beam Specimens with Unstiffened Flanges
(50XF Sheet Steel)

Spec.	BC (in.)	D (in.)	t (in.)	w/t	Span Length (in.)
4A0AX	0.913	1.999	0.077	8.83	31.0
4A1AX	0.909	2.008	0.077	8.78	31.0
4A1BX	0.914	2.001	0.077	8.84	31.0
4A2AX	0.913	2.005	0.077	8.83	31.0
4A2BX	0.915	1.995	0.077	8.85	31.0
4B0AX	1.410	2.267	0.077	15.28	41.0
4B1AX	1.412	2.279	0.077	15.31	41.0
4B1BX	1.412	2.289	0.077	15.31	41.0
4B2AX	1.418	2.263	0.077	15.39	41.0
4B2BX	1.415	2.273	0.077	15.35	41.0
4C0AX	1.810	2.756	0.077	20.48	59.0
4C1AX	1.810	2.763	0.077	20.48	59.0
4C1BX	1.812	2.755	0.077	20.50	59.0
4C2AX	1.817	2.756	0.077	20.57	59.0
4C2BX	1.815	2.760	0.077	20.54	59.0

Note : * For symbols of dimensions, see Figure 2.20.
* The inside bend radius (R) is 0.15625 (5/32) in. for all specimens.

Table 3.1

Comparison of Computed and Tested Critical Buckling Moments
Beam Specimens with a Stiffened Flange (Based on k=4.0)
(35XF Sheet Steel)

Spec.	S_{xc} ($in.^3$) (1)	f_{cr} (ksi) (2)	$(P_{cr})_{test}$ (kips) (3)	$(M_{cr})_{comp}$ (in.-kips) (4)	$(M_{cr})_{test}$ (in.-kips) (5)	(5)/(4) (6)
3A0A	0.342	28.12	N/A	9.62	N/A	N/A
3A1A	0.335	28.02	N/A	9.39	N/A	N/A
3A1B	0.338	28.04	N/A	9.48	N/A	N/A
3A2A	0.343	30.22	N/A	10.36	N/A	N/A
3A2B	0.338	30.09	N/A	10.17	N/A	N/A
3B0A	1.011	23.55	5.833	23.81	26.61	1.117
3B1A	1.010	23.73	6.214	23.97	28.35	1.183
3B1B	1.005	23.55	5.774	23.67	26.34	1.113
3B2A	1.003	25.66	6.106	25.74	27.86	1.082
3B2B	1.009	25.63	N/A	25.86	N/A	N/A
3C0A	1.615	18.38	5.042	29.68	28.68	0.966
3C1A	1.635	18.16	5.291	29.69	30.10	1.014
3C1B	1.638	18.19	5.217	29.79	29.67	0.996
3C2A	1.626	18.17	5.823	29.54	33.12	1.121
3C2B	1.624	18.45	5.760	29.96	32.76	1.093
Mean						1.076
Standard Deviation						0.066

Note: The dynamic compressive yield stress was used for calculating the critical local buckling moment ($(M_{cr})_{comp}$).

Table 3.2

Comparison of Computed and Tested Critical Buckling Moments
Beam Specimens with a Stiffened Flange (Based on k=4.0)
(50XF Sheet Steel)

Spec.	S_{xc} ($in.^3$) (1)	f_{cr} (ksi) (2)	$(P_{cr})_{test}$ (kips) (3)	$(M_{cr})_{comp}$ (in.-kips) (4)	$(M_{cr})_{test}$ (in.-kips) (5)	(5)/(4) (6)
3A0AX	0.206	45.70	N/A	9.41	N/A	N/A
3A1AX	0.209	46.80	N/A	9.80	N/A	N/A
3A1BX	0.211	46.81	N/A	9.86	N/A	N/A
3A2AX	0.210	49.14	N/A	10.31	N/A	N/A
3A2BX	0.206	49.17	N/A	10.14	N/A	N/A
3B0AX	0.570	40.81	5.57	23.25	19.84	0.853
3B1AX	0.568	41.18	5.79	23.40	20.63	0.882
3B1BX	0.570	41.18	6.03	23.48	21.48	0.915
3B2AX	0.570	42.54	5.76	24.24	20.52	0.847
3B2BX	0.570	42.61	6.11	24.29	21.78	0.897
3C0AX	1.002	24.42	6.68	24.47	27.97	1.143
3C1AX	0.996	25.01	6.28	24.92	26.29	1.055
3C1BX	0.998	24.43	6.21	24.39	26.00	1.066
3C2AX	0.987	24.42	6.17	24.10	25.84	1.072
3C2BX	0.992	25.01	6.17	24.81	25.84	1.042
Mean						0.977
Standard Deviation						0.109

Note: The dynamic compressive yield stress was used for calculating the critical local buckling moment ($(M_{cr})_{comp}$).

Table 3.3(a)

Comparison of Computed and Tested Yield Moments
Beam Specimens with a Stiffened Flange
(35XF Sheet Steel)
(Based on Static Tensile Yield Stress)

Spec.	S_e ($in.^3$) (1)	F_y (ksi) (2)	$(P_y)_{test}$ (kips) (3)	$(M_y)_{comp}$ (in.-kips) (4)	$(M_y)_{test}$ (in.-kips) (5)	(5)/(4) (6)
3A0A	0.268	32.02	3.773	8.58	10.14	1.182
3A1A	0.258	32.02	3.936	8.25	10.58	1.282
3A1B	0.262	32.02	4.137	8.39	11.12	1.325
3A2A	0.271	32.02	4.799	8.68	12.90	1.486
3A2B	0.260	32.02	4.844	8.32	13.02	1.565
3B0A	0.635	32.02	5.824	20.32	26.57	1.307
3B1A	0.646	32.02	4.894	20.69	22.33	1.079
3B1B	0.629	32.02	5.668	20.15	25.86	1.283
3B2A	0.626	32.02	6.511	20.04	29.71	1.482
3B2B	0.632	32.02	7.130	20.23	32.53	1.608
3C0A	0.924	32.02	6.038	29.58	34.34	1.161
3C1A	0.930	32.02	6.825	29.79	38.82	1.303
3C1B	0.932	32.02	6.112	29.86	34.76	1.164
3C2A	0.925	32.02	6.873	29.61	39.09	1.320
3C2B	0.930	32.02	6.684	29.78	38.01	1.276
Mean						1.321
Standard Deviation						0.148

(Considering Cold-Work of Forming)

3A0A	0.268	38.42	3.773	10.30	10.14	0.984
3A1A	0.258	38.40	3.936	9.90	10.58	1.069
3A1B	0.262	38.38	4.137	10.06	11.12	1.105
3A2A	0.271	38.36	4.799	10.40	12.90	1.240
3A2B	0.260	38.40	4.844	9.98	13.02	1.305
Mean(with consideration of cold-work)						1.141
Standard Deviation(with consideration of cold-work)						0.130
Mean(without consideration of cold-work)						1.368
Standard Deviation(without consideration of cold-work)						0.155

Table 3.3(b)

Comparison of Computed and Tested Yield Moments
Beam Specimens with a Stiffened Flange
(35XF Sheet Steel)
(Based on Dynamic Tensile Yield Stress)

Spec.	S_e ($in.^3$) (1)	F_y (ksi) (2)	$(P_y)_{test}$ (kips) (3)	$(M_y)_{comp}$ (in.-kips) (4)	$(M_y)_{test}$ (in.-kips) (5)	(5)/(4) (6)
3A0A	0.268	32.02	3.773	8.58	10.14	1.182
3A1A	0.258	32.87	3.936	8.46	10.58	1.251
3A1B	0.262	32.87	4.137	8.62	11.12	1.290
3A2A	0.271	36.40	4.799	9.87	12.90	1.307
3A2B	0.260	36.40	4.844	9.45	13.02	1.378
3B0A	0.635	32.02	5.824	20.32	26.57	1.307
3B1A	0.645	32.87	4.894	21.21	22.33	1.053
3B1B	0.629	32.87	5.668	20.66	25.86	1.252
3B2A	0.623	36.40	6.511	22.66	29.71	1.311
3B2B	0.628	36.40	7.130	22.87	32.53	1.422
3C0A	0.924	32.02	6.038	29.58	34.34	1.161
3C1A	0.929	32.87	6.825	30.53	38.82	1.271
3C1B	0.931	32.87	6.112	30.61	34.76	1.135
3C2A	0.917	36.40	6.873	34.33	39.09	1.139
3C2B	0.922	36.40	6.684	34.52	38.01	1.101
Mean						1.237
Standard Deviation						0.102

Considering Cold-Work of Forming

3A0A	0.268	38.42	3.773	10.30	10.14	0.984
3A1A	0.258	39.17	3.936	10.09	10.58	1.049
3A1B	0.262	39.14	4.137	10.26	11.12	1.084
3A2A	0.271	42.54	4.799	11.54	12.90	1.118
3A2B	0.260	42.59	4.844	11.06	13.02	1.177
Mean(with consideration of cold-work)						1.082
Standard Deviation(with consideration of cold-work)						0.072
Mean(without consideration of cold-work)						1.282
Standard Deviation(without consideration of cold-work)						0.072

Table 3.4(a)

Comparison of Computed and Tested Yield Moments
Beam Specimens with a Stiffened Flange
(50XF Sheet Steel)
(Based on Static Tensile Yield Stress)

Spec.	S_e ($in.^3$) (1)	F_y (ksi) (2)	$(P_y)_{test}$ (kips) (3)	$(M_y)_{comp}$ (in.-kips) (4)	$(M_y)_{test}$ (in.-kips) (5)	(5)/(4) (6)
3A0AX	0.152	48.81	2.90	7.40	6.71	0.907
3A1AX	0.151	48.81	3.21	7.38	7.42	1.005
3A1BX	0.152	48.81	3.02	7.44	6.98	0.938
3A2AX	0.152	48.81	3.22	7.40	7.45	1.007
3A2BX	0.150	48.81	3.34	7.33	7.72	1.053
3B0AX	0.371	48.81	5.80	18.10	20.66	1.141
3B1AX	0.374	48.81	5.86	18.23	20.88	1.145
3B1BX	0.375	48.81	6.33	18.29	22.58	1.234
3B2AX	0.376	48.81	6.41	18.34	22.84	1.245
3B2BX	0.376	48.81	6.72	18.33	23.94	1.306
3C0AX	0.591	48.81	6.38	28.84	26.72	0.926
3C1AX	0.596	48.81	6.79	29.09	28.42	0.977
3C1BX	0.588	48.81	6.80	28.70	28.45	0.991
3C2AX	0.588	48.81	6.82	28.72	28.54	0.994
3C2BX	0.589	48.81	6.72	28.77	28.14	0.978
Mean						1.057
Standard Deviation						0.126

Table 3.4(b)

Comparison of Computed and Tested Yield Moments
Beam Specimens with a Stiffened Flange
(50XF Sheet Steel)
(Based on Dynamic Tensile Yield Stress)

Spec.	S_e ($in.^3$) (1)	F_y (ksi) (2)	$(P_y)_{test}$ (kips) (3)	$(M_y)_{comp}$ (in.-kips) (4)	$(M_y)_{test}$ (in.-kips) (5)	(5)/(4) (6)
3A0AX	0.152	48.81	2.90	7.40	6.71	0.907
3A1AX	0.151	49.50	3.21	7.48	7.42	0.992
3A1BX	0.152	49.50	3.02	7.54	6.98	0.926
3A2AX	0.152	51.60	3.22	7.81	7.45	0.954
3A2BX	0.150	51.60	3.34	7.75	7.72	0.996
3B0AX	0.371	48.81	5.80	18.10	20.66	1.141
3B1AX	0.373	49.50	5.86	18.48	20.88	1.130
3B1BX	0.375	49.50	6.33	18.54	22.58	1.218
3B2AX	0.375	51.60	6.41	19.34	22.84	1.181
3B2BX	0.375	51.60	6.72	19.33	23.94	1.238
3C0AX	0.591	48.81	6.38	28.84	26.72	0.926
3C1AX	0.595	49.50	6.79	29.48	28.42	0.964
3C1BX	0.587	49.50	6.80	29.08	28.45	0.978
3C2AX	0.586	51.60	6.82	30.26	28.54	0.943
3C2BX	0.587	51.60	6.72	30.31	28.14	0.928
Mean						1.028
Standard Deviation						0.117

Table 3.5(a)

Comparison of Computed and Tested Failure Moments Based on the Effective width Formulas in the 1991 AISI Automotive Steel Design Manual for Beam Specimens with a Stiffened Flange (35XF Sheet Steel) (Based on Static Tensile Yield Stress)

Spec.	Strain Rate in./in./sec. (1)	F_y (ksi) (2)	$(P_u)_{test}$ (kips) (3)	$(M_u)_{comp}$ (in.-kips) (4)	$(M_u)_{test}$ (in.-kips) (5)	(5)/(4) (6)
3A0A	0.00001	32.02	5.69	10.73	15.29	1.425
3A1A	0.0001	32.02	5.43	10.33	14.59	1.412
3A1B	0.0001	32.02	5.72	10.49	15.37	1.465
3A2A	0.01	32.02	6.31	10.85	16.96	1.563
3A2B	0.01	32.02	6.39	10.41	17.17	1.649
3B0A	0.00001	32.02	6.38	25.41	29.11	1.146
3B1A	0.0001	32.02	6.54	25.86	29.84	1.154
3B1B	0.0001	32.02	6.49	25.17	29.61	1.037
3B2A	0.01	32.02	6.97	25.05	31.80	1.176
3B2B	0.01	32.02	7.63	25.29	34.81	1.376
3C0A	0.00001	32.02	6.53	36.98	37.14	1.004
3C1A	0.0001	32.02	6.99	37.22	39.75	1.068
3C1B	0.0001	32.02	6.96	37.30	39.58	1.061
3C2A	0.01	32.02	7.45	37.02	42.37	1.144
3C2B	0.01	32.02	7.42	37.22	42.20	1.134
Mean						1.270
Standard Deviation						0.198

Note : The cold-work of forming was not considered for the Specimen 3A because the inelastic reserve capacity was used for the calculation of ultimate moments.

Table 3.5(b)

Comparison of Computed and Tested Failure Moments Based on the Effective width Formulas in the 1991 AISI Automotive Steel Design Manual for Beam Specimens with a Stiffened Flange (35XF Sheet Steel) (Based on Dynamic Tensile Yield Stress)

Spec.	Strain Rate in./in./sec. (1)	F_y (ksi) (2)	$(P_u)_{test}$ (kips) (3)	$(M_u)_{comp}$ (in.-kips) (4)	$(M_u)_{test}$ (in.-kips) (5)	(5)/(4) (6)
3A0A	0.00001	32.02	5.69	10.73	15.29	1.425
3A1A	0.0001	32.87	5.43	10.57	14.59	1.380
3A1B	0.0001	32.87	5.72	10.77	15.37	1.427
3A2A	0.01	36.40	6.31	12.34	16.96	1.374
3A2B	0.01	36.40	6.39	11.81	17.17	1.454
3B0A	0.00001	32.02	6.38	25.40	29.11	1.146
3B1A	0.0001	32.87	6.54	26.51	29.84	1.126
3B1B	0.0001	32.87	6.49	25.82	29.61	1.147
3B2A	0.01	36.40	6.97	28.32	31.80	1.123
3B2B	0.01	36.40	7.63	28.59	34.81	1.217
3C0A	0.00001	32.02	6.53	36.97	37.14	1.004
3C1A	0.0001	32.87	6.99	38.16	39.75	1.042
3C1B	0.0001	32.87	6.96	38.26	39.58	1.034
3C2A	0.01	36.40	7.45	42.91	42.37	0.987
3C2B	0.01	36.40	7.42	43.15	42.20	0.978
Mean						1.191
Standard Deviation						0.169

Note : The cold-work of forming was not considered for the Specimen 3A because the inelastic reserve capacity was used for the calculation of ultimate moments.

Table 3.6(a)

Comparison of Computed and Tested Failure Moments Based on the Effective width Formulas in the 1991 AISI Automotive Steel Design Manual for Beam Specimens with a Stiffened Flange (50XF Sheet Steel) (Based on Static Tensile Yield Stress)

Spec.	Strain Rate in./in./sec. (1)	F_y (ksi) (2)	$(P_u)_{test}$ (kips) (3)	$(M_u)_{comp}$ (in.-kips) (4)	$(M_u)_{test}$ (in.-kips) (5)	(5)/(4) (6)
3A0AX	0.00001	48.81	4.42	9.25	10.22	1.105
3A1AX	0.0001	48.81	4.51	9.22	10.44	1.132
3A1BX	0.0001	48.81	4.44	9.29	10.26	1.104
3A2AX	0.01	48.81	4.56	9.24	10.55	1.142
3A2BX	0.01	48.81	4.93	9.16	11.41	1.246
3B0AX	0.00001	48.81	6.25	22.62	22.28	0.985
3B1AX	0.0001	48.81	6.50	22.79	23.15	1.016
3B1BX	0.0001	48.81	6.67	22.87	23.76	1.039
3B2AX	0.01	48.81	6.69	22.92	23.84	1.040
3B2BX	0.01	48.81	6.98	22.91	24.87	1.086
3C0AX	0.00001	48.81	8.16	34.62	34.16	0.987
3C1AX	0.0001	48.81	8.04	34.69	33.67	0.971
3C1BX	0.0001	48.81	8.25	34.49	34.53	1.001
3C2AX	0.01	48.81	8.72	34.10	36.54	1.072
3C2BX	0.01	48.81	8.43	34.52	35.31	1.023
Mean						1.063
Standard Deviation						0.075

Note : The cold-work of forming was not considered for the Specimen 3A because the inelastic reserve capacity was used for the calculation of ultimate moments.

Table 3.6(b)

Comparison of Computed and Tested Failure Moments Based on the Effective width Formulas in the 1991 AISI Automotive Steel Design Manual for Beam Specimens with a Stiffened Flange (50XF Sheet Steel) (Based on Dynamic Tensile Yield Stress)

Spec.	Strain Rate in./in./sec. (1)	F_y (ksi) (2)	$(P_u)_{test}$ (kips) (3)	$(M_u)_{comp}$ (in.-kips) (4)	$(M_u)_{test}$ (in.-kips) (5)	(5)/(4) (6)
3A0AX	0.00001	48.81	4.42	9.25	10.22	1.105
3A1AX	0.0001	49.50	4.51	9.35	10.44	1.117
3A1BX	0.0001	49.50	4.44	9.43	10.26	1.088
3A2AX	0.01	51.60	4.56	9.77	10.55	1.080
3A2BX	0.01	51.60	4.93	9.69	11.41	1.178
3B0AX	0.00001	48.81	6.25	22.62	22.28	0.985
3B1AX	0.0001	49.50	6.50	23.10	23.15	1.002
3B1BX	0.0001	49.50	6.67	23.18	23.76	1.025
3B2AX	0.01	51.60	6.69	24.17	23.84	0.986
3B2BX	0.01	51.60	6.98	24.16	24.87	1.029
3C0AX	0.00001	48.81	8.16	34.62	34.16	0.987
3C1AX	0.0001	49.50	8.04	35.06	33.67	0.960
3C1BX	0.0001	49.50	8.25	34.86	34.53	0.991
3C2AX	0.01	51.60	8.72	35.56	36.54	1.028
3C2BX	0.01	51.60	8.43	36.01	35.31	0.981
Mean						1.036
Standard Deviation						0.063

Note : The cold-work of forming was not considered for the Specimen 3A because the inelastic reserve capacity was used for the calculation of ultimate moments.

Table 3.7

Average Tested Failure Moments for Beam Specimens with a Stiffened Flange (35XF Sheet Steel)

Strain Rate in./in./sec.	w/t		
	29.64	55.74	76.41
0.00001	15.29	29.11	37.14
0.0001	14.98	29.73	39.67
0.01	17.07	33.31	42.29

Table 3.8

Average Tested Failure Moments for Beam Specimens with a Stiffened Flange (50XF Sheet Steel)

Strain Rate in./in./sec.	w/t		
	26.68	46.09	65.77
0.00001	10.22	22.28	34.16
0.0001	10.35	23.46	34.10
0.01	10.98	24.36	35.93

Table 3.9

Comparison of Computed and Tested Critical Buckling Moments
Beam Specimens with Unstiffened Flanges (Based on k=0.43)
(35XF Sheet Steel)

Spec.	S_{xc} ($in.^3$) (1)	f_{cr} (ksi) (2)	$(P_{cr})_{test}$ (kips) (3)	$(M_{cr})_{comp}$ (in.-kips) (4)	$(M_{cr})_{test}$ (in.-kips) (5)	(5)/(4) (6)
4A0A	0.384	28.22	N/A	10.84	N/A	N/A
4A1A	0.377	28.26	N/A	10.65	N/A	N/A
4A1B	0.382	28.26	N/A	10.79	N/A	N/A
4A2A	0.380	30.15	N/A	11.46	N/A	N/A
4A2B	0.377	30.23	N/A	11.40	N/A	N/A
4B0A	0.719	25.55	N/A	18.37	N/A	N/A
4B1A	0.717	25.53	N/A	18.30	N/A	N/A
4B1B	0.717	25.66	N/A	18.40	N/A	N/A
4B2A	0.717	27.22	N/A	19.52	N/A	N/A
4B2B	0.717	27.14	N/A	19.46	N/A	N/A
4C0A	1.153	21.64	8.22	24.95	33.39	1.338
4C1A	1.150	21.60	8.15	24.84	33.11	1.333
4C1B	1.148	21.64	8.63	24.84	35.06	1.411
4C2A	1.160	22.77	9.56	26.41	38.84	1.471
4C2B	1.153	22.82	9.52	26.31	38.67	1.470
Mean						1.405
Standard Deviation						0.060

Note: The dynamic compressive yield stress was used for calculating the critical local buckling moment ($(M_{cr})_{comp}$).

Table 3.10

Comparison of Computed and Tested Critical Buckling Moments
Beam Specimens with Unstiffened Flanges (Based on k=0.43)
(50XF Sheet Steel)

Spec.	S_{xc} ($in.^3$) (1)	f_{cr} (ksi) (2)	$(P_{cr})_{test}$ (kips) (3)	$(M_{cr})_{comp}$ (in.-kips) (4)	$(M_{cr})_{test}$ (in.-kips) (5)	(5)/(4) (6)
4A0AX	0.314	45.58	N/A	14.33	N/A	N/A
4A1AX	0.315	46.81	N/A	14.75	N/A	N/A
4A1BX	0.315	46.77	N/A	14.74	N/A	N/A
4A2AX	0.316	49.12	N/A	15.50	N/A	N/A
4A2BX	0.314	49.10	N/A	15.42	N/A	N/A
4B0AX	0.537	40.64	9.28	21.81	23.78	1.090
4B1AX	0.541	40.96	9.07	22.16	23.24	1.049
4B1BX	0.544	40.96	9.09	22.29	23.29	1.045
4B2AX	0.538	42.21	9.62	22.71	24.65	1.085
4B2BX	0.540	42.26	10.11	22.82	25.91	1.135
4C0AX	0.854	27.34	7.87	23.35	29.02	1.243
4C1AX	0.857	27.34	9.01	23.43	33.22	1.418
4C1BX	0.855	27.27	8.37	23.31	30.86	1.324
4C2AX	0.857	27.10	8.40	23.22	30.98	1.334
4C2BX	0.858	27.17	8.79	23.30	32.41	1.391
Mean						1.211
Standard Deviation						0.147

Note: The dynamic compressive yield stress was used for calculating the critical local buckling moment ($(M_{cr})_{comp}$).

Table 3.11(a)

Comparison of Computed and Tested Failure Moments Based on the Effective width Formulas in the 1991 AISI Automotive Steel Design Manual for Beam Specimens with Unstiffened Flanges (35XF Sheet Steel) (Based on Static Tensile Yield Stress)

Spec.	Strain Rate in./in./sec. (1)	F_y (ksi) (2)	$(P_u)_{test}$ (kips) (3)	$(M_y)_{comp}$ (in.-kips) (4)	$(M_u)_{test}$ (in.-kips) (5)	(5)/(4) (6)
4A0A	0.00001	32.02	6.41	12.29	14.82	1.206
4A1A	0.0001	32.02	7.15	12.08	16.53	1.369
4A1B	0.0001	32.02	7.18	12.23	16.60	1.357
4A2A	0.01	32.02	7.53	12.17	17.41	1.430
4A2B	0.01	32.02	7.63	12.07	17.64	1.461
4B0A	0.00001	32.02	9.77	21.73	26.26	1.208
4B1A	0.0001	32.02	10.12	21.67	27.20	1.255
4B1B	0.0001	32.02	9.87	21.78	26.52	1.218
4B2A	0.01	32.02	10.97	21.73	29.48	1.357
4B2B	0.01	32.02	10.98	21.67	29.51	1.361
4C0A	0.00001	32.02	8.49	30.47	34.49	1.132
4C1A	0.0001	32.02	8.83	30.35	35.87	1.182
4C1B	0.0001	32.02	9.15	30.33	37.17	1.225
4C2A	0.01	32.02	10.23	30.62	41.56	1.357
4C2B	0.01	32.02	10.22	30.47	41.52	1.363
Mean						1.299
Standard Deviation						0.096

Considering Cold-Work of Forming

4A0A	0.00001	38.30	6.41	14.70	14.82	1.008
4A1A	0.0001	38.36	7.15	14.47	16.53	1.142
4A1B	0.0001	38.36	7.18	14.65	16.60	1.133
4A2A	0.01	38.33	7.53	14.57	17.41	1.195
4A2B	0.01	38.42	7.63	14.49	17.64	1.217
Mean(with consideration of cold-work)						1.139
Standard Deviation(with consideration of cold-work)						0.081
Mean(without consideration of cold-work)						1.365
Standard Deviation(without consideration of cold-work)						0.098

Note : $(M_y)_{comp}=(M_u)_{comp}$

Table 3.11(b)

Comparison of Computed and Tested Failure Moments Based on the Effective width Formulas in the 1991 AISI Automotive Steel Design Manual for Beam Specimens with Unstiffened Flanges (35XF Sheet Steel) (Based on Dynamic Tensile Yield Stress)

Spec.	Strain Rate in./in./sec. (1)	F_y (ksi) (2)	$(P_u)_{test}$ (kips) (3)	$(M_y)_{comp}$ (in.-kips) (4)	$(M_u)_{test}$ (in.-kips) (5)	(5)/(4) (6)
4A0A	0.00001	32.02	6.41	12.29	14.82	1.206
4A1A	0.0001	32.87	7.15	12.40	16.53	1.333
4A1B	0.0001	32.87	7.18	12.55	16.60	1.322
4A2A	0.01	36.40	7.53	13.83	17.41	1.259
4A2B	0.01	36.40	7.63	13.73	17.64	1.285
4B0A	0.00001	32.02	9.77	21.73	26.26	1.208
4B1A	0.0001	32.87	10.12	22.14	27.20	1.228
4B1B	0.0001	32.87	9.87	22.26	26.52	1.191
4B2A	0.01	36.40	10.97	24.14	29.48	1.221
4B2B	0.01	36.40	10.98	24.07	29.51	1.226
4C0A	0.00001	32.02	8.49	30.47	34.49	1.132
4C1A	0.0001	32.87	8.83	30.99	35.87	1.157
4C1B	0.0001	32.87	9.15	30.97	37.17	1.200
4C2A	0.01	36.40	10.23	33.89	41.56	1.226
4C2B	0.01	36.40	10.22	33.72	41.52	1.231
Mean						1.228
Standard Deviation						0.052

Considering Cold-Work of Forming

4A0A	0.00001	38.30	6.41	14.70	14.82	1.008
4A1A	0.0001	39.13	7.15	14.76	16.53	1.120
4A1B	0.0001	39.13	7.18	14.94	16.60	1.111
4A2A	0.01	42.51	7.53	16.16	17.41	1.077
4A2B	0.01	42.60	7.63	16.07	17.64	1.098
Mean(with consideration of cold-work)						1.083
Standard Deviation(with consideration of cold-work)						0.045
Mean(without consideration of cold-work)						1.281
Standard Deviation(without consideration of cold-work)						0.051

Note : $(M_y)_{comp}=(M_u)_{comp}$

Table 3.12(a)

Comparison of Computed and Tested Failure Moments Based on the Effective width Formulas in the 1991 AISI Automotive Steel Design Manual for Beam Specimens with Unstiffened Flanges (50XF Sheet Steel) (Based on Static Tensile Yield Stress)

Spec.	Strain Rate in./in./sec. (1)	F_y (ksi) (2)	$(P_u)_{test}$ (kips) (3)	$(M_y)_{comp}$ (in.-kips) (4)	$(M_u)_{test}$ (in.-kips) (5)	(5)/(4) (6)
4A0AX	0.00001	48.81	8.84	15.34	17.13	1.117
4A1AX	0.0001	48.81	8.92	15.38	17.27	1.123
4A1BX	0.0001	48.81	8.75	15.38	16.94	1.101
4A2AX	0.01	48.81	9.45	15.41	18.31	1.189
4A2BX	0.01	48.81	9.36	15.33	18.13	1.183
4B0AX	0.00001	48.81	9.87	22.78	25.29	1.110
4B1AX	0.0001	48.81	10.01	22.95	25.66	1.118
4B1BX	0.0001	48.81	10.16	23.09	26.04	1.128
4B2AX	0.01	48.81	10.28	22.77	26.35	1.157
4B2BX	0.01	48.81	10.31	22.89	26.41	1.154
4C0AX	0.00001	48.81	8.94	31.92	32.96	1.033
4C1AX	0.0001	48.81	9.48	32.03	34.95	1.091
4C1BX	0.0001	48.81	9.28	31.92	34.20	1.071
4C2AX	0.01	48.81	9.67	31.95	35.67	1.116
4C2BX	0.01	48.81	9.77	32.01	36.03	1.126
Mean						1.121
Standard Deviation						0.040

Considering Cold-Work of Forming

4A0AX	0.00001	58.20	8.84	18.29	17.13	0.937
4A1AX	0.0001	58.24	8.92	18.35	17.27	0.941
4A1BX	0.0001	58.19	8.75	18.33	16.94	0.924
4A2AX	0.01	58.20	9.45	18.37	18.31	0.997
4A2BX	0.01	58.18	9.36	18.27	18.13	0.992
Mean(with consideration of cold-work)						0.958
Standard Deviation(with consideration of cold-work)						0.034
Mean(without consideration of cold-work)						1.143
Standard Deviation(without consideration of cold-work)						0.040

Note : $(M_y)_{comp}=(M_u)_{comp}$

Table 3.12(b)

Comparison of Computed and Tested Failure Moments Based on the Effective width Formulas in the 1991 AISI Automotive Steel Design Manual for Beam Specimens with Unstiffened Flanges (50XF Sheet Steel) (Based on Dynamic Tensile Yield Stress)

Spec.	Strain Rate in./in./sec. (1)	F_y (ksi) (2)	$(P_u)_{test}$ (kips) (3)	$(M_y)_{comp}$ (in.-kips) (4)	$(M_u)_{test}$ (in.-kips) (5)	(5)/(4) (6)
4A0AX	0.00001	48.81	8.84	15.34	17.13	1.117
4A1AX	0.0001	49.50	8.92	15.60	17.27	1.107
4A1BX	0.0001	49.50	8.75	15.60	16.94	1.086
4A2AX	0.01	51.60	9.45	16.29	18.31	1.124
4A2BX	0.01	51.60	9.36	16.20	18.13	1.119
4B0AX	0.00001	48.81	9.87	22.78	25.29	1.110
4B1AX	0.0001	49.50	10.01	23.21	25.66	1.106
4B1BX	0.0001	49.50	10.16	23.35	26.04	1.115
4B2AX	0.01	51.60	10.28	23.81	26.35	1.107
4B2BX	0.01	51.60	10.31	23.94	26.41	1.103
4C0AX	0.00001	48.81	8.94	31.92	32.96	1.033
4C1AX	0.0001	49.50	9.48	32.39	34.95	1.079
4C1BX	0.0001	49.50	9.28	32.27	34.20	1.060
4C2AX	0.01	51.60	9.67	33.40	35.67	1.068
4C2BX	0.01	51.60	9.77	33.45	36.03	1.077
Mean						1.094
Standard Deviation						0.026

Considering Cold-Work of Forming

4A0AX	0.00001	58.20	8.84	18.29	17.13	0.937
4A1AX	0.0001	58.84	8.92	18.55	17.27	0.931
4A1BX	0.0001	58.80	8.75	18.52	16.94	0.915
4A2AX	0.01	60.97	9.45	19.24	18.31	0.952
4A2BX	0.01	60.95	9.36	19.14	18.13	0.947
Mean(with consideration of cold-work)						0.936
Standard Deviation(with consideration of cold-work)						0.015

Mean(without consideration of cold-work)	1.111
Standard Deviation(without consideration of cold-work)	0.015

Note : $(M_y)_{comp}=(M_u)_{comp}$

Table 3.13

Average Tested Failure Moments for Beam Specimens with Unstiffened Flanges (35XF Sheet Steel)

Strain Rate in./in./sec.	w/t		
	9.17	15.08	20.95
0.00001	14.82	26.26	34.49
0.0001	16.57	26.86	36.52
0.01	17.53	29.49	41.54

Table 3.14

Average Tested Failure Moments for Beam Specimens with Unstiffened Flanges (50XF Sheet Steel)

Strain Rate in./in./sec.	w/t		
	8.83	15.33	20.51
0.00001	17.13	25.29	32.96
0.0001	17.11	25.85	34.58
0.01	18.22	26.38	35.85

Table 3.15

Delflections under Service Moments Based on Effective Sections
for Hat-Beam Specimens with a Stiffened Flange
(35XF Sheet Steel)

Spec.	$(M_s)_{test}$ (kips-in.) (1)	$(d)_{test}$ (in.) (2)	$(d)_{comp}$ (in.) (3)	(2)/(3) (4)
3B1A	12.73	0.1213	0.1658	0.732
3B1B	12.40	0.1319	0.1661	0.794
3B2A	13.60	0.1350	0.1830	0.738
3B2B	13.72	0.1396	0.1827	0.764
3C0A	17.75	0.1518	0.2003	0.758
3C1A	18.32	0.1974	0.2037	0.969
3C1B	18.37	0.2002	0.2033	0.985
3C2A	20.60	0.1835	0.2329	0.788
3C2B	20.71	0.1727	0.2325	0.743
Mean				0.808
Standard Deviation				0.093

Table 3.16

Delflections under Service Moments Based on Effective Sections for Hat-Beam Specimens with a Stiffened Flange (50XF Sheet Steel)

Spec.	$(M_s)_{test}$ (kips-in.) (1)	$(d)_{test}$ (in.) (2)	$(d)_{comp}$ (in.) (3)	(2)/(3) (4)
3A0AX	4.44	0.1410	0.1327	1.063
3A1AX	4.49	0.1034	0.1329	0.778
3A1BX	4.52	0.1472	0.1322	1.113
3A2AX	4.69	0.1291	0.1383	0.933
3A2BX	4.65	0.1225	0.1406	0.871
3B0AX	10.86	0.1424	0.1858	0.766
3B1AX	11.09	0.1964	0.1899	1.034
3B1BX	11.12	0.1824	0.1894	0.963
3B2AX	11.60	0.1821	0.1977	0.921
3B2BX	11.60	0.1912	0.1971	0.970
3C0AX	17.30	0.1469	0.1960	0.749
3C1AX	17.67	0.1521	0.1996	0.762
3C1BX	17.45	0.1596	0.1992	0.801
3C2AX	18.16	0.1512	0.2117	0.714
3C2BX	18.17	0.1970	0.2079	0.948
Mean				0.892
Standard Deviation				0.126

Table 3.17

Delflections under Service Moments Based on Effective Sections
for Channel Specimens with Unstiffened Flanges
(35XF Sheet Steel)

Spec.	$(M_s)_{test}$ (kips-in.) (1)	$(d)_{test}$ (in.) (2)	$(d)_{comp}$ (in.) (3)	(2)/(3) (4)
4A0A	7.37	0.0639	0.0620	1.031
4A1A	7.44	0.0609	0.0641	0.950
4A1B	7.53	0.0715	0.0649	1.102
4A2A	8.30	0.0542	0.0708	0.765
4A2B	8.24	0.0471	0.0706	0.667
4B0A	13.04	0.0511	0.0635	0.805
4B1A	13.28	0.0491	0.0650	0.755
4B1B	13.36	0.0445	0.0649	0.701
4B2A	14.48	0.0588	0.0706	0.833
4B2B	14.44	0.0527	0.0707	0.745
4C0A	18.28	0.0929	0.1097	0.847
4C1A	18.59	0.0924	0.1126	0.821*
4C1B	18.58	0.0630	0.1127	0.559*
4C2A	20.33	0.0992	0.1227	0.808*
4C2B	20.23	0.0639	0.1232	0.519*
Mean				0.833
Standard Deviation				0.121

(*) This value was not considered in the calculation of mean and standard deviation because the LVDT which measured the midspan deflection was not functioning properly during the test.

Table 3.18

Delflections under Service Moments Based on Effective Sections
for Channel Specimens with Unstiffened Flanges
(50XF Sheet Steel)

Spec.	$(M_s)_{test}$ (kips-in.) (1)	$(d)_{test}$ (in.) (2)	$(d)_{comp}$ (in.) (3)	(2)/(3) (4)
4A0AX	9.21	0.0422	0.0671	0.629
4A1AX	9.36	0.0537	0.0678	0.792
4A1BX	9.36	0.0401	0.0680	0.590
4A2AX	9.77	0.0471	0.0707	0.666
4A2BX	9.72	0.0401	0.0711	0.564
4B0AX	13.67	0.0442	0.0914	0.484
4B1AX	13.93	0.0392	0.0920	0.426
4B1BX	14.01	0.0412	0.0916	0.450
4B2AX	14.26	0.0621	0.0960	0.647
4B2BX	14.36	0.0466	0.0957	0.487
4C0AX	19.15	0.0841	0.1465	0.574
4C1AX	19.44	0.0965	0.1480	0.652
4C1BX	19.36	0.0980	0.1483	0.661
4C2AX	20.04	0.1094	0.1541	0.710
4C2BX	20.07	0.1026	0.1539	0.667
Mean				0.600
Standard Deviation				0.103

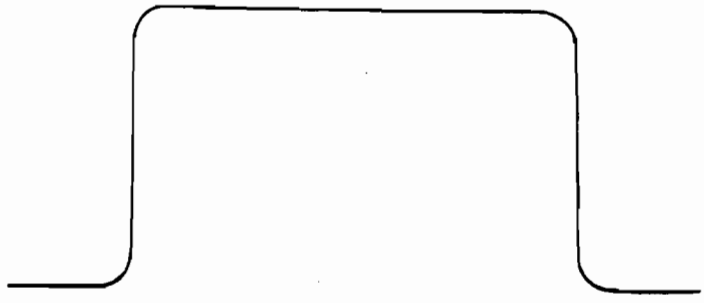

Figure 2.1 Configuration of Beam Test Specimens for Members with a Stiffened Compression Flange

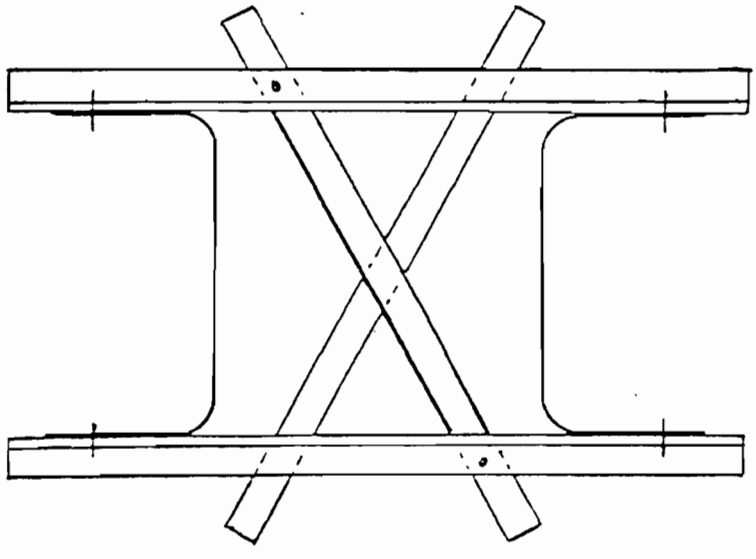

Figure 2.2 Configuration of Beam Test Specimens for Members with Unstiffened Compression Flanges

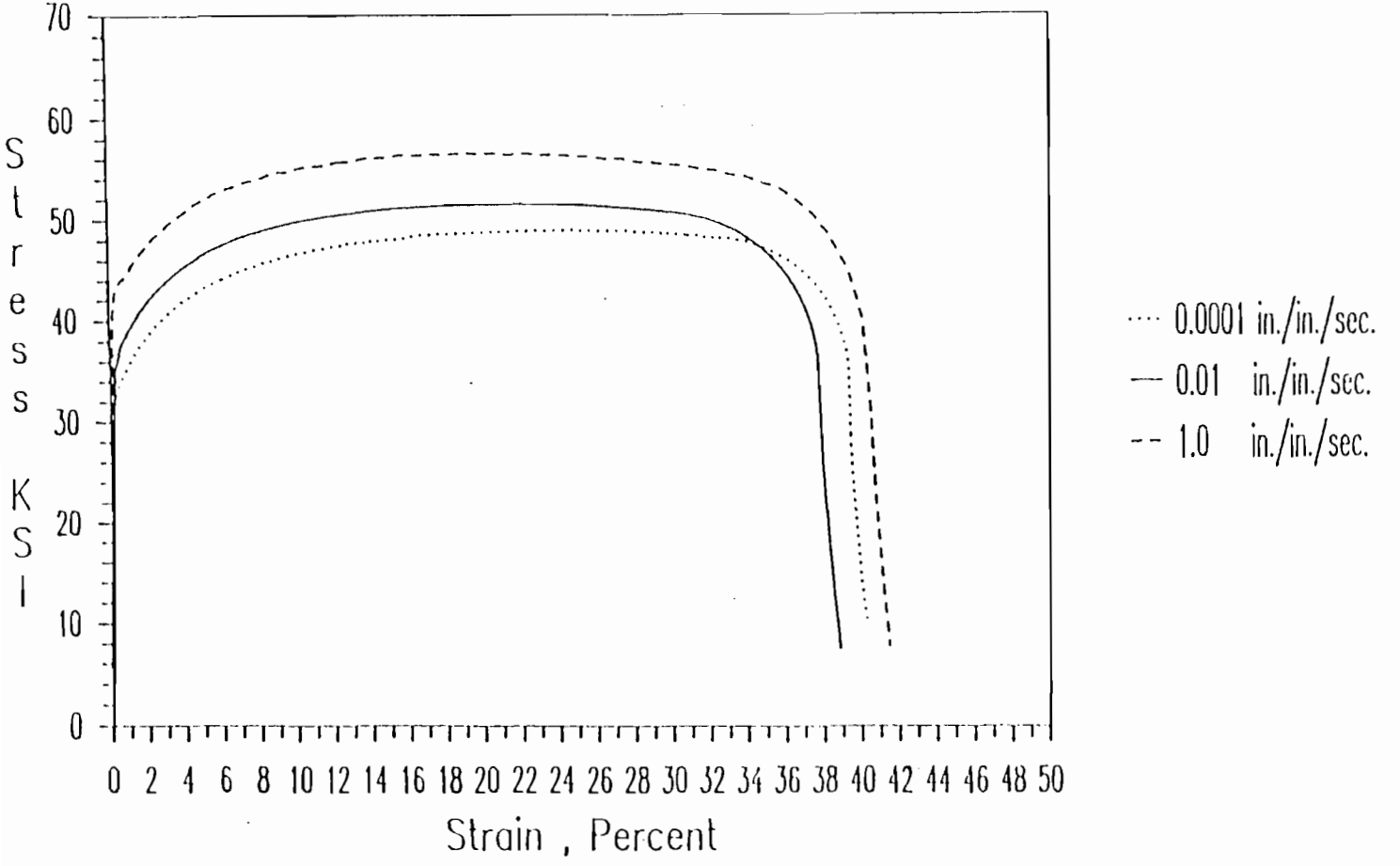

Figure 2.3 Stress-Strain Curves for 35XF Sheet Steel Tested under Different Strain Rates (Longitudinal Tension)

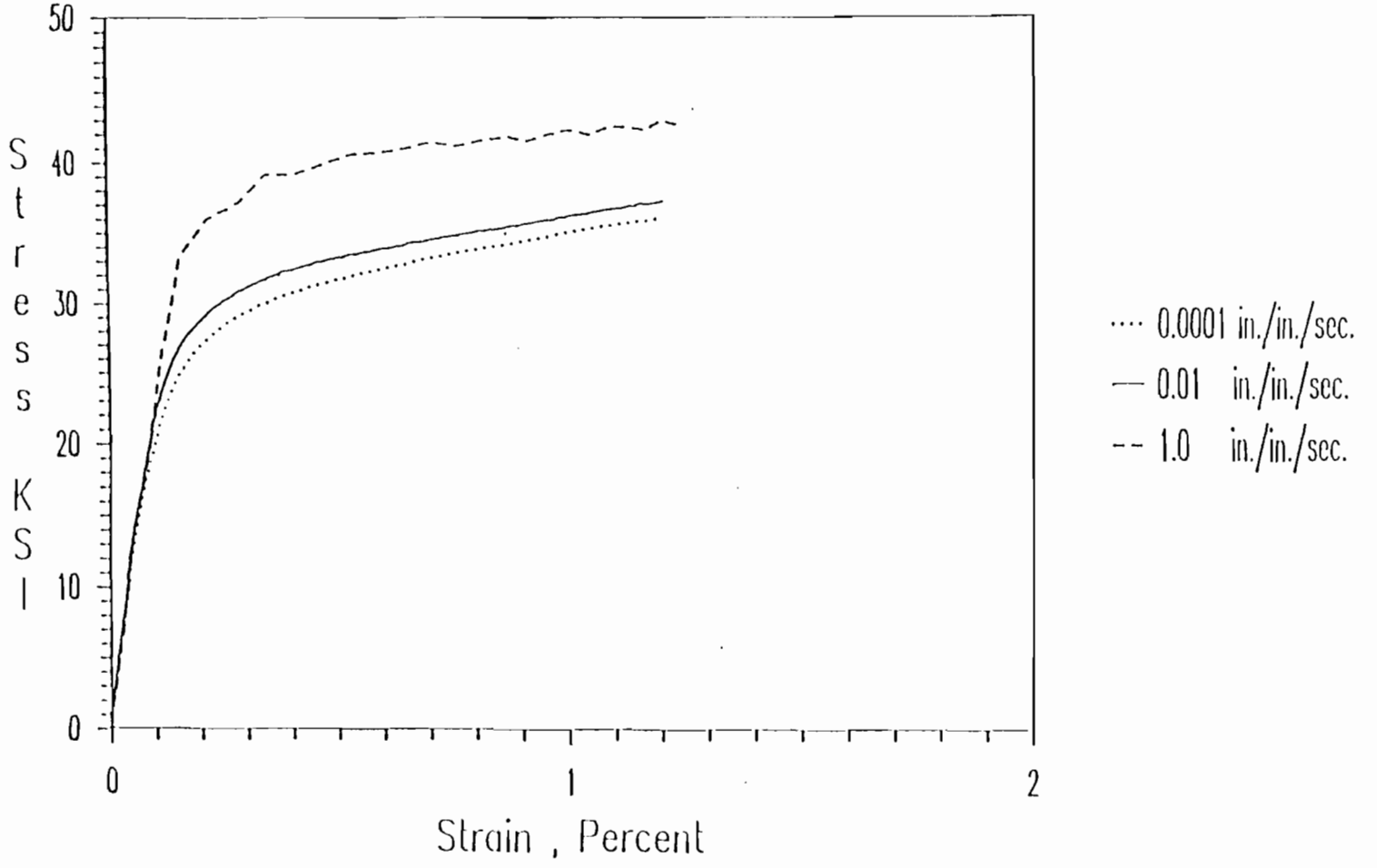

Figure 2.4 Stress-Strain Curves for 35XF Sheet Steel Tested under Different Strain Rates (Longitudinal Compression)

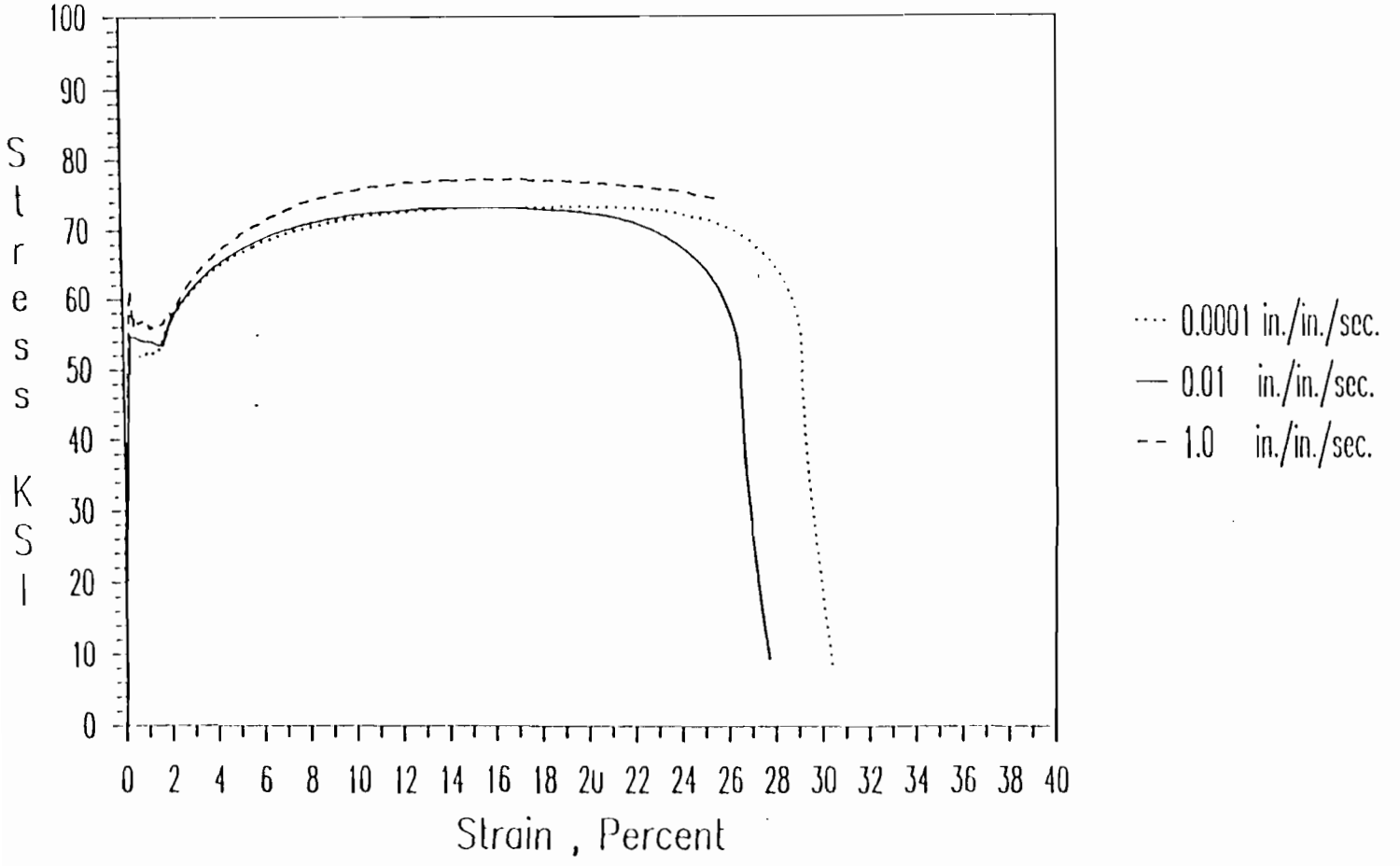

Figure 2.5 Stress-Strain Curves for 50XF Sheet Steel Tested under Different Strain Rates (Longitudinal Tension)

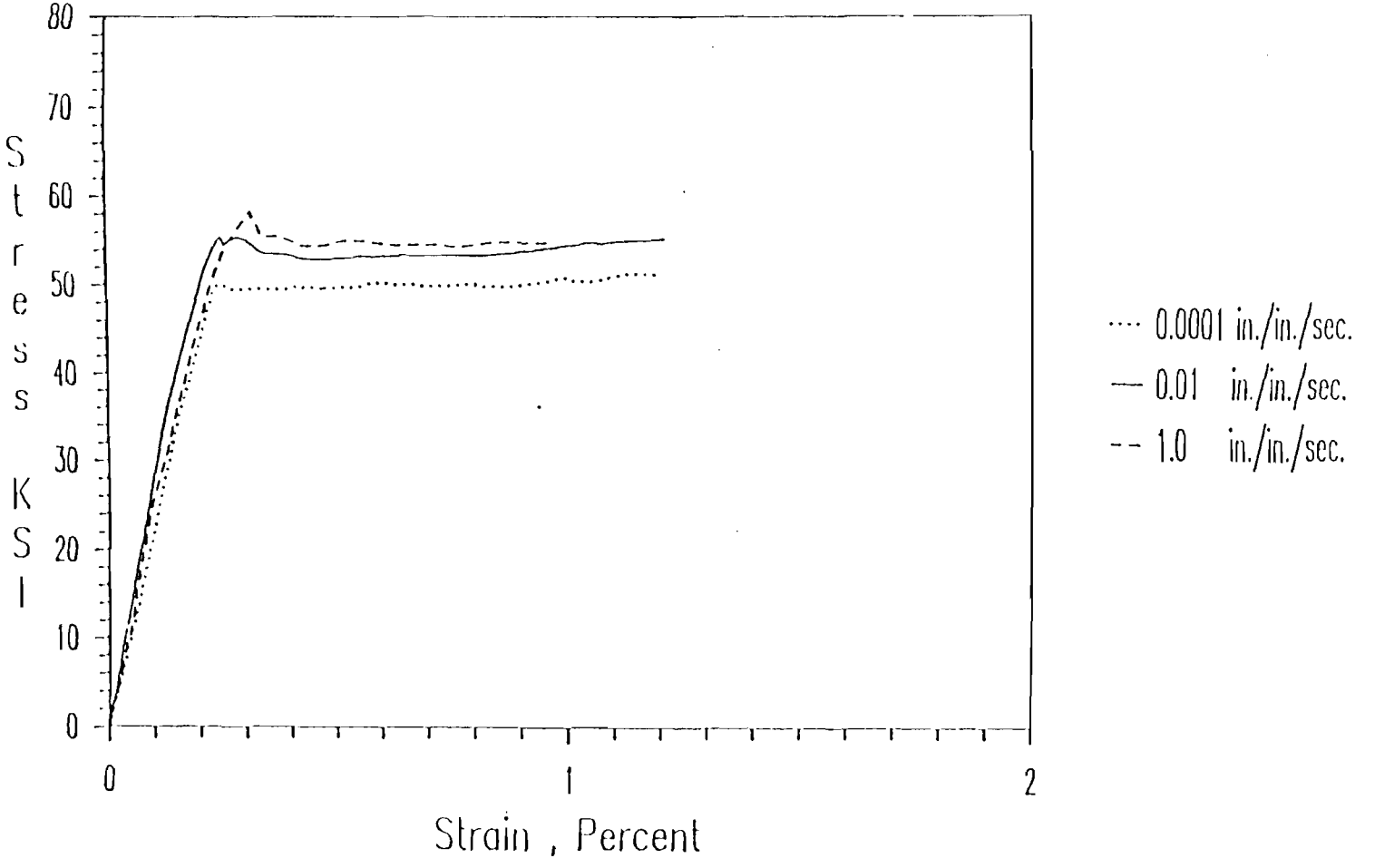

Figure 2.6 Stress-Strain Curves for 50XF Sheet Steel Tested under Different Strain Rates (Longitudinal Compression)

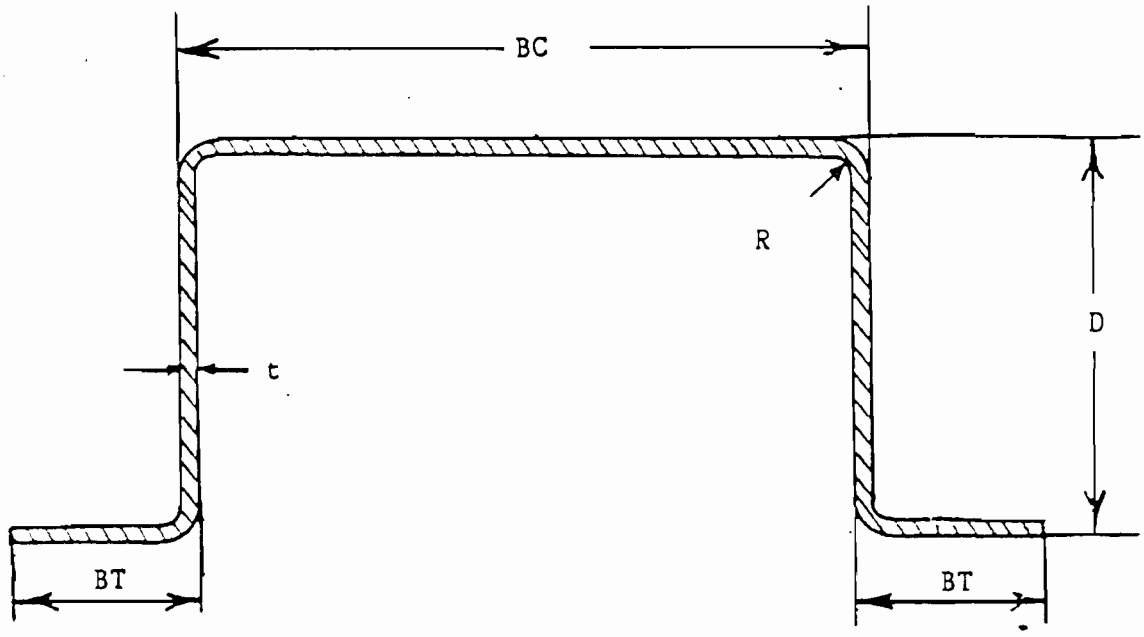

Figure 2.7 Hat Sections Used for Beam Tests

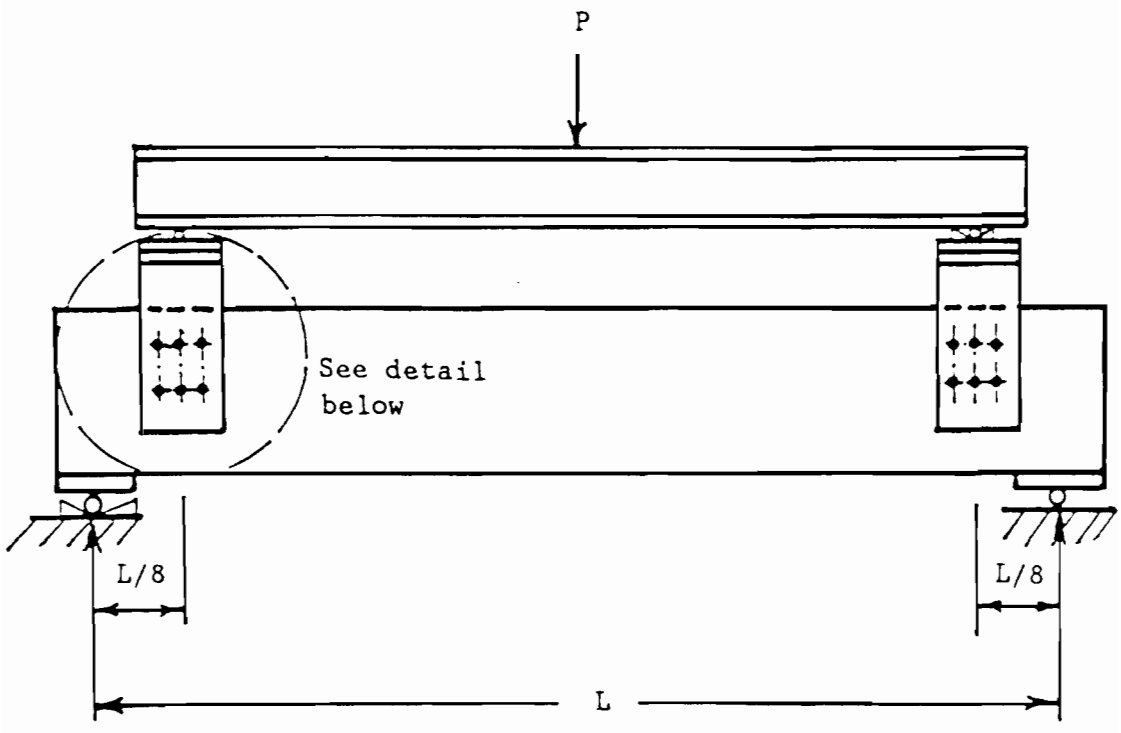

(a) Test Setup

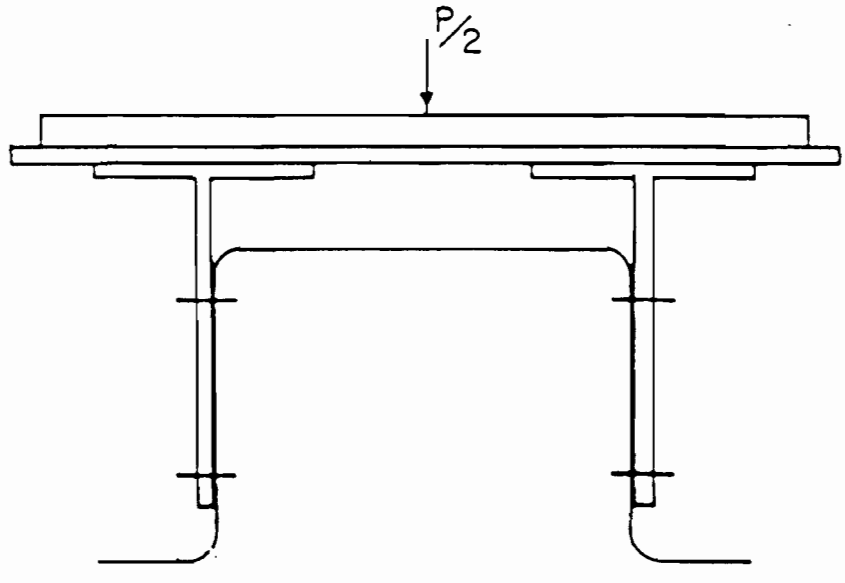

(b) Detail at Loading Points

Figure 2.8 Test Setup for Beams with a Stiffened Flange

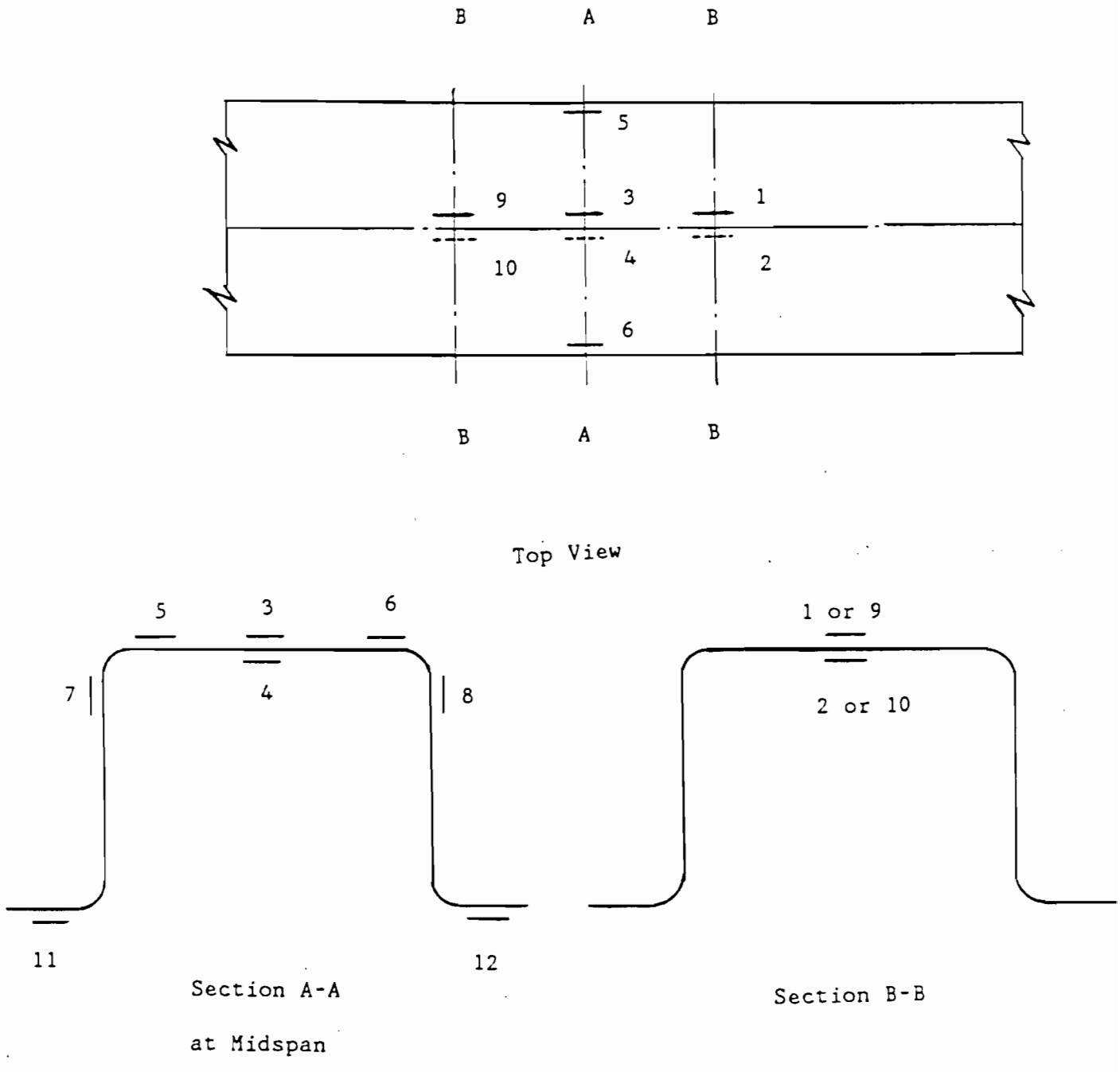

Figure 2.9 Locations of Strain Gages on Hat Sections

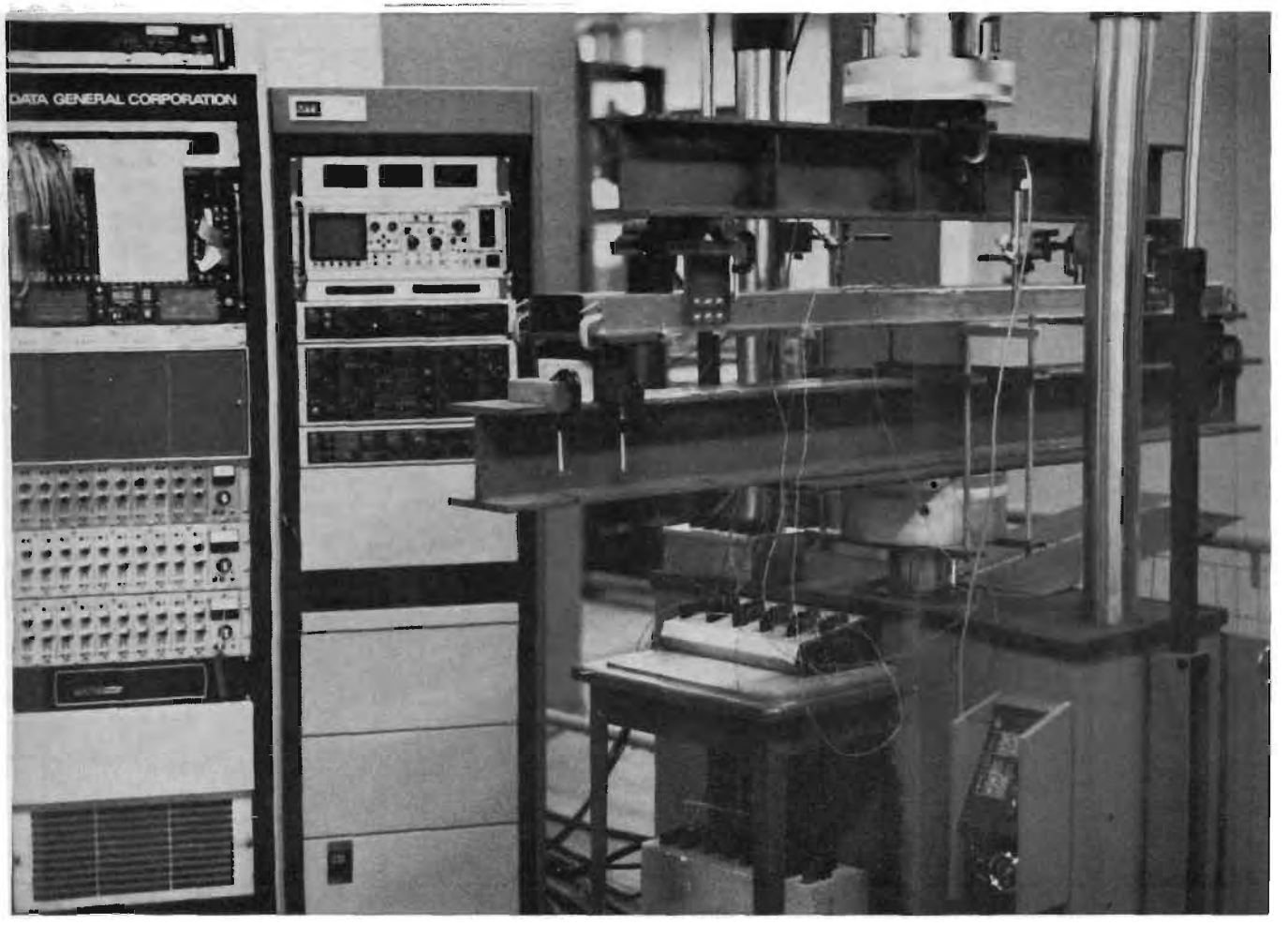

Figure 2.10 MTS 880 Material Test System and CAMAC Data Acquisition System Used for Beam Tests

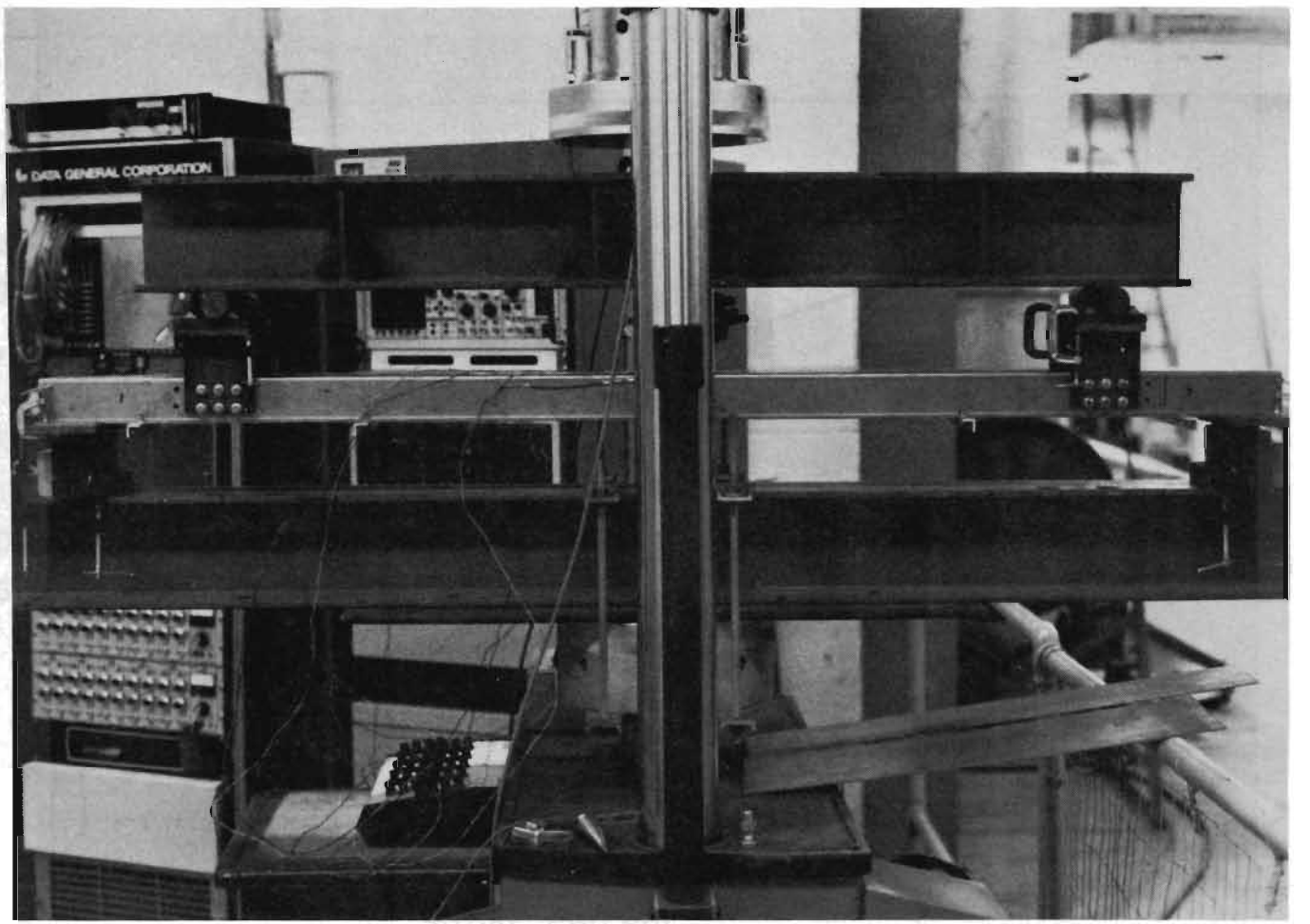

Figure 2.11 Photograph of Test Setup for Hat-Shaped Beam Specimen

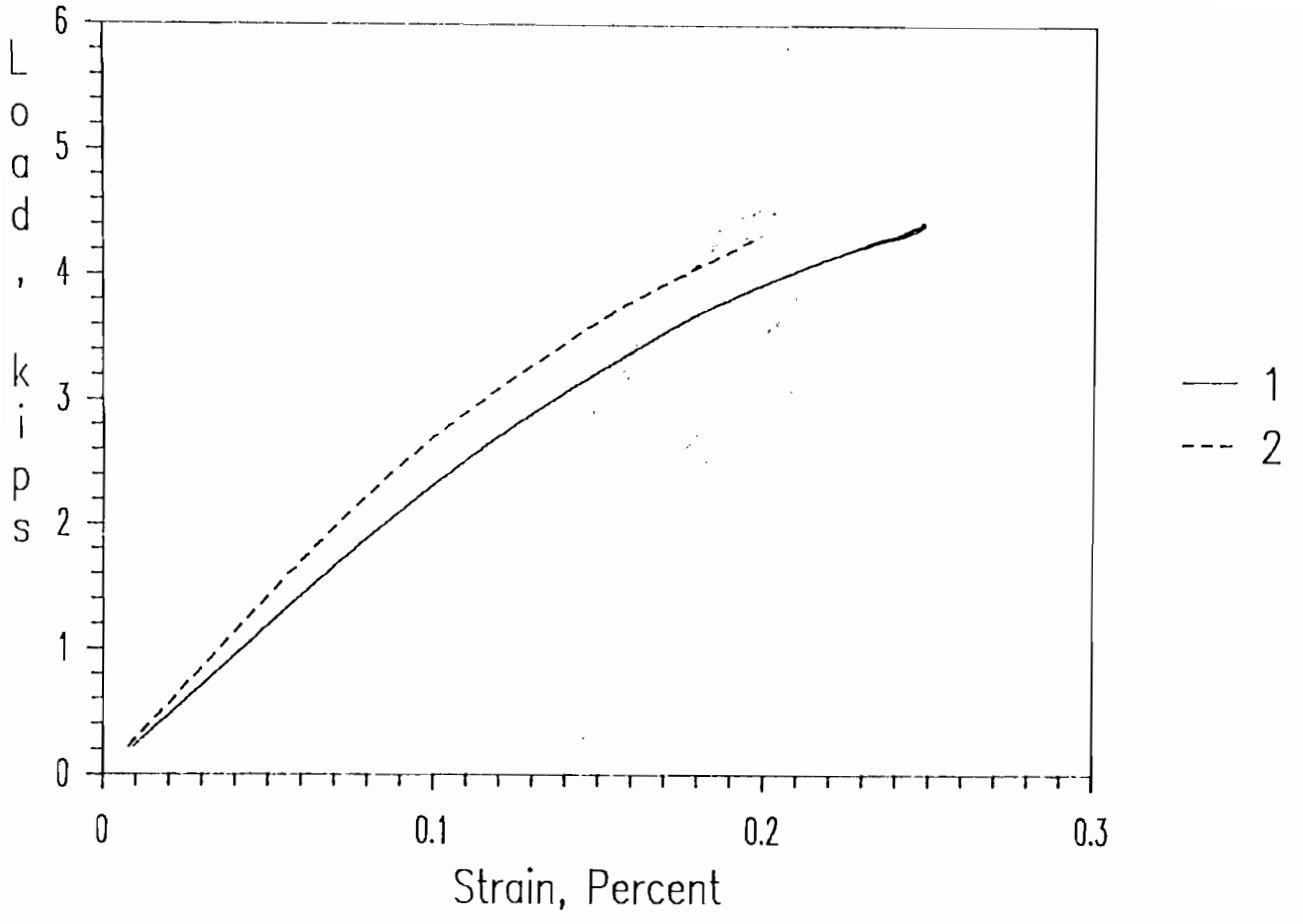

Figure 2.12 Load-Strain Curves of Strain Gages # 1 and 2 Installed at the Center of the Stiffened Flange (Spec. 3A1BX)

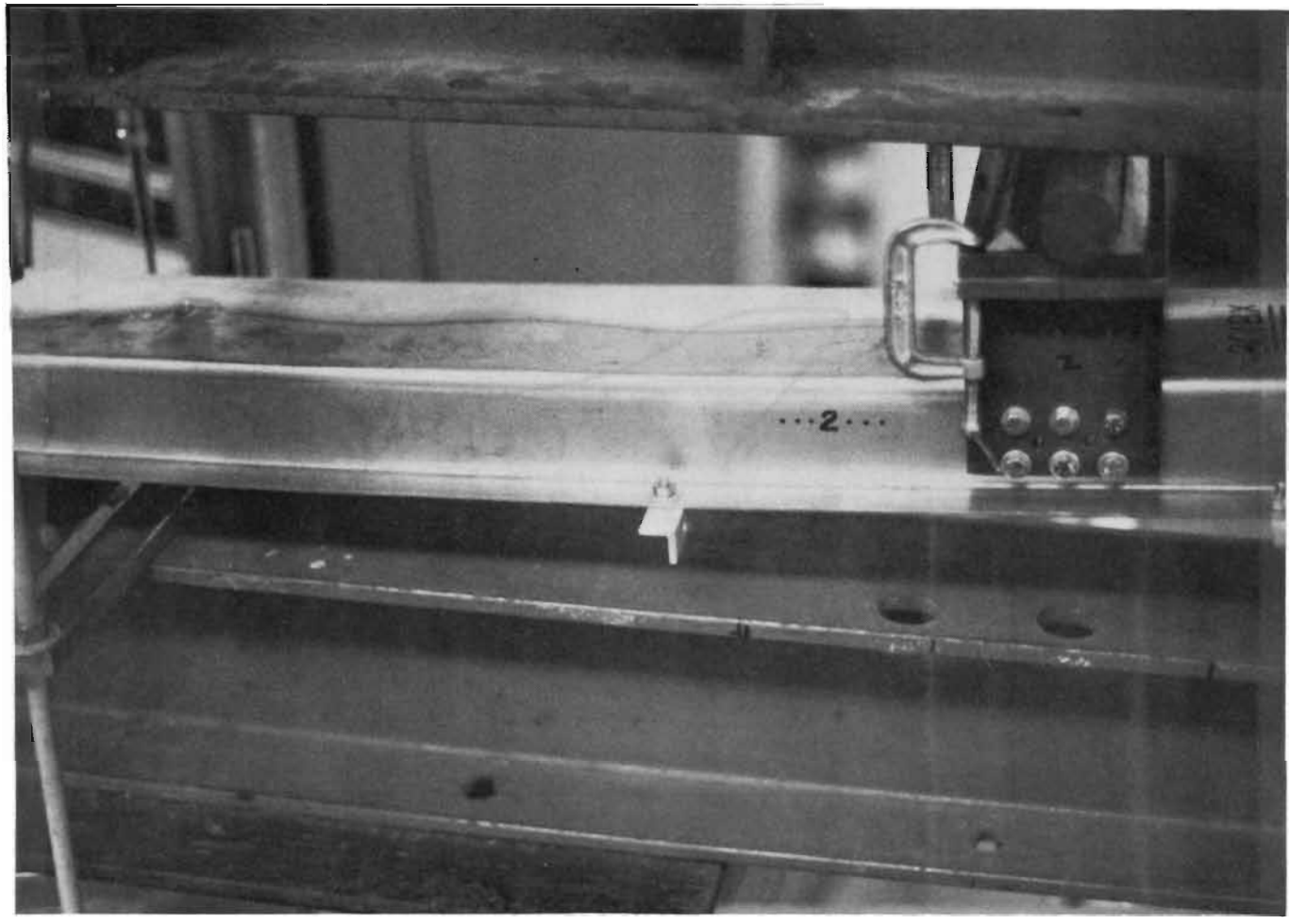

Figure 2.13 Development of Stiffened Flange Buckling Waves During a Medium Speed Test

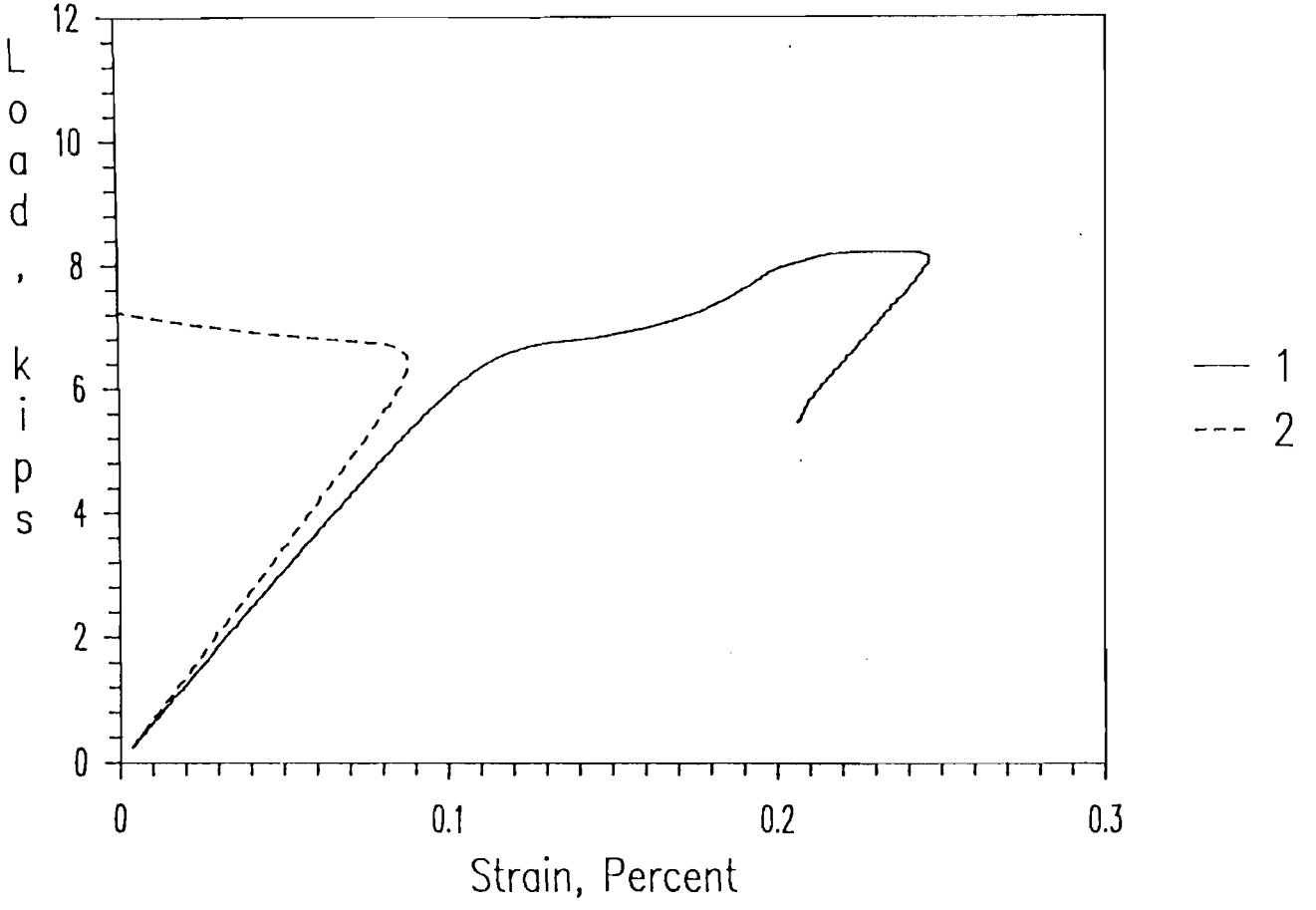

Figure 2.14 Load-Strain Curves of Strain Gages # 1 and 2 Installed at the Center of the Stiffened Flange (Spec. 3C1BX)

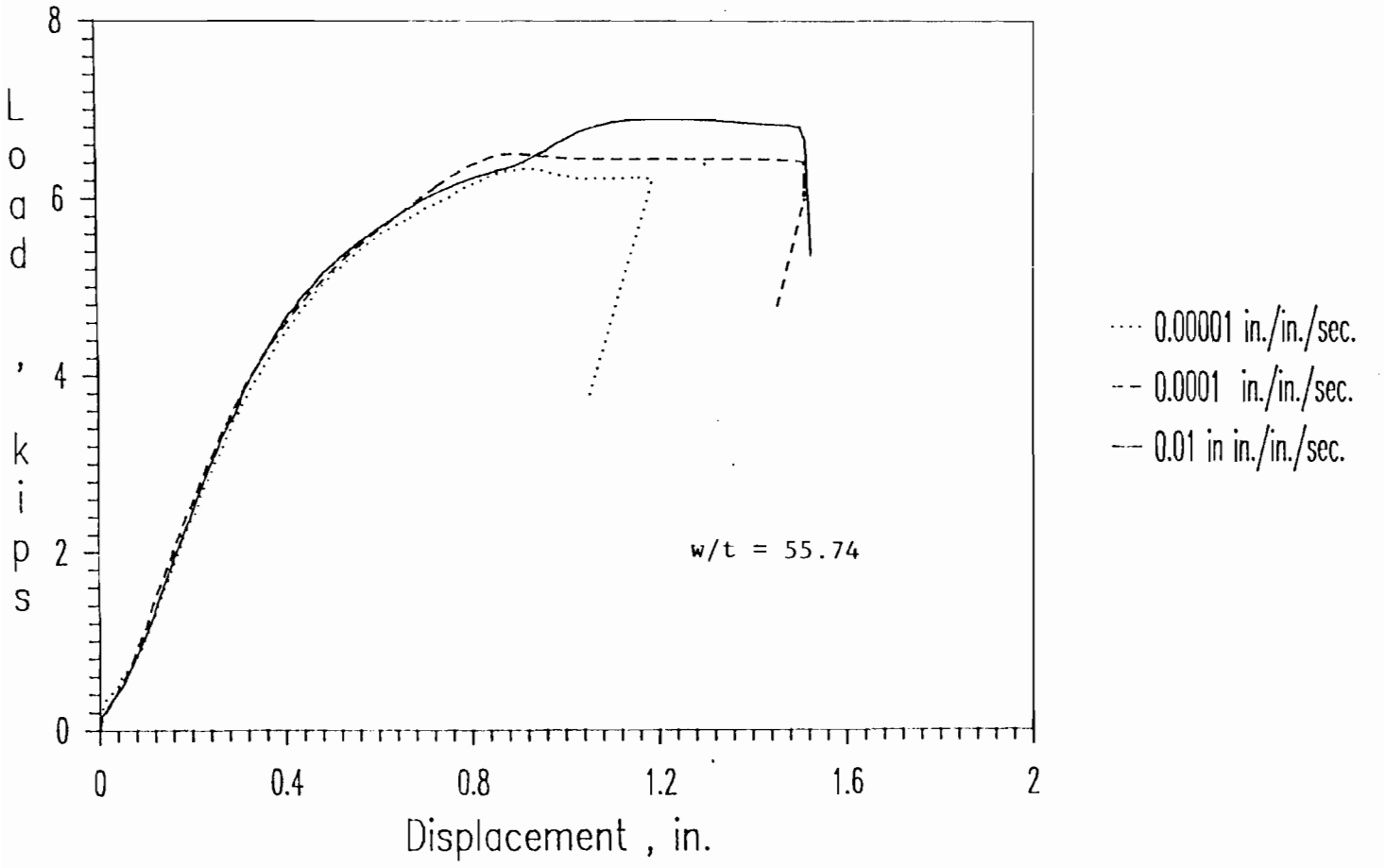

Figure 2.15 Load-Displacement Curves for Hat-Shaped Beam Specimens 3B0A, 3B1A, and 3B2A

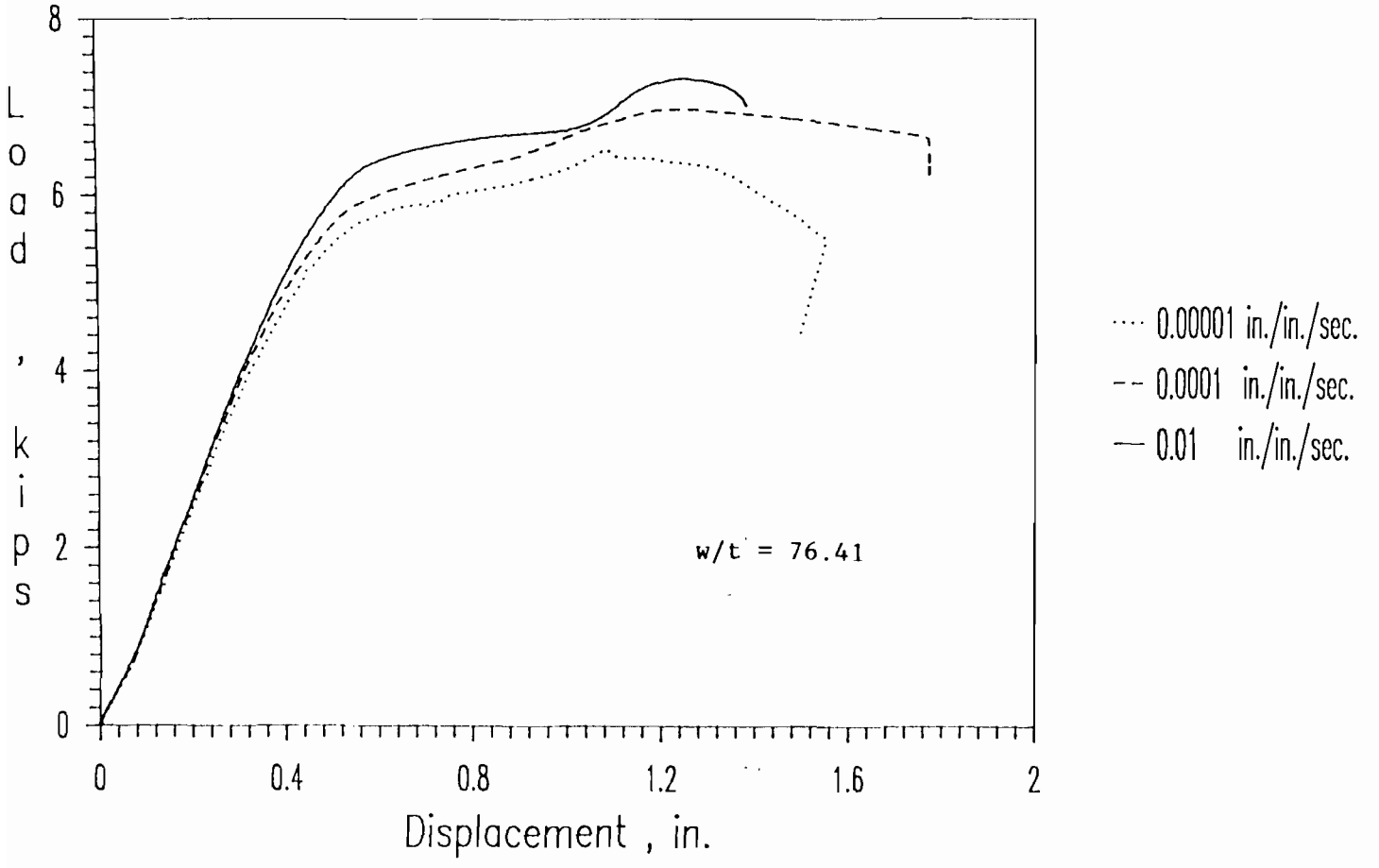

Figure 2.16 Load-Displacement Curves for Hat-Shaped Beam Specimens 3C0A, 3C1A, and 3C2A

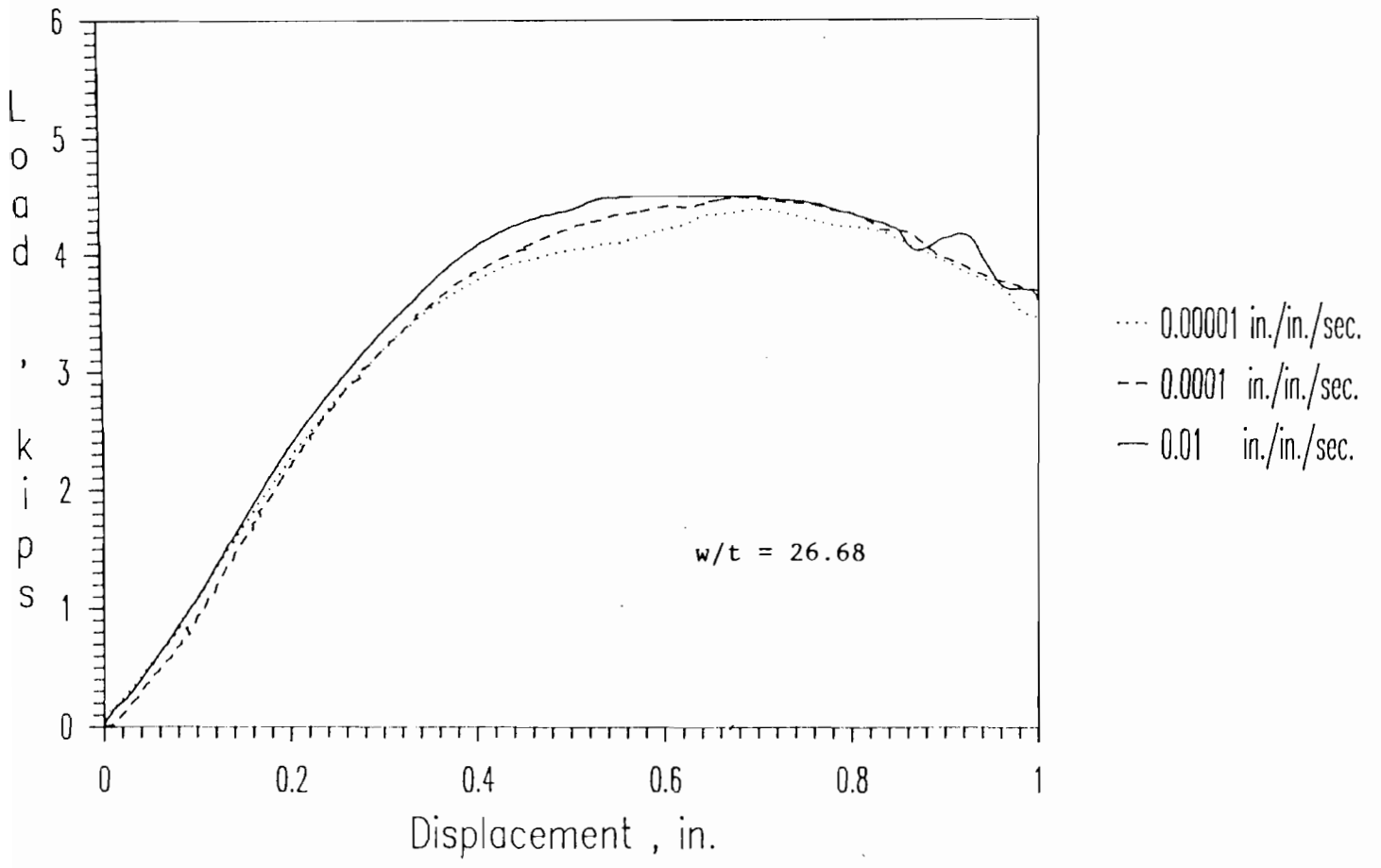

Figure 2.17 Load-Displacement Curves for Hat-Shaped Beam Specimens 3A0AX, 3A1AX, and 3A2AX

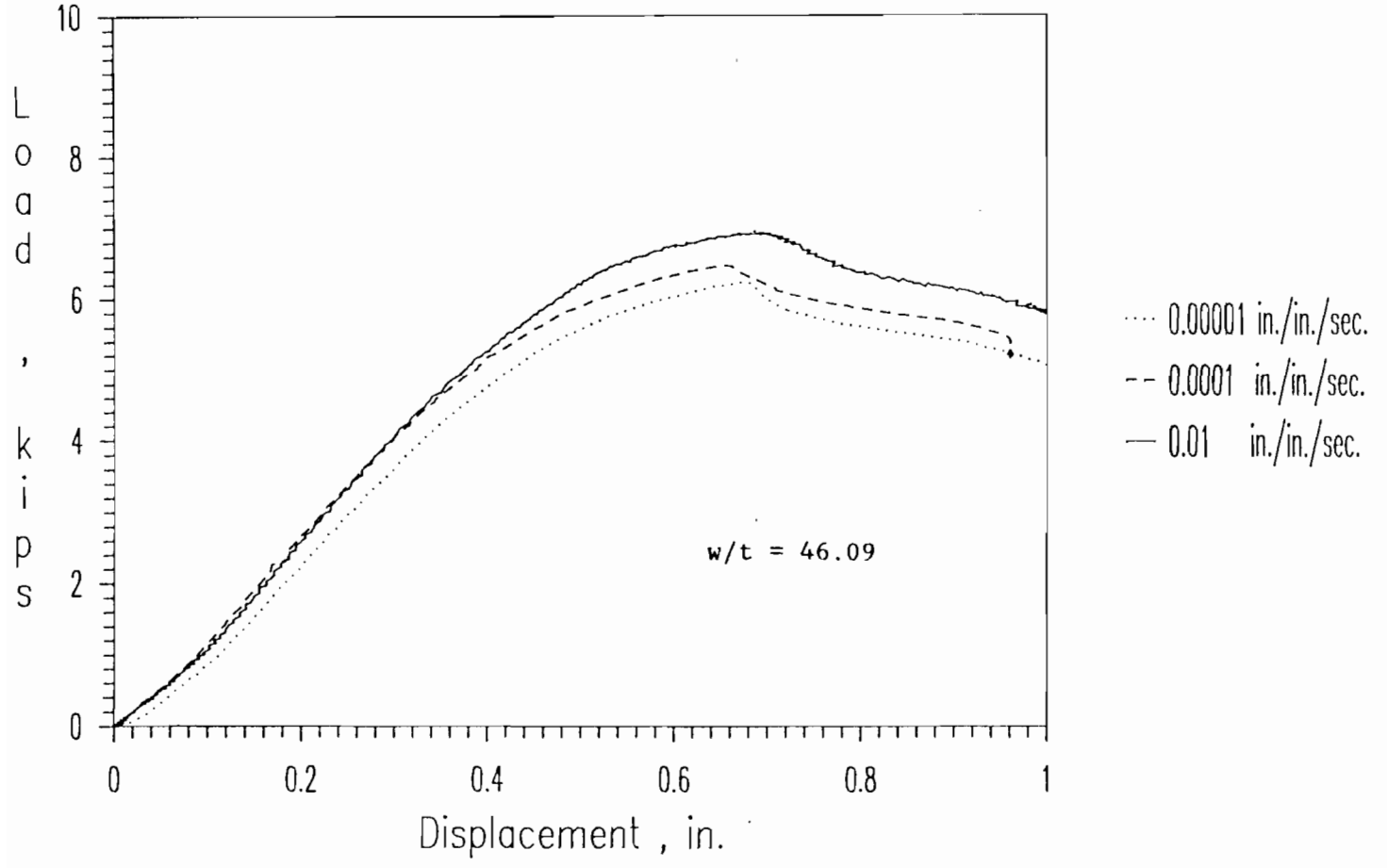

Figure 2.18 Load-Displacement Curves for Hat-Shaped Beam Specimens 3B0AX, 3B1AX, and 3B2BX

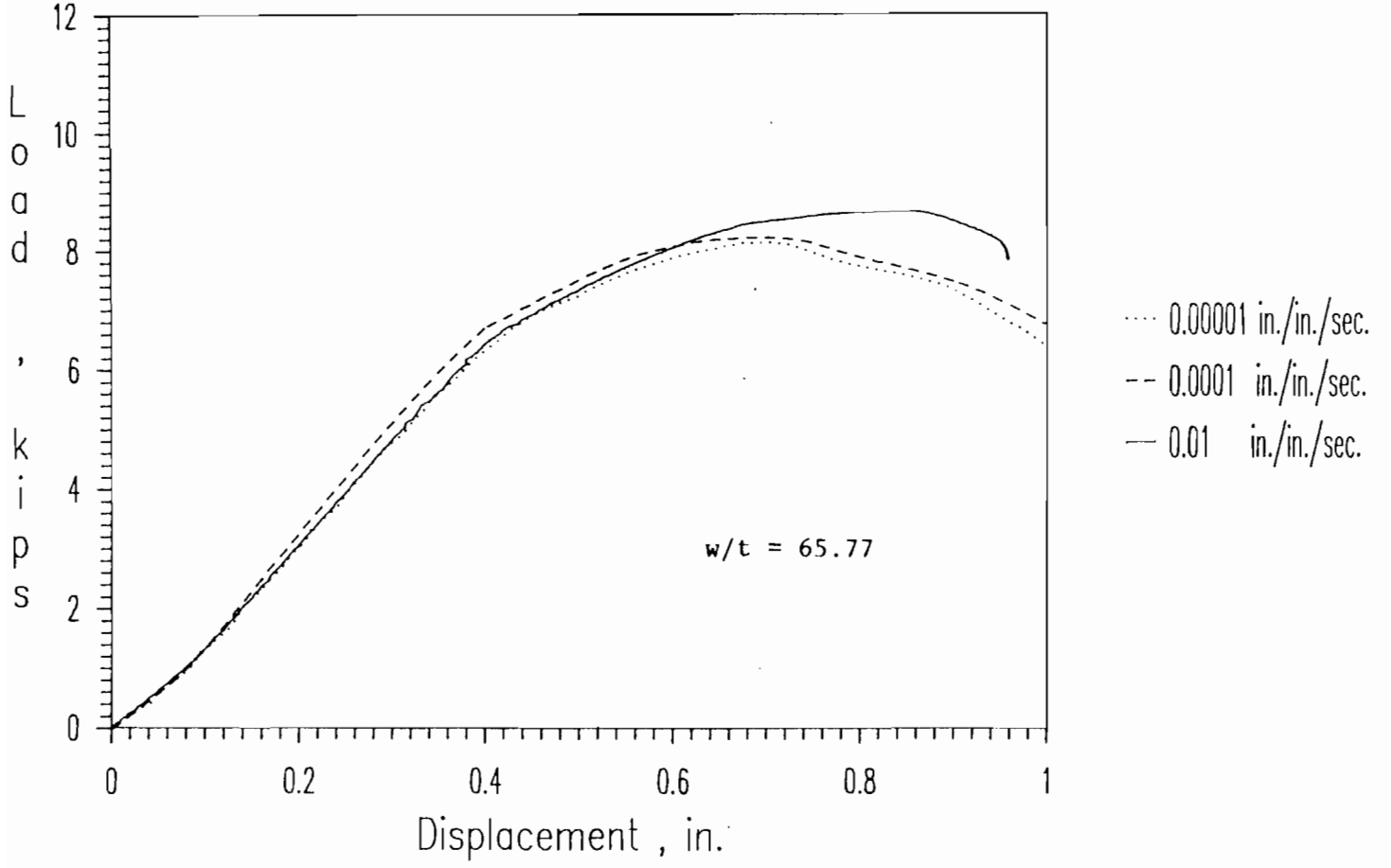

Figure 2.19 Load-Displacement Curves for Hat-Shaped Beam Specimens 3C0AX, 3C1BX, and 3C2AX

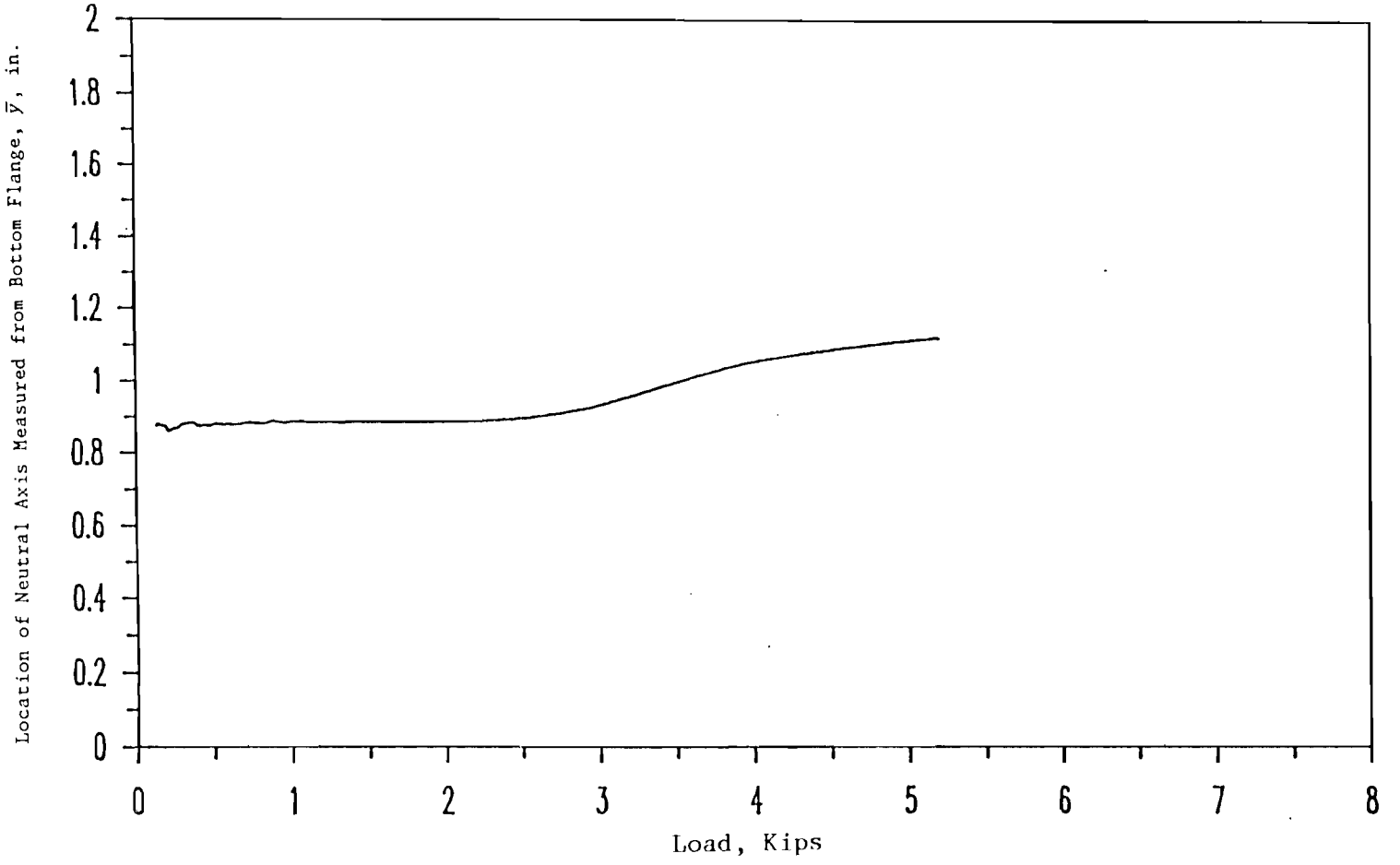

Figure 2.20 Typical Plot of Load vs. Location of Neutral Axis for Beam with a Stiffened Flange (Spec. 3A0A)

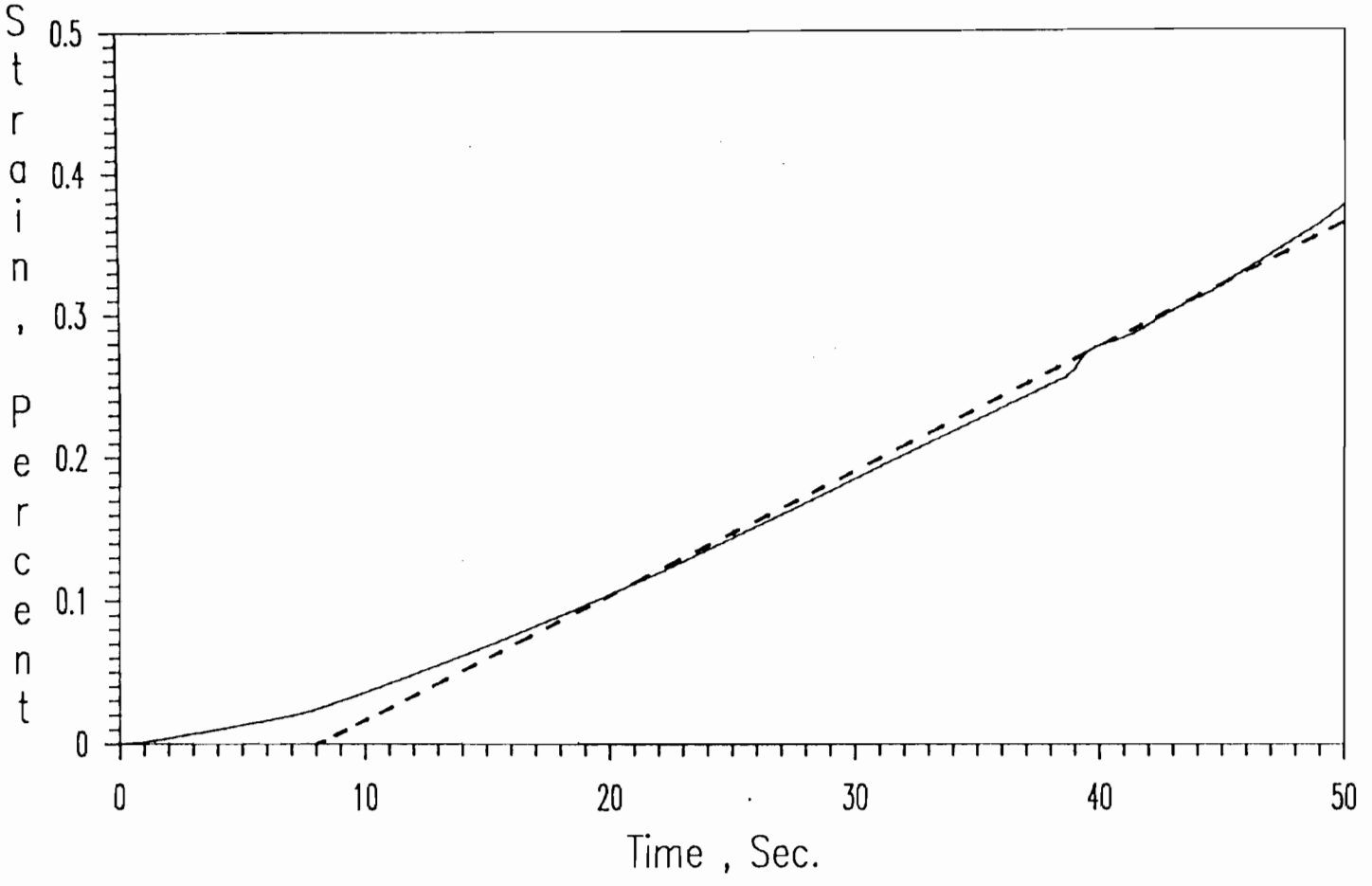

Figure 2.21 Typical Plot of Strain-Time Relationship for Hat-Shaped Beam Specimen Under a Strain Rate of 10^{-4} in./in./sec. (Spec. 3A1AX)

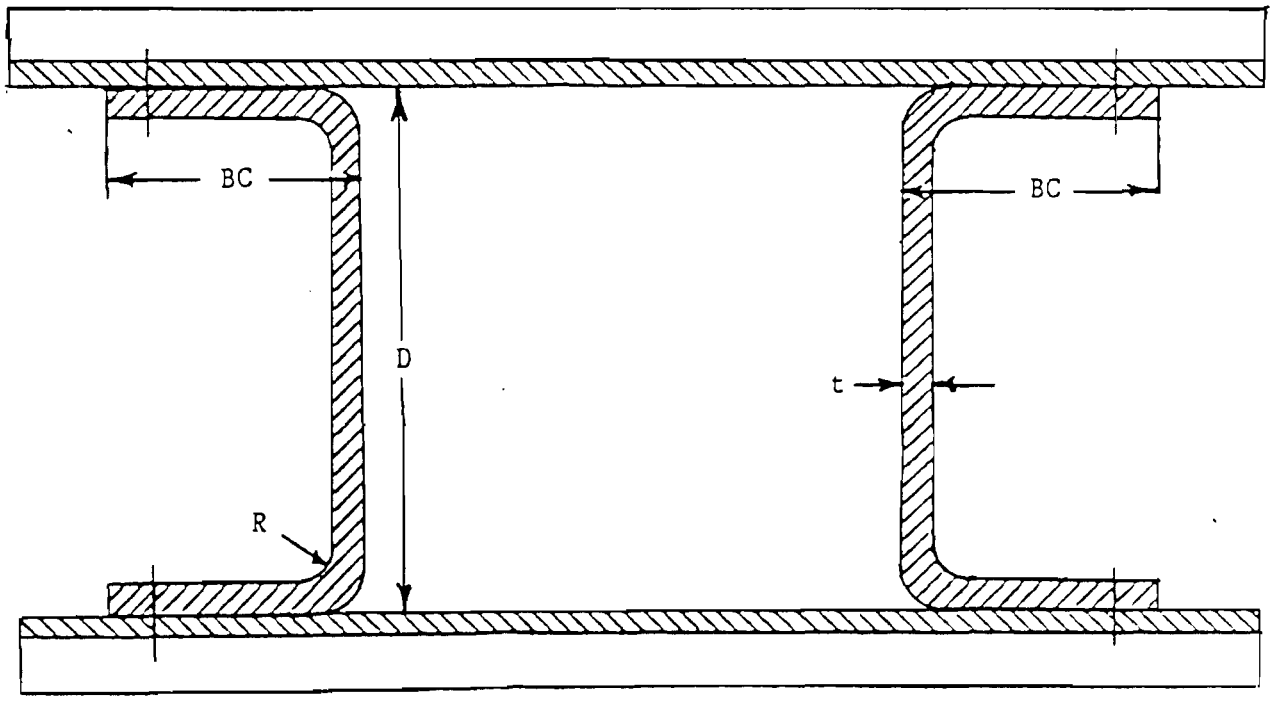

Figure 2.22 Cross Sections of Channel Beams Used for the Study of Unstiffened Elements

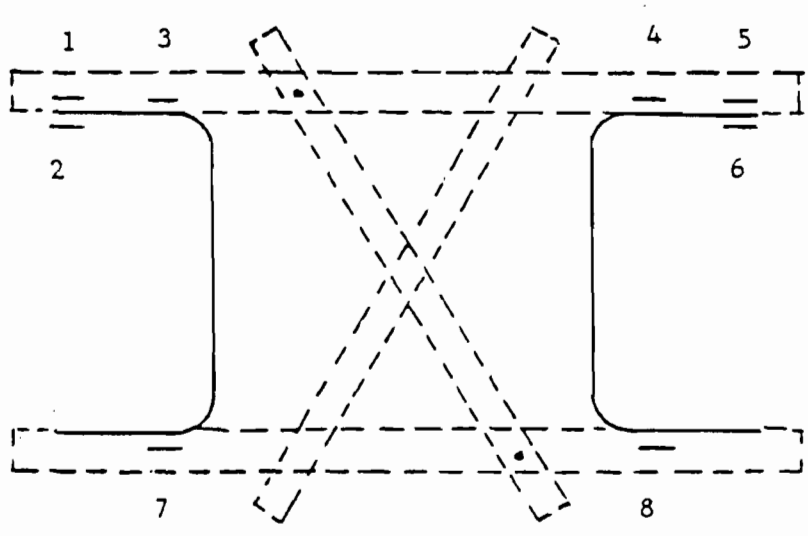

Figure 2.23 Locations of Strain Gages at Midspan Section of Channel Beams

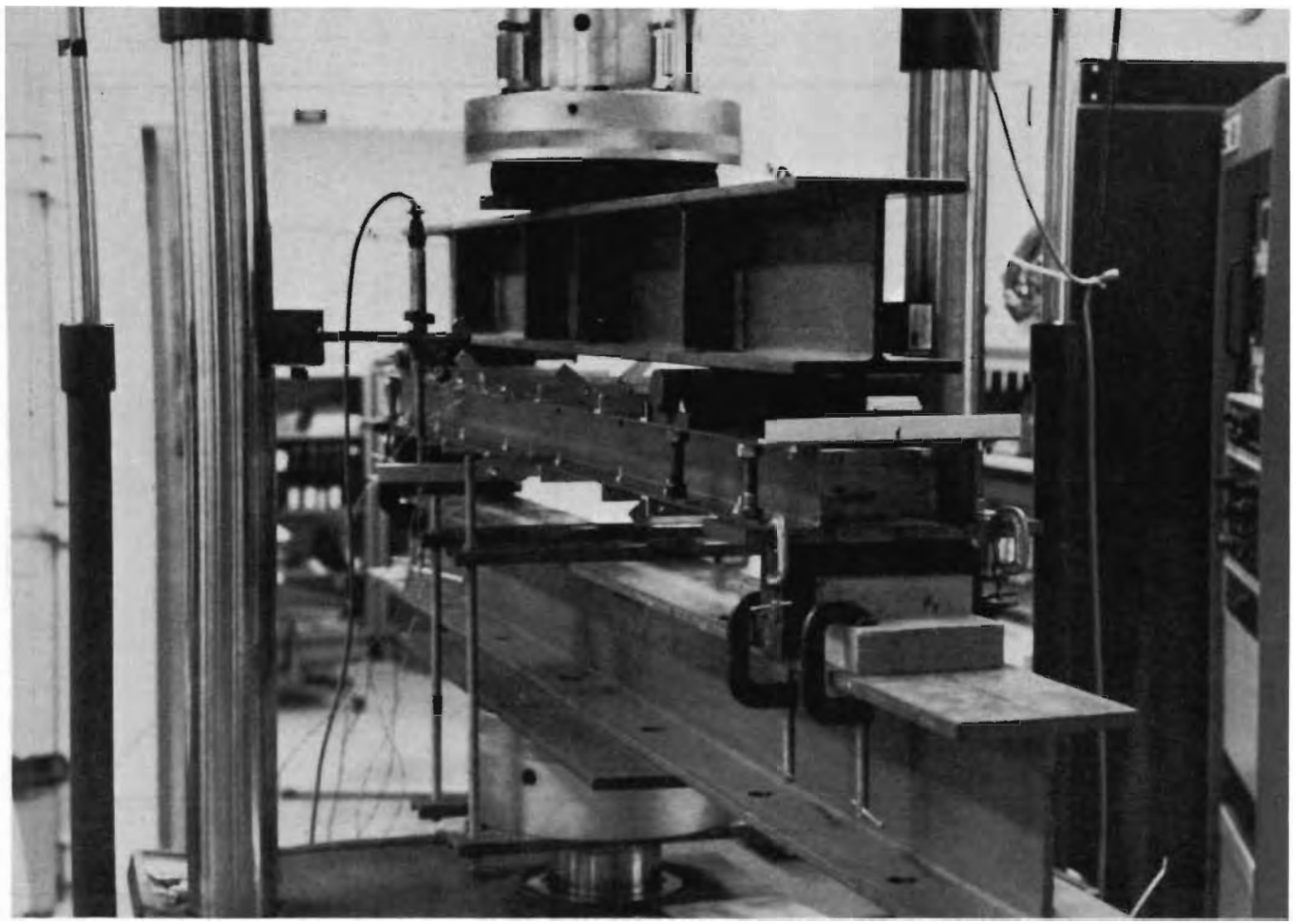

Figure 2.24 Photograph of Test Setup for Channel Beam Specimens

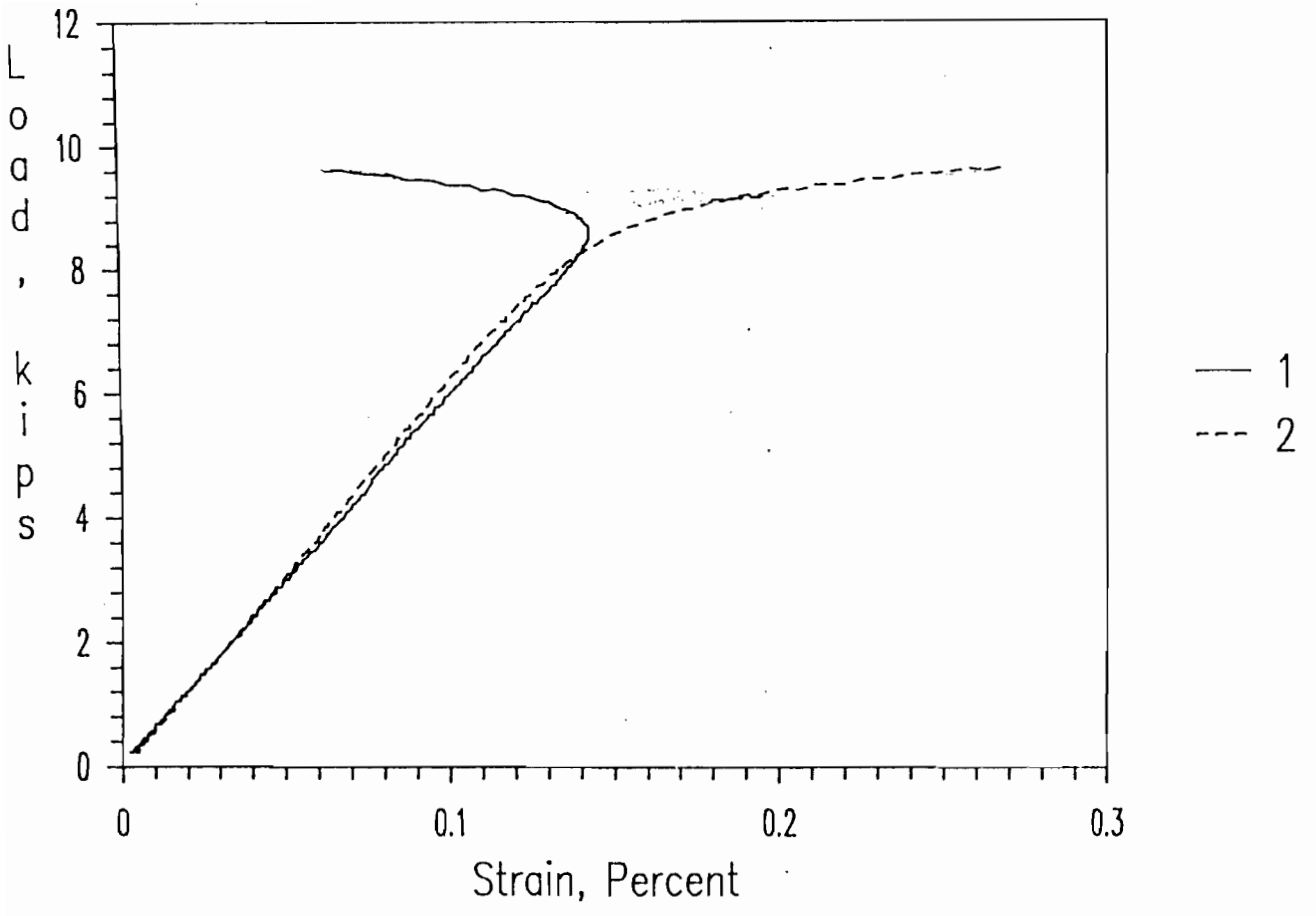

Figure 2.25 Load-Strain Curves of Strain Gages # 1 and 2 Installed at the Center of the Stiffened Flange (Spec. 4C2AX)

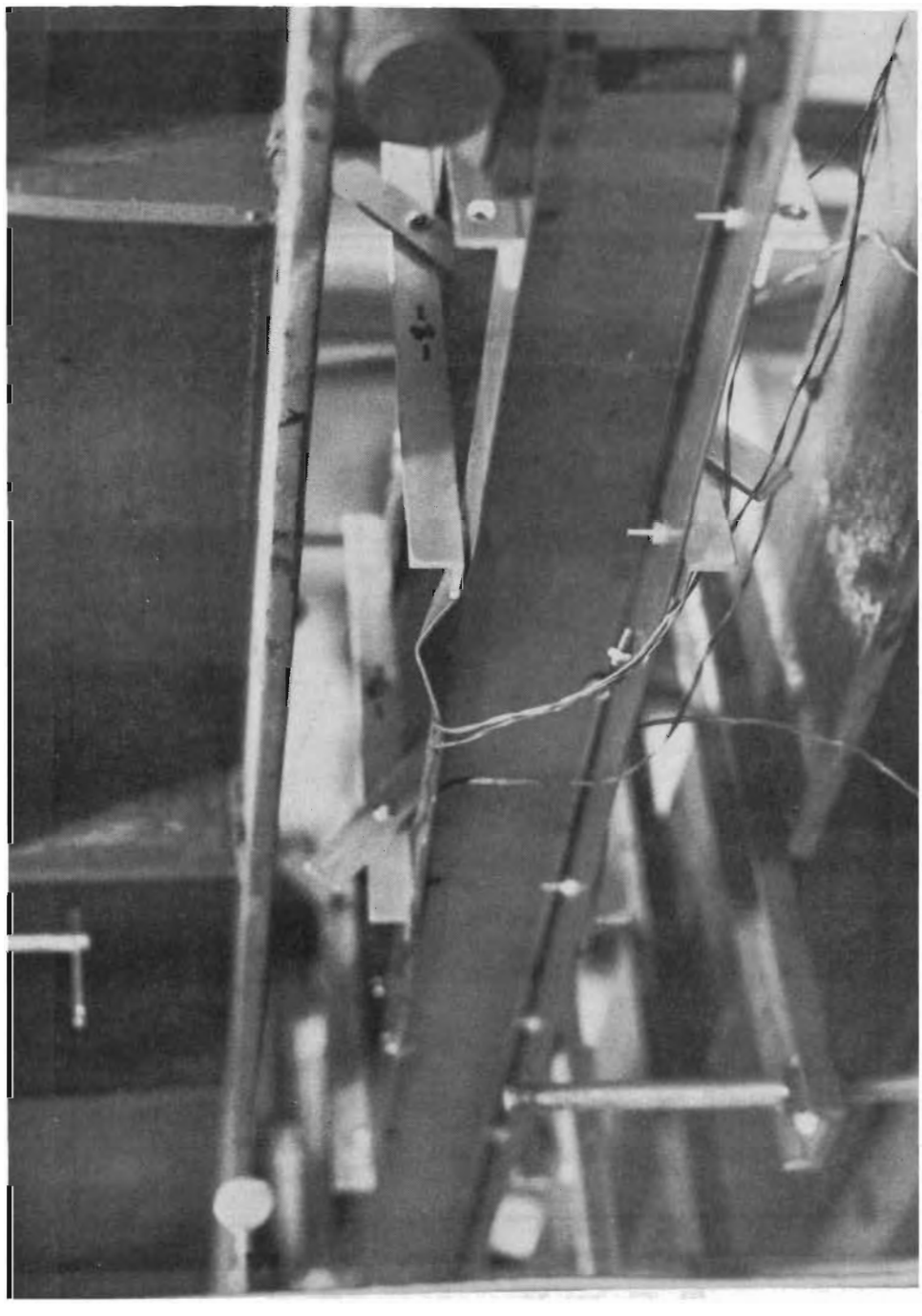

Figure 2.26 Typical Failure of Channel Beam Specimens

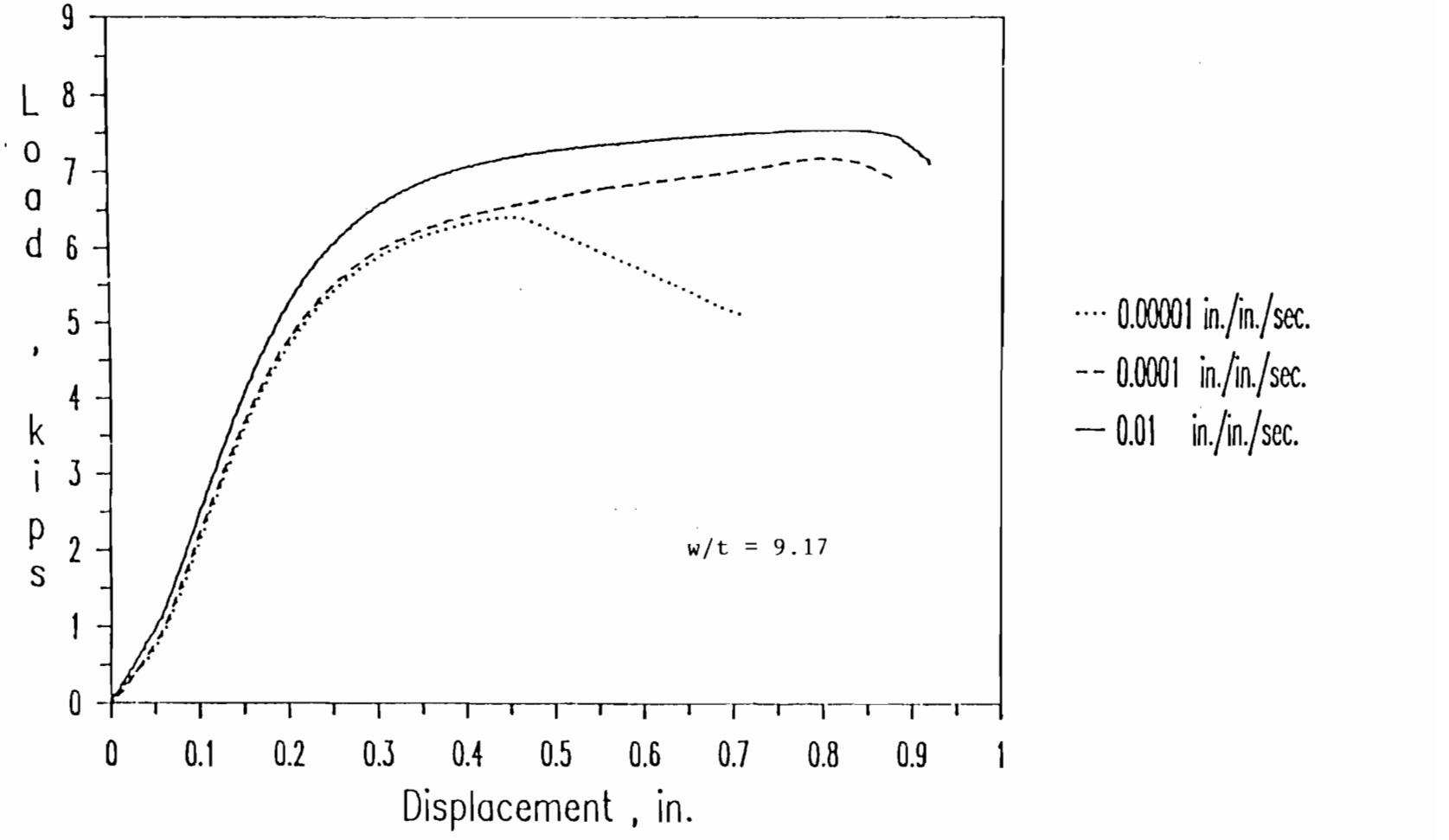

Figure 2.27 Load-Displacement Curves for Channel Beam Specimens 4A0A, 4A1A, and 4A2A

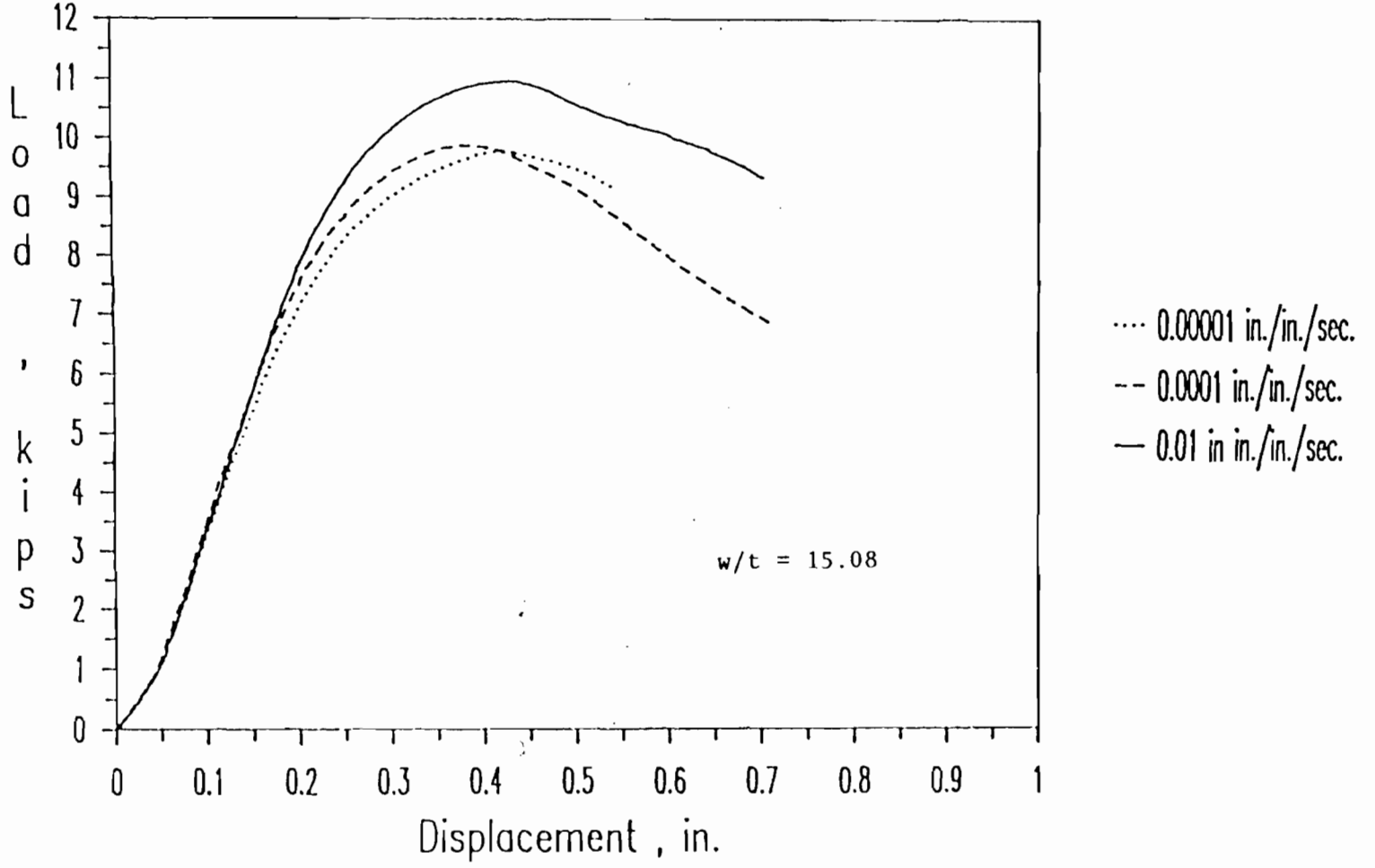

Figure 2.28 Load-Displacement Curves for Channel Beam Specimens 4B0A, 4B1A, and 4B2A

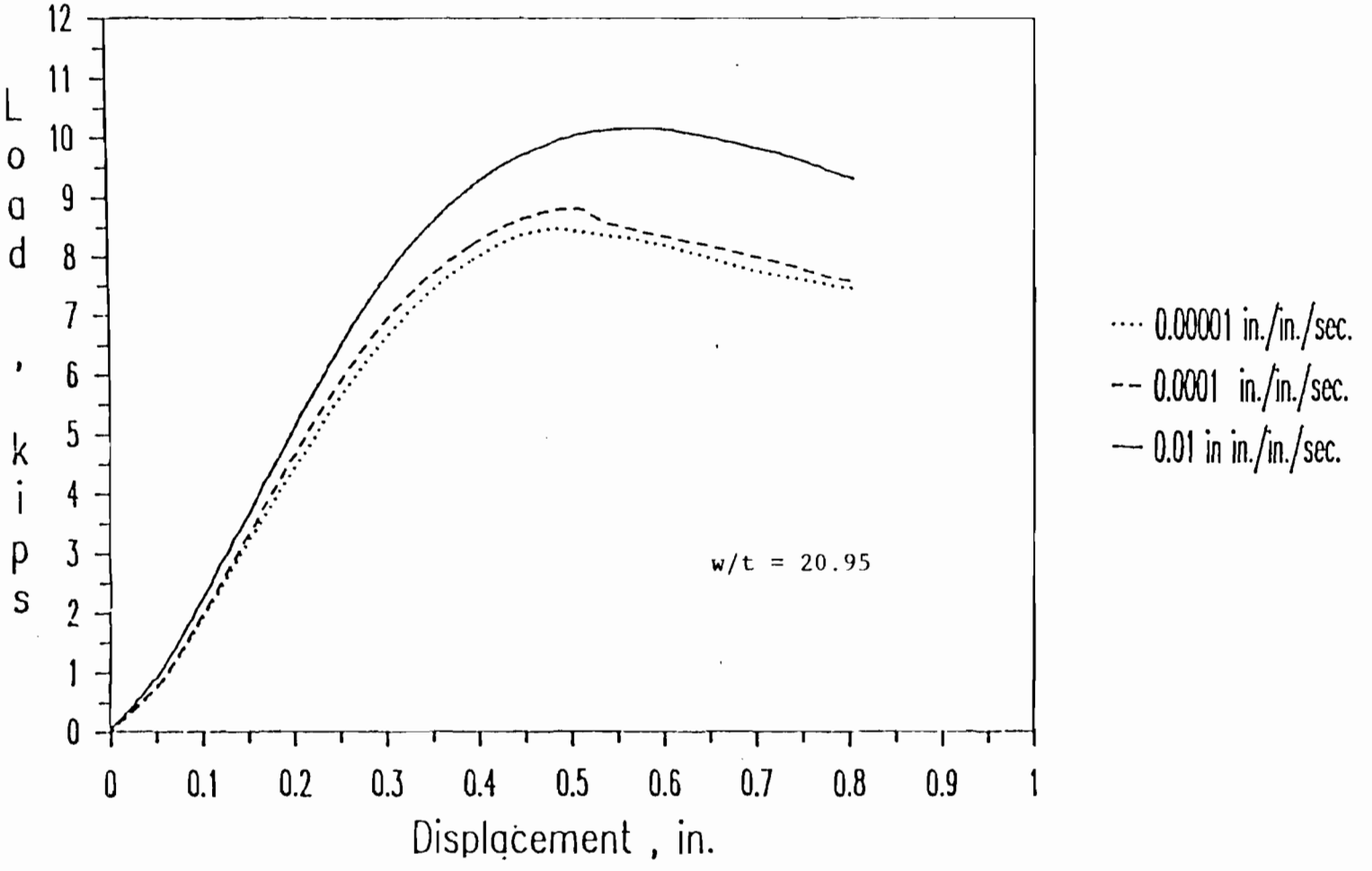

Figure 2.29 Load-Displacement Curves for Channel Beam Specimens 4C0A, 4C1A, and 4C2A

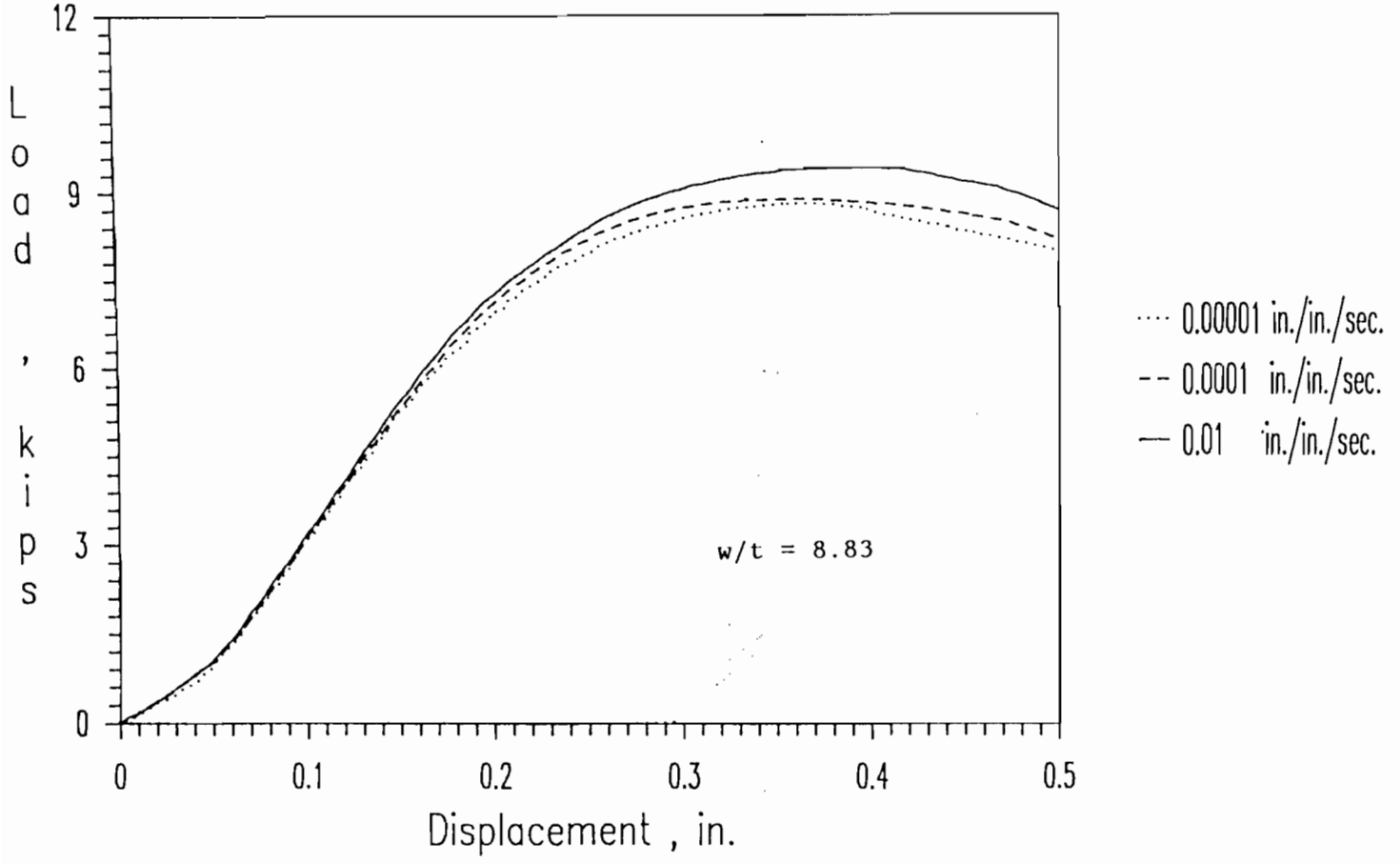

Figure 2.30 Load-Displacement Curves for Channel Beam Specimens 4A0AX, 4A1AX, and 4A2AX

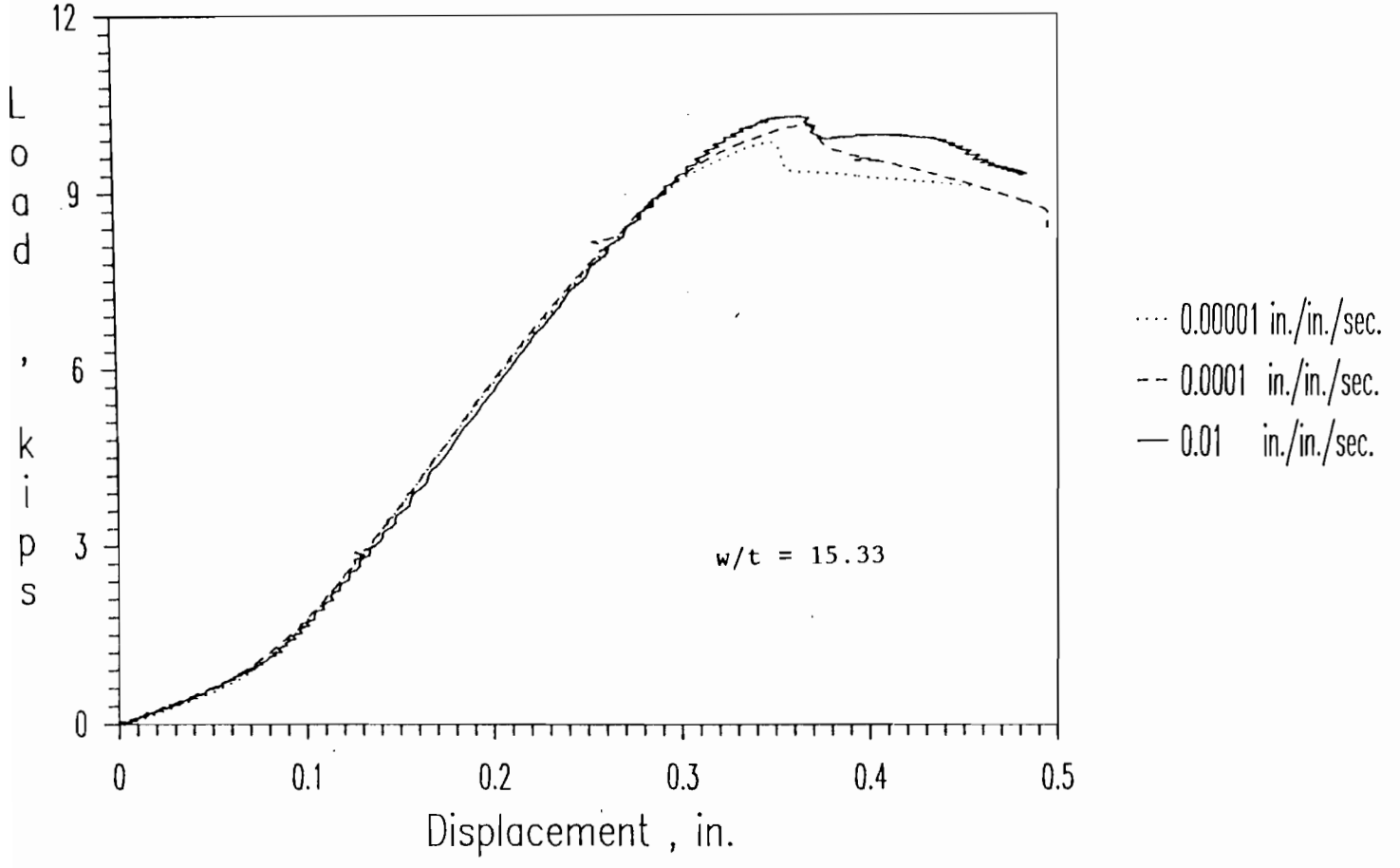

Figure 2.31 Load-Displacement Curves for Channel Beam Specimens 4B0AX, 4B1BX, and 4B2BX

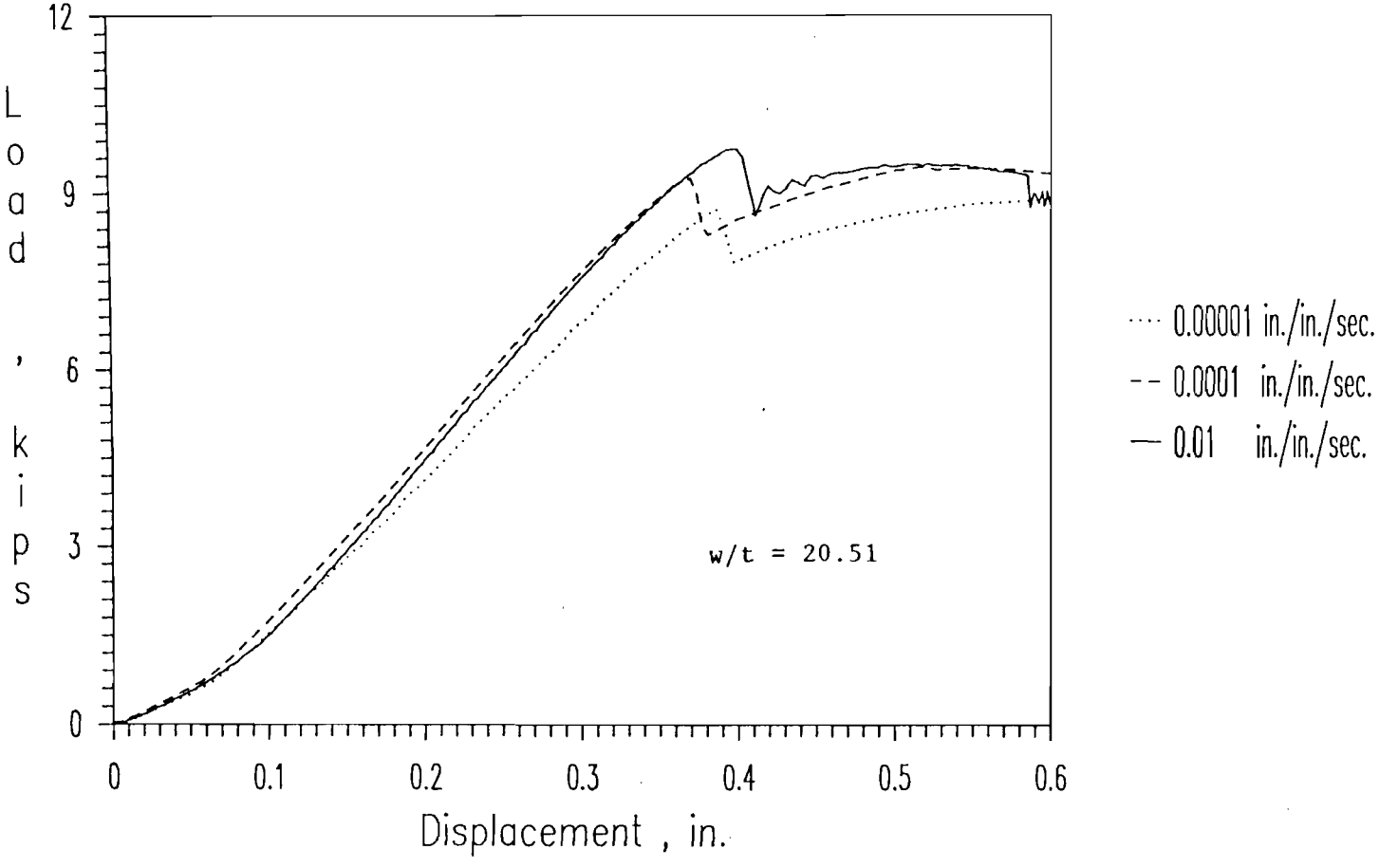

Figure 2.32 Load-Displacement Curves for Channel Beam Specimens 4C0AX, 4C1AX, and 4C2BX

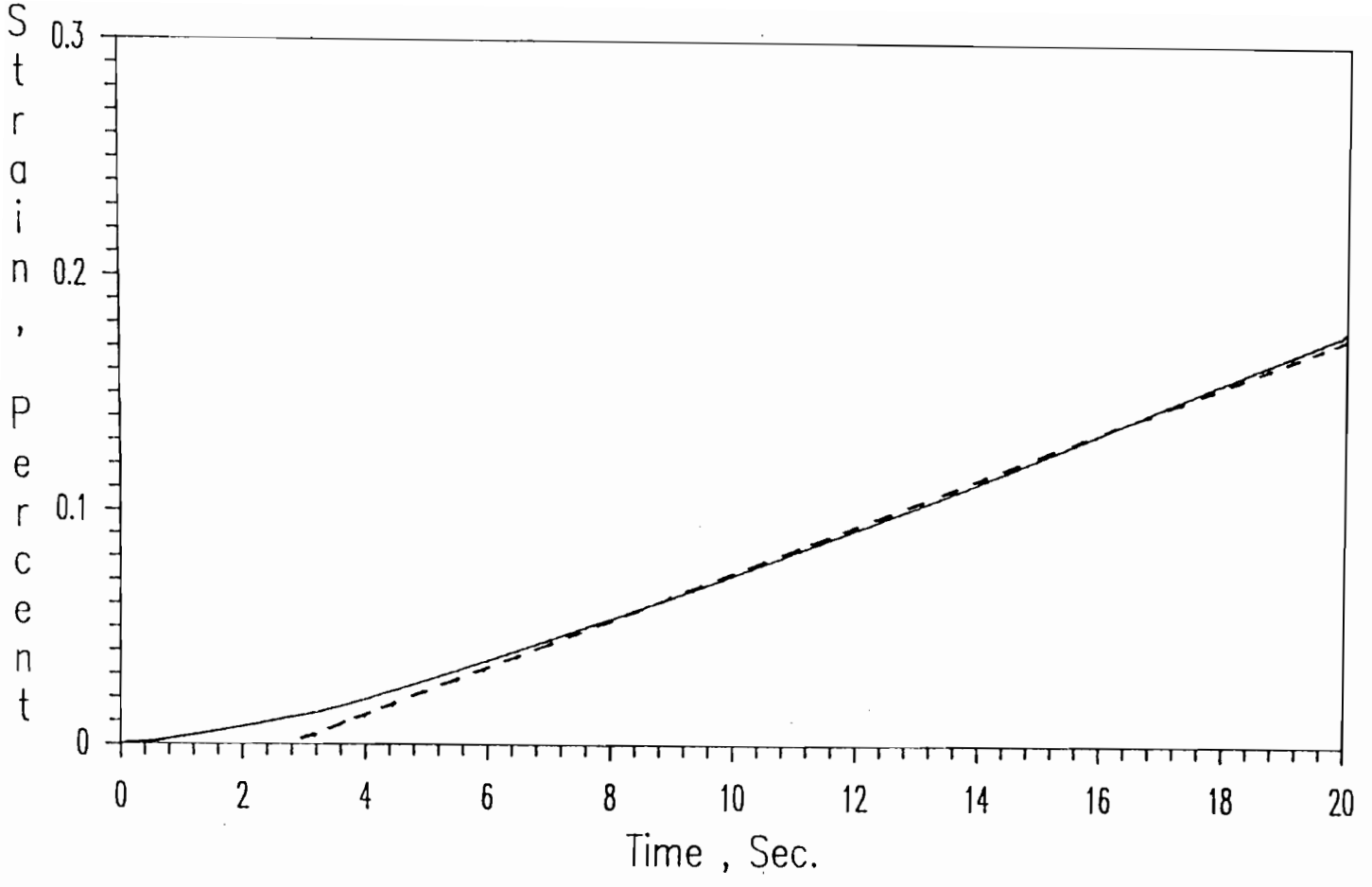

Figure 2.33 Typical Plot of Strain-Time Relationship for Channel Beam Specimen Under a Strain Rate of 10^{-4} in./in./sec. (Spec. 4C1AX)

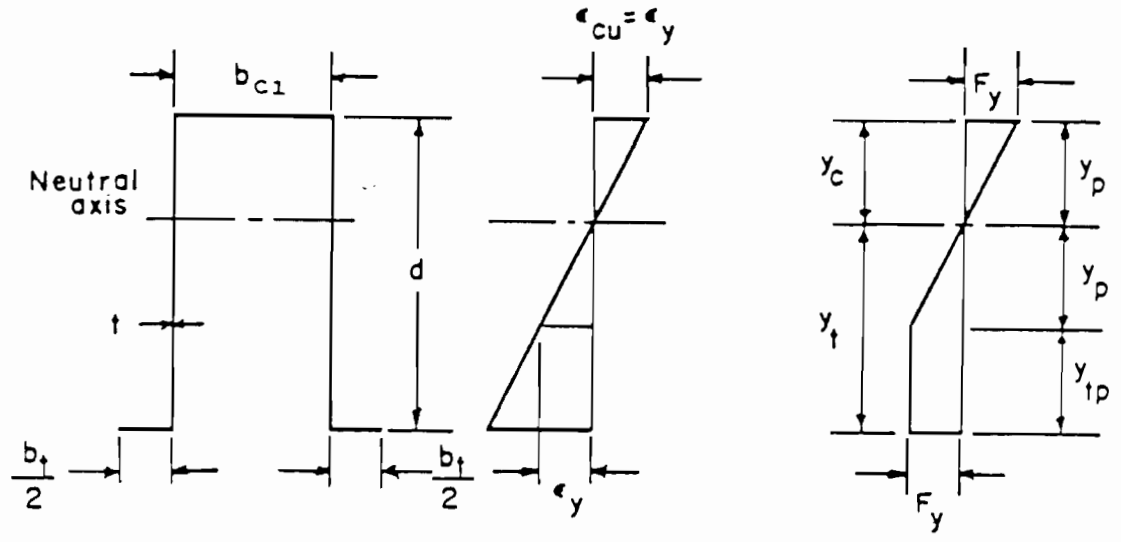

(a)

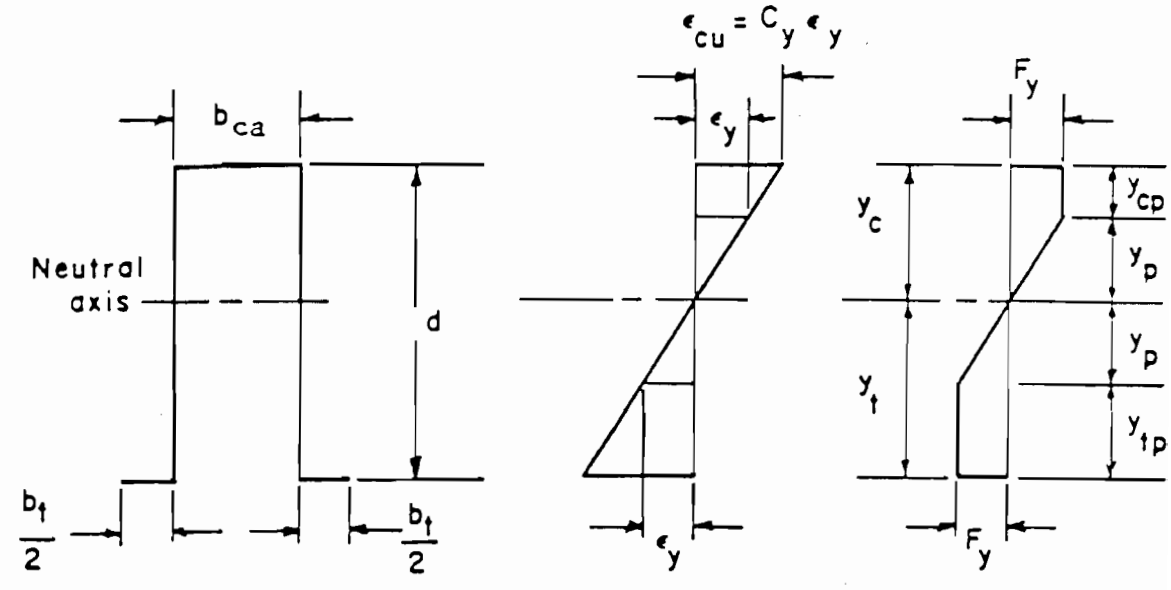

(b)

Figure 3.1 Stress Distribution in Sections with Yielded Tension Flanges at Ultimate Moments[12]

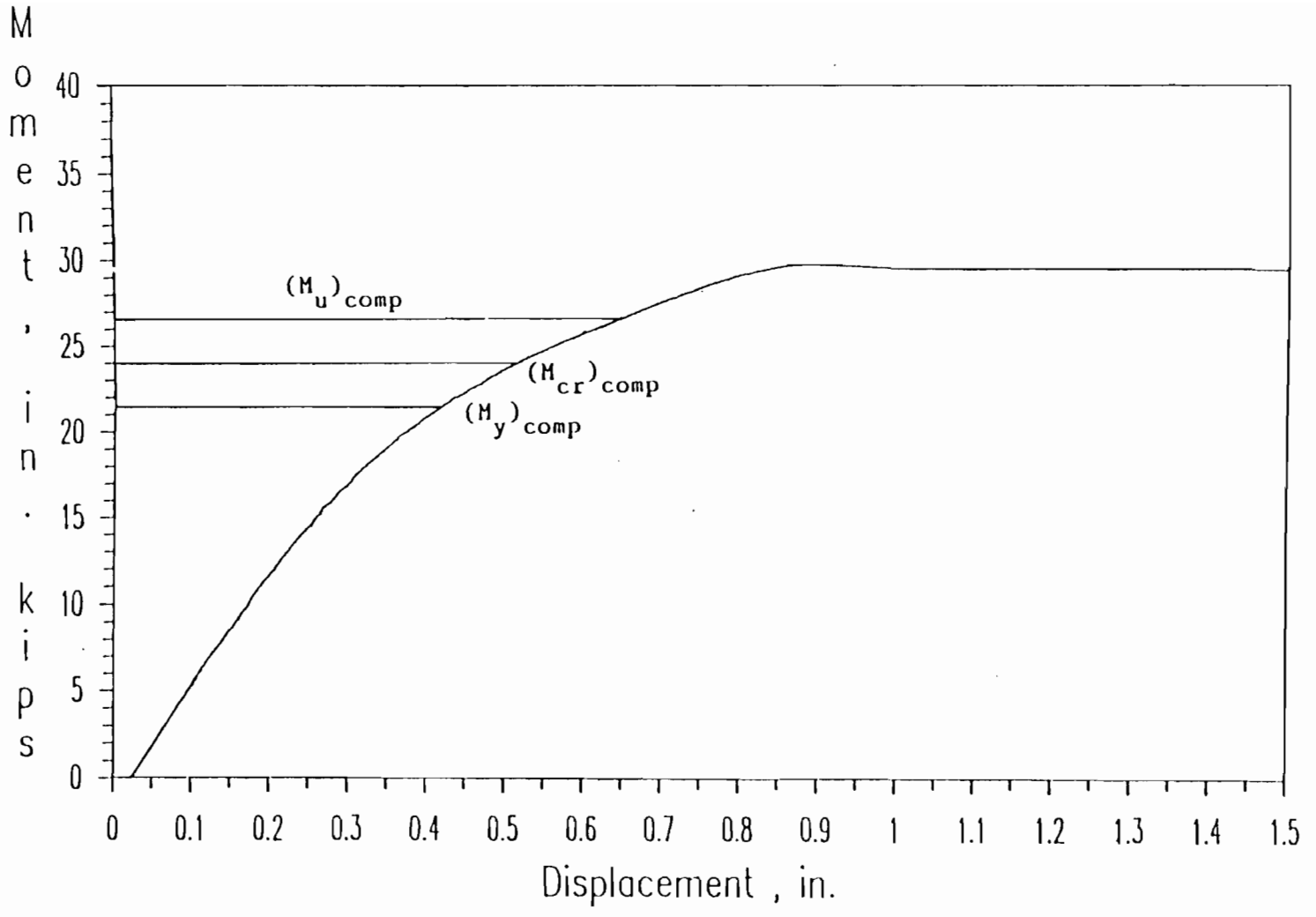

Figure 3.2 Moment-Displacement Curve for Hat-Shaped Beam Specimens (Spec. 3B1A)

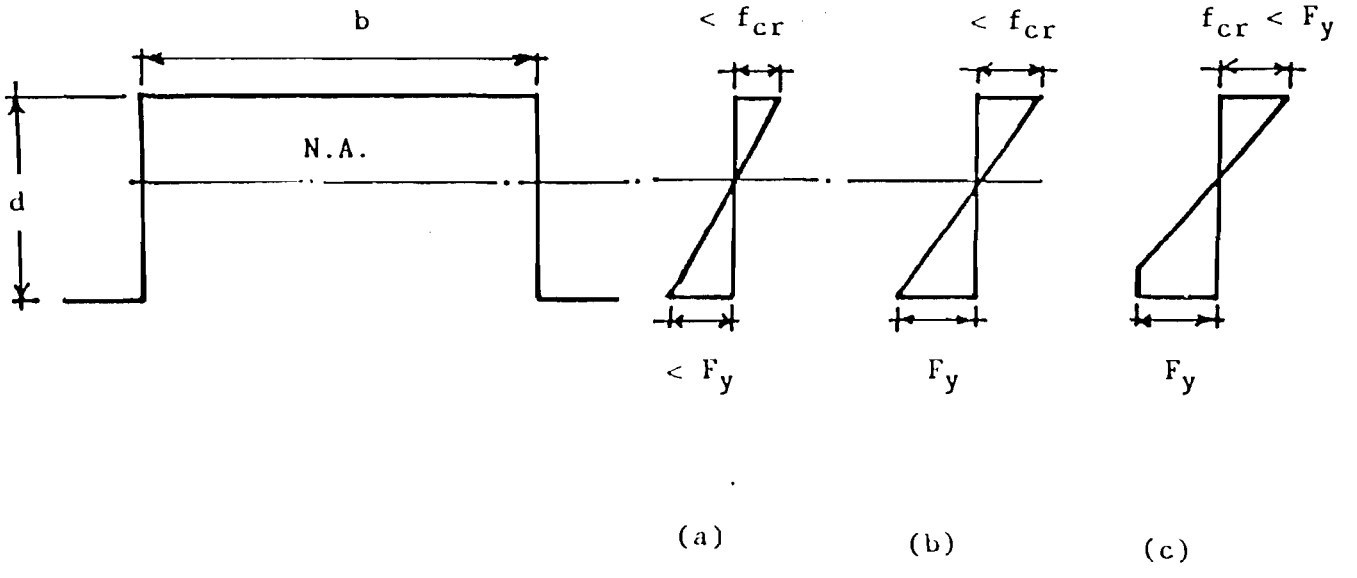

Figure 3.3 Stress Distribution in Hat Sections

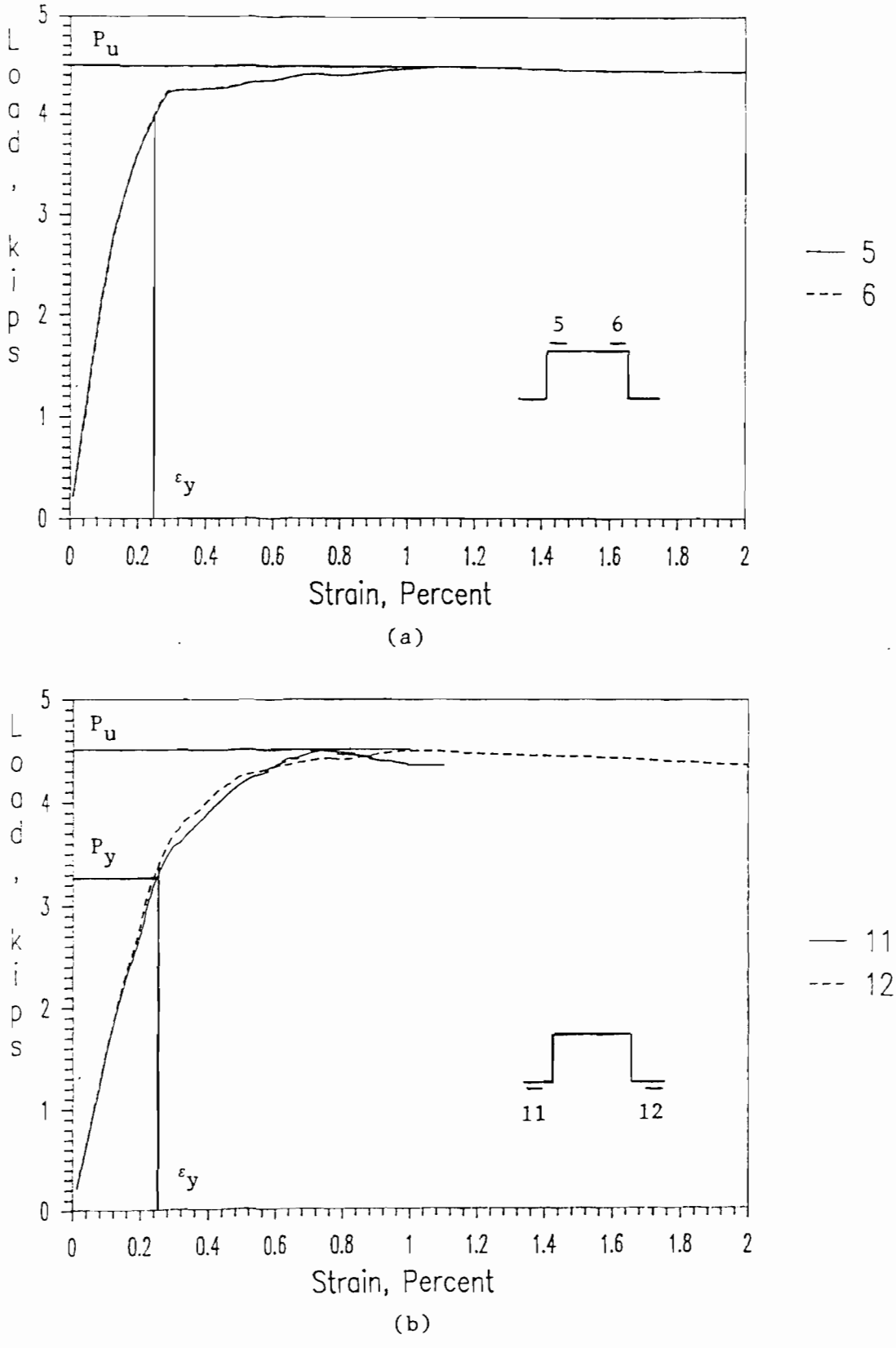

Figure 3.4 Load-Strain Curves for Hat-Shaped Beam Specimen Using 50XF Sheet Steel (3A1AX) (a) Compressive Strain (b) Tensile Strain

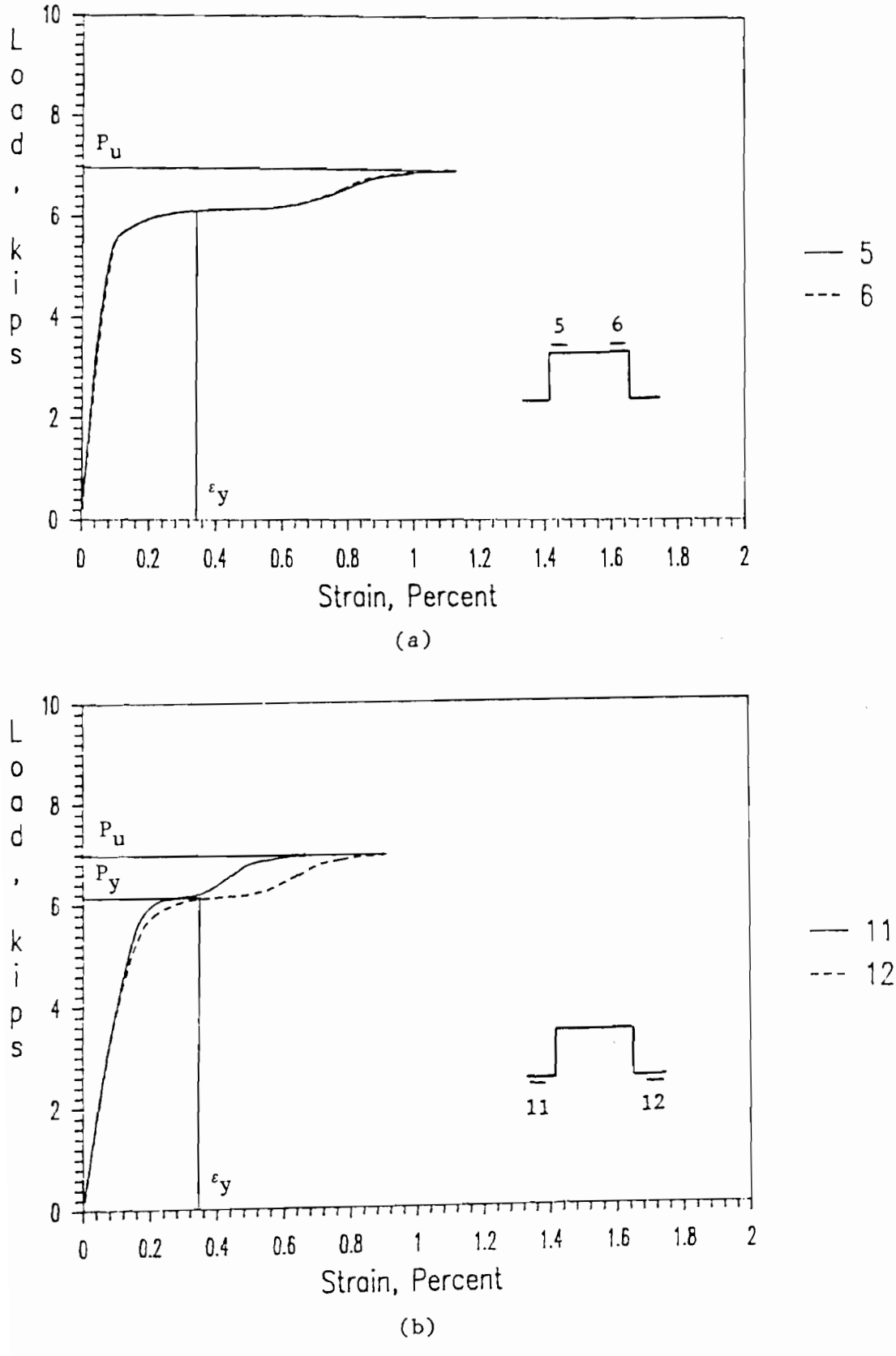

Figure 3.5 Load-Strain Curves for Hat-Shaped Beam Specimen Using 35XF Sheet Steel (3C1B) (a) Compressive Strain (b) Tensile Strain

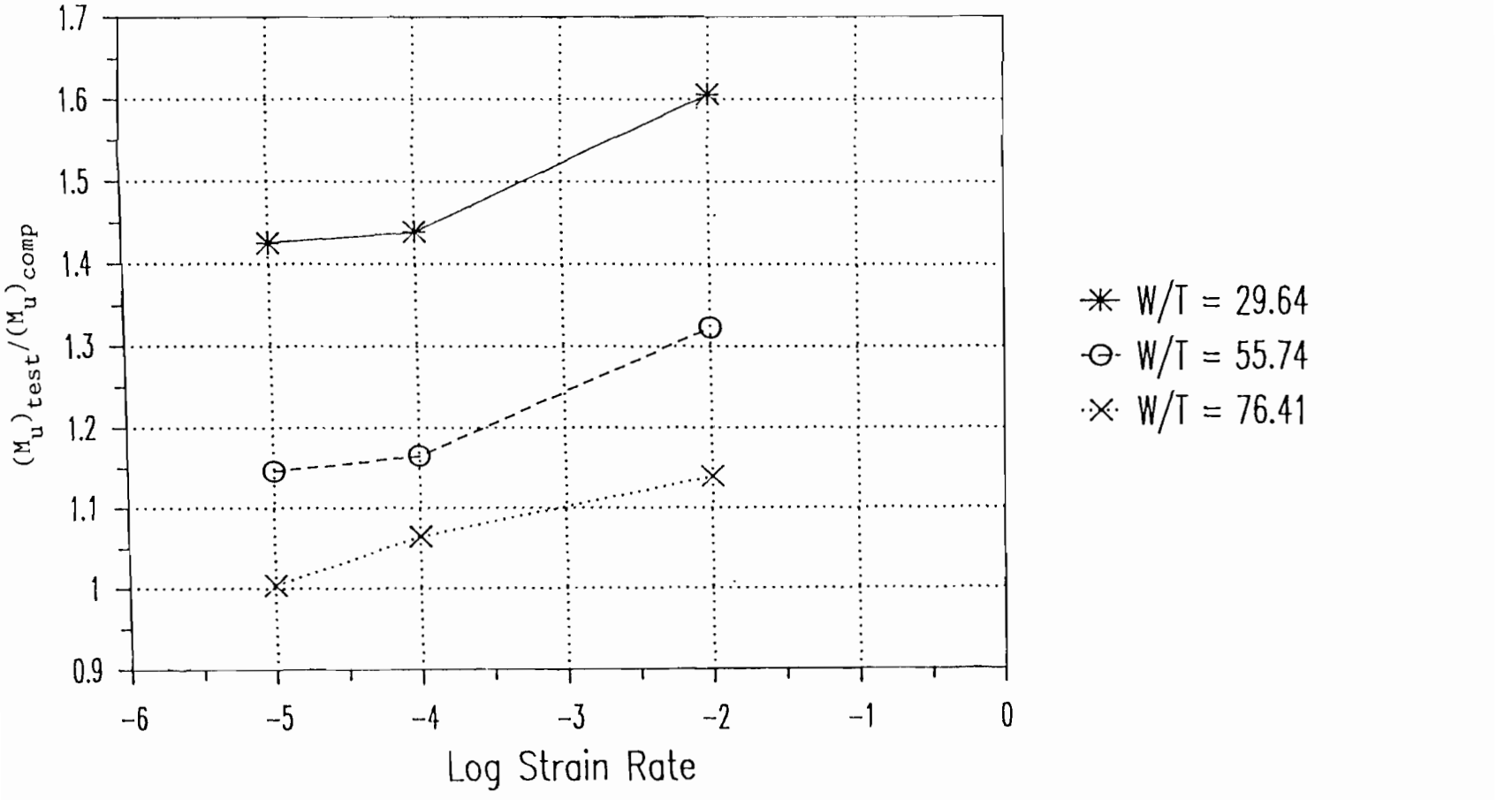

Figure 3.6 Ratios of Tested Failure Moments to Computed Failure Moments (Based on Static Yield Stress) vs. Logarithmic Strain Rate for Hat-Shaped Beams (35XF Sheet Steel)

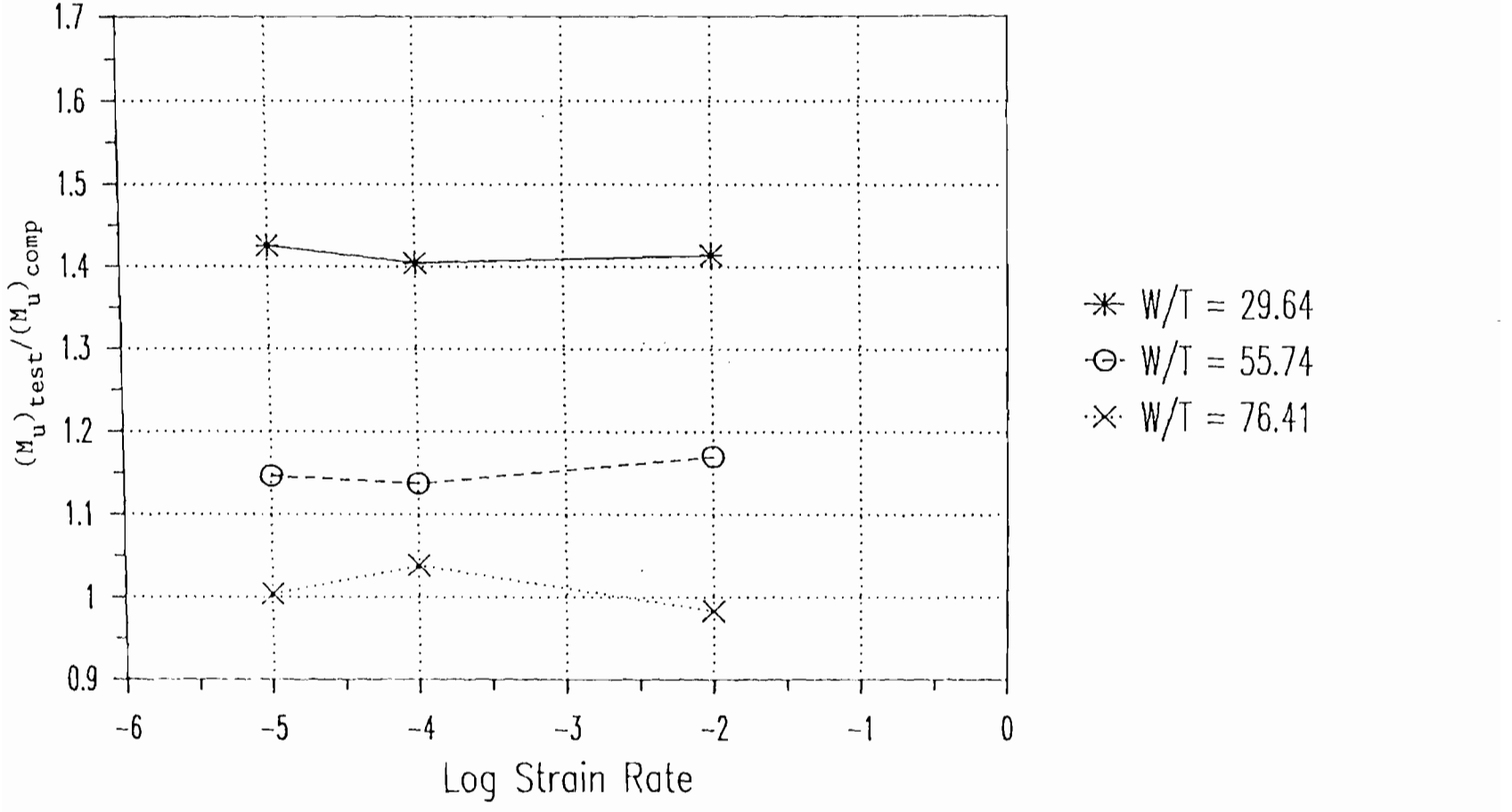

Figure 3.7 Ratios of Tested Failure Moments to Computed Failure Moments (Based on Dynamic Yield Stress) vs. Logarithmic Strain Rate for Hat-Shaped Beams (35XF Sheet Steel)

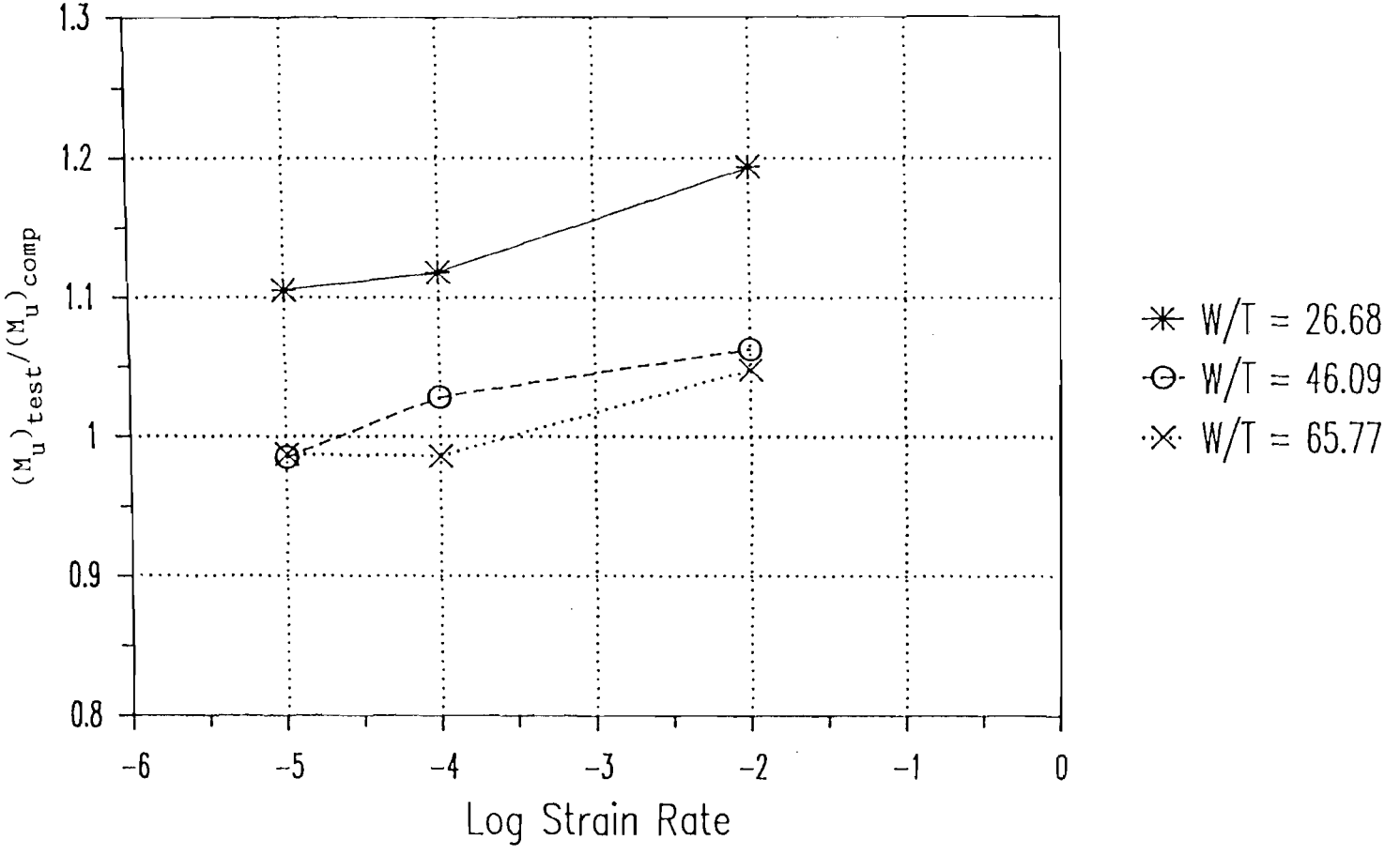

Figure 3.8 Ratios of Tested Failure Moments to Computed Failure Moments (Based on Static Yield Stress) vs. Logarithmic Strain Rate for Hat-Shaped Beams (50XF Sheet Steel)

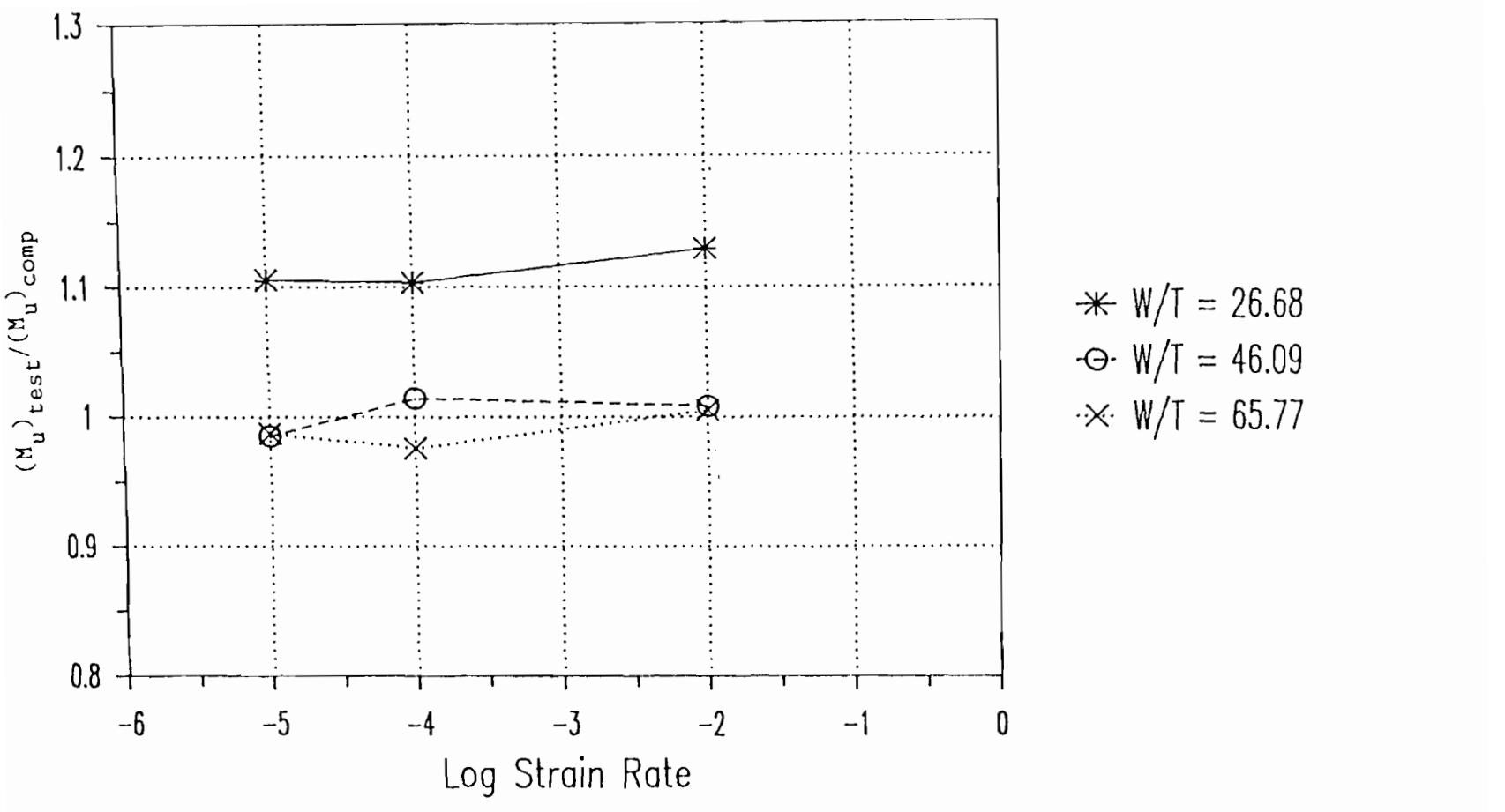

Figure 3.9 Ratios of Tested Failure Moments to Computed Failure Moments (Based on Dynamic Yield Stress) vs. Logarithmic Strain Rate for Hat-Shaped Beams (50XF Sheet Steel)

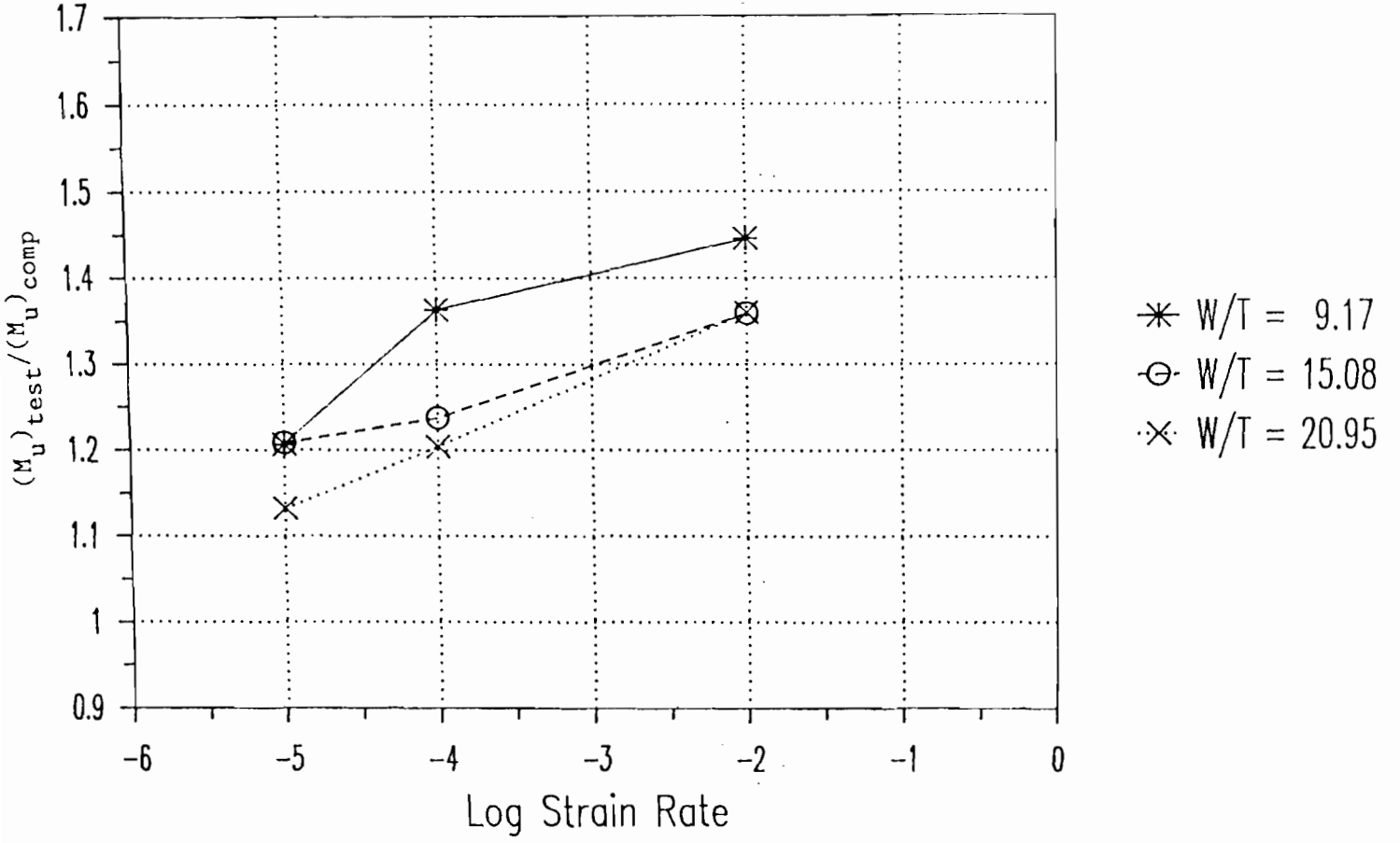

Figure 3.10 Ratios of Tested Failure Moments to Computed Failure Moments (Based on Static Yield Stress) vs. Logarithmic Strain Rate for Channel Beams (35XF Sheet Steel)

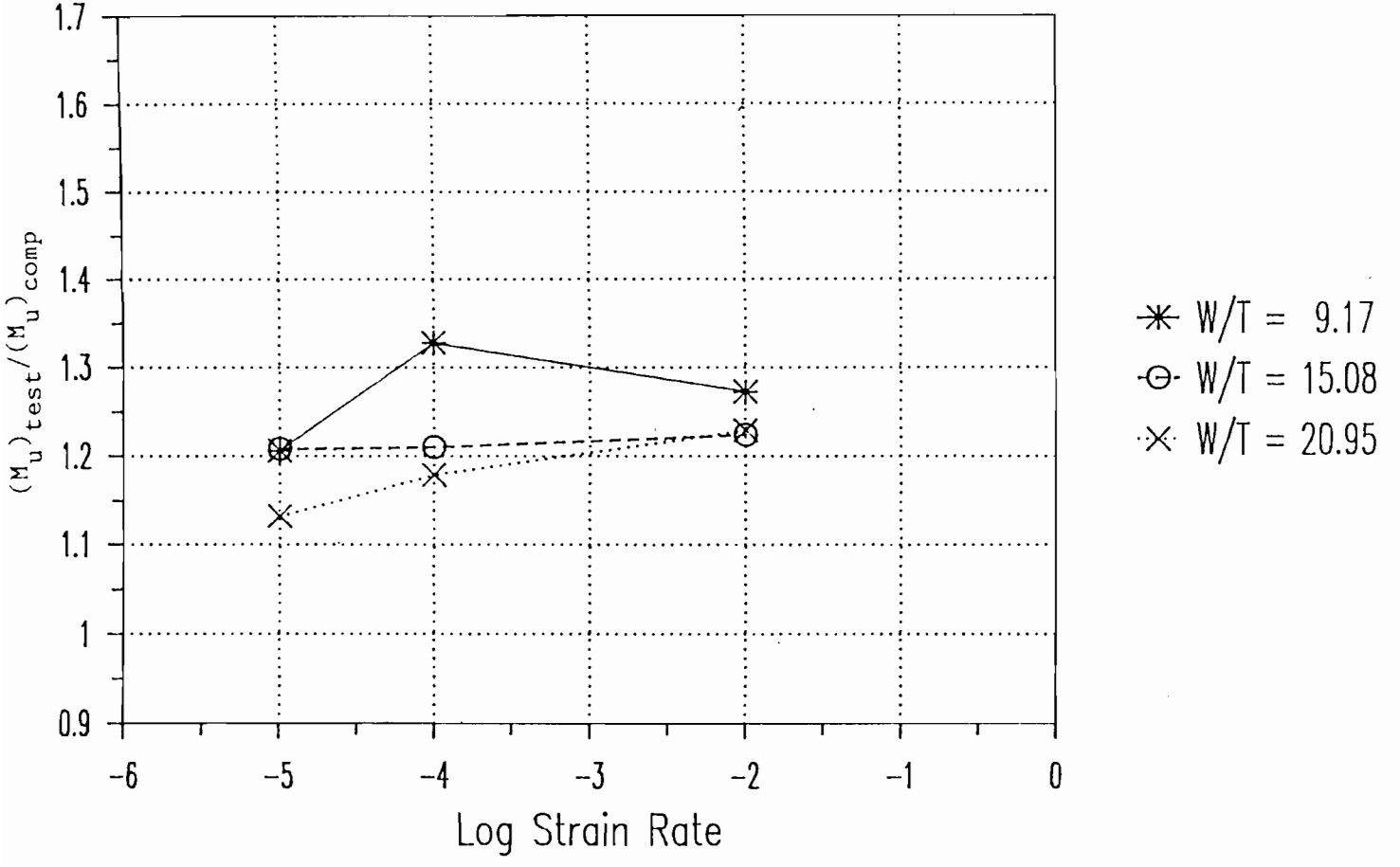

Figure 3.11 Ratios of Tested Failure Moments to Computed Failure Moments (Based on Dynamic Yield Stress) vs. Logarithmic Strain Rate for Channel Beams (35XF Sheet Steel)

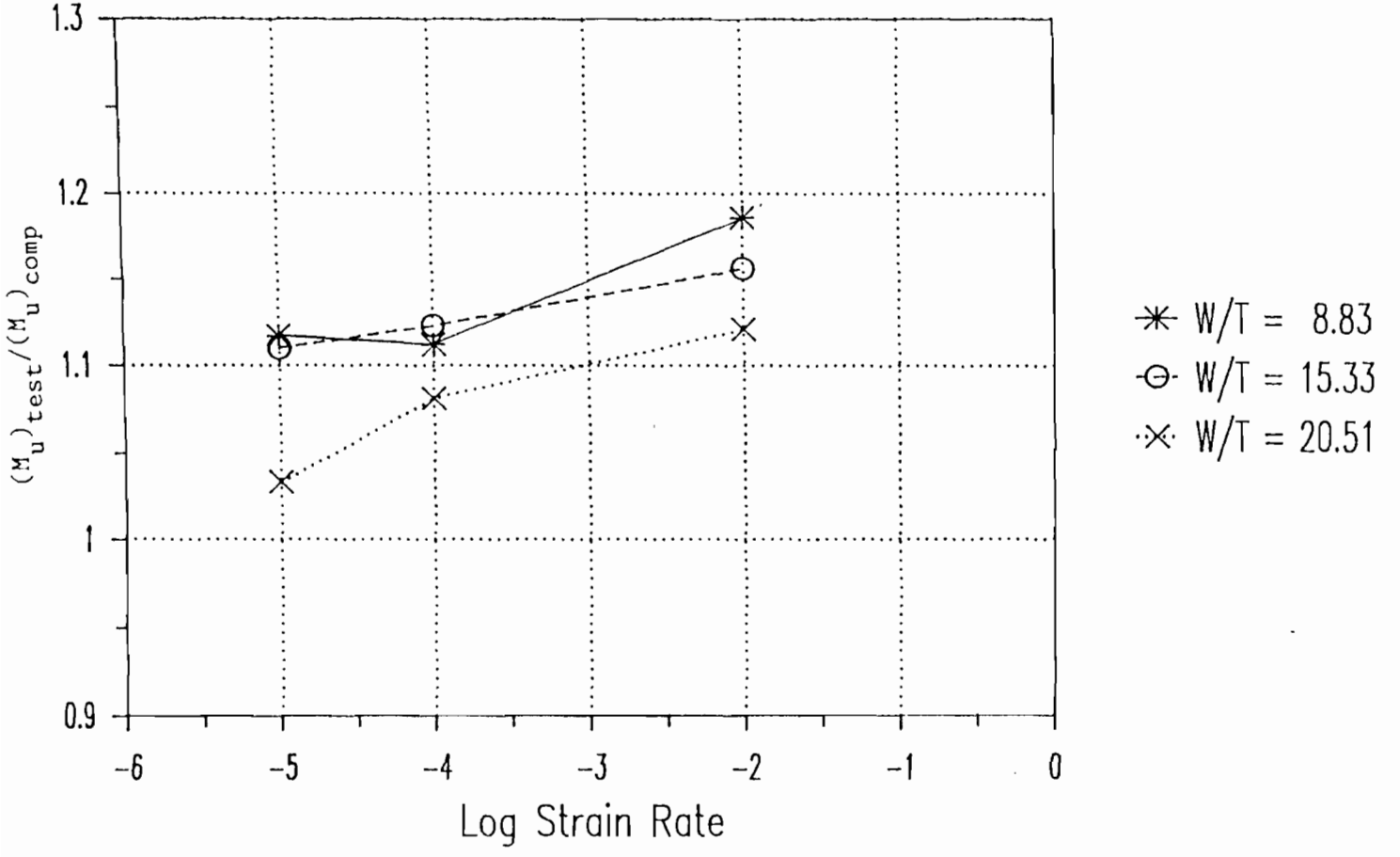

Figure 3.12 Ratios of Tested Failure Moments to Computed Failure Moments (Based on Static Yield Stress) vs. Logarithmic Strain Rate for Channel Beams (50XF Sheet Steel)

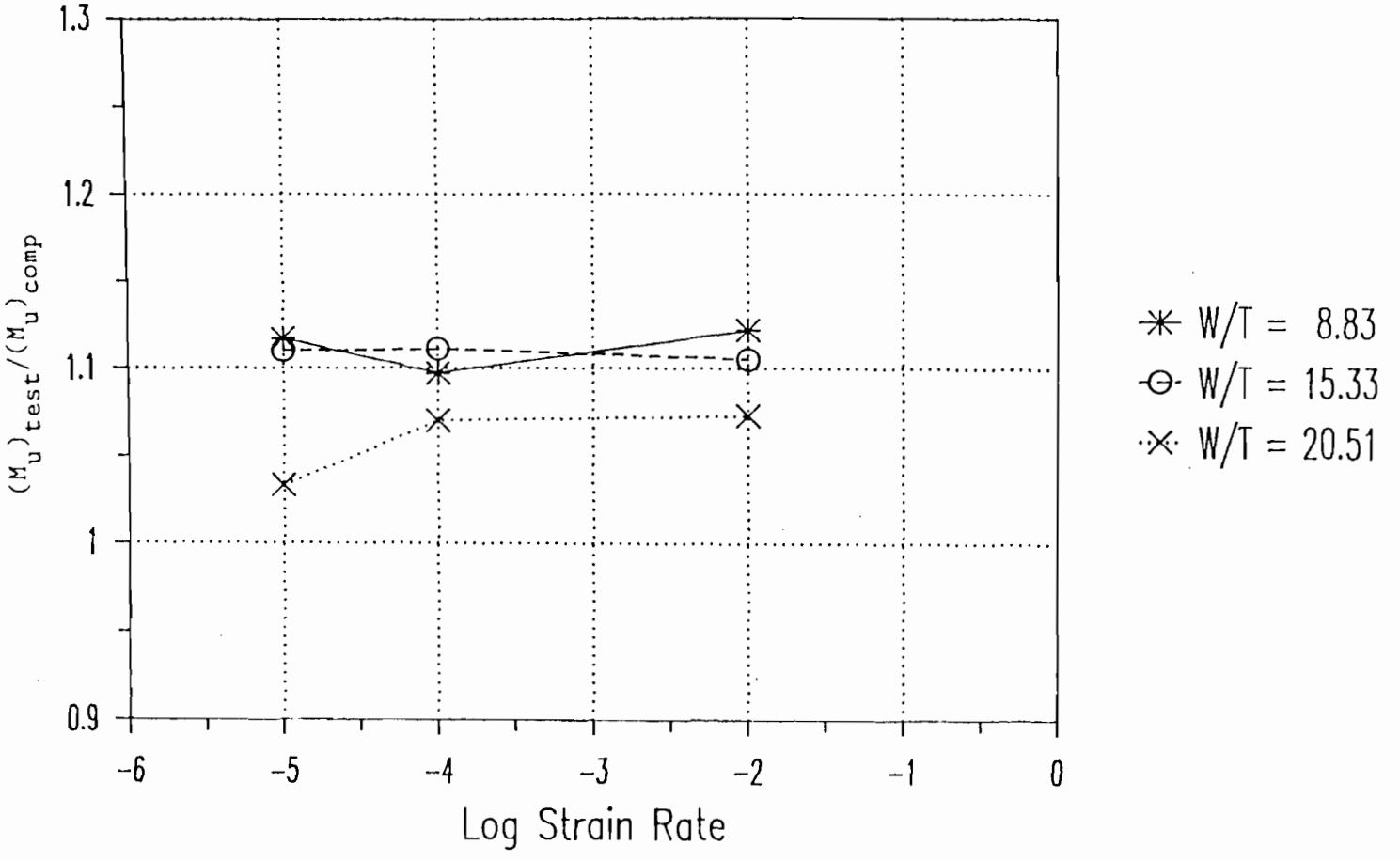

Figure 3.13 Ratios of Tested Failure Moments to Computed Failure Moments (Based on Dynamic Yield Stress) vs. Logarithmic Strain Rate for Channel Beams (50XF Sheet Steel)

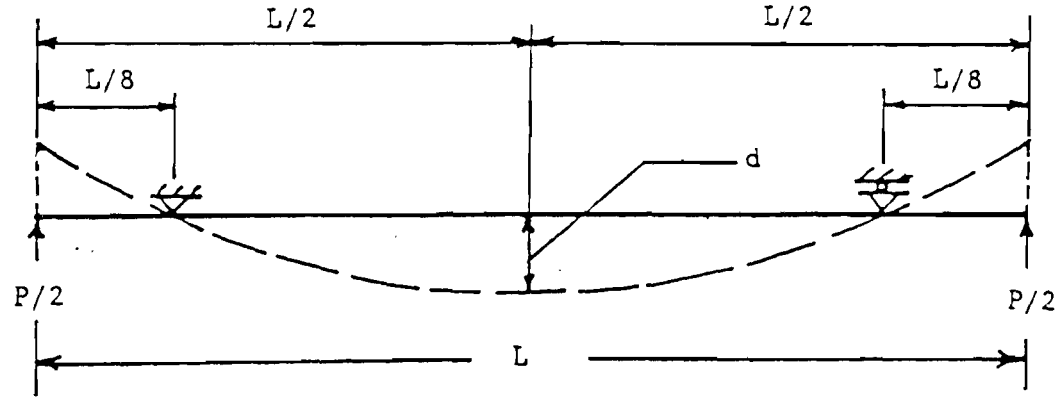

Figure 3.14 Schematic Diagram for Beam Specimen Showing Midspan Deflection

APPENDIX A

EFFECTIVE DESIGN WIDTH FORMULAS USED IN THE AISI COLD-FORMED STEEL DESIGN MANUAL

According to the AISI Cold-Formed Steel Design Manual[7], the effective design widths of stiffened and unstiffened compression elements can be determined by using the following equation :

(a) For Load Capacity Determination : The effective width (b) for computing the load-carrying capacity of uniformly compressed elements can be determined from the following formulas :

$$b = w \qquad \text{when} \quad \lambda \leq 0.673, \qquad (A-1a)$$

$$b = \rho w \qquad \text{when} \quad \lambda > 0.673, \qquad (A-1b)$$

where b = effective width of a compression element

w = flat width of a compression element

$$\rho = (1 - 0.22/\lambda)/\lambda \qquad (A-2)$$

λ = a slenderness factor

$$\lambda = \frac{1.052}{\sqrt{k}} \left(\frac{w}{t}\right)\left(\sqrt{\frac{f}{E}}\right) \qquad (A-3)$$

where f = the edge stress

E = modulus of elasticity, 29500 ksi

k = plate buckling coefficient

= 4.0 for stiffened elements supported by a web on each longitudinal edge

= 0.43 for unstiffened elements supported by a web on a longitudinal edge and free on the other

(b) For Deflection Determination : The effective width (b_d) in computing deflections shall be determined from the following formulas :

$$b_d = w \qquad \text{when} \quad \lambda \leq 0.673, \qquad (A-4a)$$

$$b_d = \rho w \qquad \text{when} \quad \lambda > 0.673, \qquad (A-4b)$$

where ρ = reduction factor determined by either of the following two procedures :

(1) Procedure I.

A low estimate of the effective width may be obtained from Equations A-2 and A-3 where f_d is substituted for f. f_d is defined as the computed compressive stress in the element being considered (calculations are based on the effective section at the load for which deflections are determined).

(2) Procedure II.

For stiffened elements supported by a web on each longitudinal edge an improved estimate of the effective width can be obtained by calculating ρ as follows :

$$\rho = 1 \qquad \text{when} \quad \lambda \leq 0.673 \qquad (A-5a)$$

$$\rho = (1.358 - 0.461/\lambda)/\lambda \qquad \text{when} \quad 0.673 < \lambda < \lambda_c \qquad (A-5b)$$

$$\rho = (0.41 + 0.59\sqrt{F_y/f} - 0.22/\lambda)/\lambda \qquad \text{when} \qquad \lambda \geq \lambda_c \qquad (A-5c)$$

$$\text{where} \qquad \lambda_c = 0.256 + 0.328(w/t)(\sqrt{F_y/E}). \qquad (A-6)$$

and λ is as defined by Equation A-2 except that f_d is substituted for f.

For the uniformly compressed unstiffened elements, the effective width used in computing deflections shall be determined in accordance with Procedure I except that f_d is substituted for f.

The effective width formulas used in the current AISI Automotive Steel Design Manual[1] are the same as that used in the AISI Cold-Formed Steel Design Manual[7]. According to the AISI Automotive Steel Design Manual[1], for stiffened and unstiffened compression elements with higher yield strength (F_y > 80 ksi), it is suggested that a reduced yield strength be substituted for the value of f in Equation A-3 and used in all subsequent calculations to determine the ultimate moment.

APPENDIX B

NOTATION

The following symbols are used in this report:

b	Effective width of a compression element
C	Ratio of the total corner cross-sectional area of the controlling flange to the full cross-sectional area of the controlling flange for beam
D	Flexural rigidity of plate
E	Modulus of elasticity of steel, 29,500 ksi
f	Edge stress in the compression element
f_{cr}	Critical local buckling stress
$(f_{cr})_E$	Elastic critical local buckling stress
$(f_{cr})_I$	Inelastic critical local buckling stress
f_x	Stress component normal to the edges of the plate
F_{pr}	Proportional limit
F_y	Yield stress
F_{ya}	Average tensile yield stress of steel
F_{yc}	Corner yield stress
F_{yf}	Weighted average tensile stress point of flat portions
F_{yv}	Tensile yield stress of virgin steel
F_u	Ultimate tensile strength
F_{uv}	Ultimate tensile strength of virgin steel
k	Buckling coefficient
$(M_{cr})_{comp}$	Computed critical local buckling moment
$(M_{cr})_{test}$	Tested critical local buckling moment
$(M_s)_{test}$	Service moment

$(M_u)_{comp}$	Computed ultimate moment
$(M_u)_{test}$	Tested ultimate moment
$(M_y)_{comp}$	Computed yield moment
$(M_y)_{test}$	Tested yield moment
P_{cr}	Critical local buckling load
$(P_{cr})_{test}$	Tested critical local buckling load
P_u	Ultimate load
$(P_u)_{test}$	Tested ultimate load
$(P_y)_{test}$	Tested yield load
R	Inside bend radius
t	Thickness of element
w	Flat width of a compression element
λ	Slenderness factor
ω	Lateral deflection of the plate
μ	Poisson's ratio
ρ	Reduction factor